Defence Research and Development Canada
Recherche et développement pour la défense Canada

DEFENCE R&D DÉFENSE

Processing and Analysis of Polarimetric Ship Signatures from MARSIE

Report on Results for Polar Epsilon

Paris W. Vachon, Marina Dragosevic, Nathan Kashyap, Chen Liu, David Schlingmeier, Alan Meek, Terry Potter, Bing Yue and James Kraft

Defence R&D Canada – Ottawa
TECHNICAL MEMORANDUM
DRDC Ottawa TM 2006-202
October 2006

Canada

Processing and Analysis of Polarimetric Ship Signatures from MARSIE

Report on Results for Polar Epsilon

Paris W. Vachon
DRDC Ottawa

Marina Dragošević
TerraBytes Consulting

Nathan Kashyap, Chen Liu, David Schlingmeier
DRDC Ottawa

Allan Meek
MacDonald, Dettwiler & Associates Ltd.

Terry Potter
Terry M. Potter Consulting

Bing Yue
W.E. Thorpe Associates Ltd.

James Kraft
J. Kraft Consulting Inc.

Defence R&D Canada – Ottawa

Technical Memorandum
DRDC Ottawa TM 2006-202
October 2006

Principal Author

Original signed by Paris W. Vachon

Paris W. Vachon

Defence Scientist

Approved by

Original signed by Gary W. Geling

Gary W. Geling

Head, Radar Applications and Space Technologies Section

Approved for release by

Original signed by Cam Boulet

Cam Boulet

Chair, Document Review Panel

This work was supported in part by an SLA between the Polar Epsilon Project and DRDC Ottawa concerning Exploitation Tool development.

Abstract

This report presents the initial analysis of a polarimetric synthetic aperture radar (SAR) data set that was acquired during the Oct. 2005 Maritime Sensor Integration Experiment (MARSIE). MARSIE, as part of a larger TTCP activity, was designed to explore the benefits of sensor fusion to solve the target detection and tracking problem. The MARSIE trial was conducted off the East Coast of Canada and brought many sensors to bear on a set of known ship targets that were engaged in a simulated maritime incursion scenario. The Environment Canada CV-580 polarimetric SAR was used as a proxy sensor for RADARSAT-2 polarimetry. MARSIE polarimetry results include observations of ship target radar cross section for co-polarization and cross-polarization channels, the reduction in the probability of missed detection for polarimetric relative to single channel radar operation, and the potential benefit of polarimetric target decomposition to generate ship target classification features and to segment the ship target of interest from the ocean background. A main recommendation of this report is that polarimetry could improve Polar Epsilon (PE) ship detection performance and enhance the PE concept of operations for the surveillance of spatially constrained maritime operational areas of interest such as choke points.

Résumé

Le présent rapport traite de l'analyse initiale d'un ensemble de données du radar à synthèse d'ouverture (SAR) polarimétrique qui a été recueilli durant l'expérience MARSIE (Maritime Sensor Integration Experiment, expérience conjointe sur l'intégration des capteurs), en octobre 2005. L'expérience MARSIE, menée dans le cadre d'une activité plus globale du TTCP, visait à explorer les avantages de la fusion des données des capteurs pour résoudre le problème de détection et de poursuite des cibles. Elle a été menée au large de la côte Est du Canada, et un grand nombre de capteurs y ont été utilisés pour recueillir des données relatives à un ensemble de navires cibles connus participant à un scénario d'incursion maritime simulée. Le SAR polarimétrique du CV 580 d'Environnement Canada a été utilisé comme détecteur de proximité pour la polarimétrie de RADARSAT-2. Les résultats polarimétriques de l'expérience MARSIE comprennent des observations de la surface équivalente radar de navires cibles pour les canaux de copolarisation et de polarisation croisée, la réduction de la probabilité de détection manquée dans le cas de l'utilisation du radar polarimétrique par comparaison à l'utilisation du radar monocanal, et l'avantage potentiel offert par la décomposition polarimétrique de cible pour générer des caractéristiques de classification de navires cibles et pour détacher le navire cible d'intérêt par rapport au fond océanique. Dans les principales recommandations du présent rapport, on indique notamment que la polarimétrie pourrait accroître l'efficacité de détection des navires dans le projet Polar Epsilon (PE) et améliorer le concept des opérations de ce projet pour la surveillance des zones opérationnelles maritimes confinées d'intérêt, comme les points d'étranglement.This page intentionally left blank.

This page intentionally left blank.

Executive summary

Processing and Analysis of Polarimetric Ship Signatures from MARSIE: Report on Results for Polar Epsilon

Vachon, P.W.; Dragošević, M.; Kashyap, N.; Liu, C.; Schlingmeier, D.; Meek, A.; Potter, T.; Yue, B.; Kraft, J.; DRDC Ottawa TM 2006-202; Defence R&D Canada – Ottawa; October 2006.

Introduction

A polarimetric synthetic aperture radar (SAR) data set was acquired during the Maritime Sensor Integration Experiment (MARSIE). DRDC Ottawa's participation in MARSIE leverages past trial experience involving the Environment Canada (EC) CV-580 polarimetric SAR. This experience has provided insight into the potential of polarimetry for ship detection and classification, and has lead directly to the development of the Chip-based Adaptive SAR Processor (CHASP), which permits adaptation of SAR processing to moving ship targets of interest.

MARSIE is a TTCP-lead activity that is exploring the benefits of sensor fusion to solve the target detection and tracking problem. The MARSIE trial was held in Oct. 2005 off the East Coast of Canada and brought many sensors to bear on a set of known ship targets that were engaged in a simulated maritime incursion scenario. The EC CV-580 polarimetric SAR was used as a proxy sensor for RADARSAT-2 polarimetry. Four flights were carried out over MARSIE trial events, providing a large collection of polarimetric SAR imagery of known vessels.

Project Polar Epsilon (PE) will use the RADARSAT-2 SAR sensor as its main maritime surveillance capability. Currently, PE focuses on the use of wide swath (i.e., ScanSAR) modes to maximize the area coverage rate. However, increased swath width comes at the expense of reduced image resolution, which in turn reduces the probability of detecting smaller vessels. As such, results from the MARSIE polarimetry experiments could have impact on the PE Concept of Operations (CONOPS). To illustrate the significance of the MARSIE analysis to Project Polar Epsilon, we have highlighted in this report the analysis of imagery taken of the ship *Dominion Victory,* which, at 25 metres length, is a vessel that matches the minimum detection criteria laid out in the PE Statement of Requirements.

This document describes the polarimetric SAR data set that was acquired during MARSIE, the data processing that was carried out, and the analysis of the resulting image products.

Results

The MARSIE trial has provided a vast and valuable polarimetric data set that has and will be beneficial to the study of polarimetric signatures of ships.

It is demonstrated that CHASP processing always improves the ship focus and that CHASP can often be used to usefully estimate the ship velocity for the case of airborne SAR geometry.

The total radar cross section (RCS) as a function of linear polarization state has been compiled for several vessels. The estimated HV and VH Total RCS values were roughly 10 dB smaller than the estimated HH and VV channel Total RCS values.

Polarimetric SAR can be used to improve ship detection and provide some classification information. For *Dominion Victory*, a six-fold to an eleven-fold reduction in the probability of missed detection was observed by using polarimetric information, as compared to a single channel radar with the same probability of false alarm.

Four polarimetric target decomposition methods were applied to the MARSIE data in order to characterize the targets of interest in terms of their constituent elemental scatterers. Some decomposition methods appear to offer potential for target classification since decomposition to a variety of scatterer types was possible. Others provide a means to segment the target signature from the surrounding ocean background.

Significance

The MARSIE trial dataset is a rich information source that could be used by Polar Epsilon to further enhance the PE system's ship detection and classification performance, including false alarm rate reduction. There is strong evidence that significant improvements could be realized as compared to lower resolution, single polarization acquisition modes. It is recommended that Polar Epsilon use RADARSAT-2 polarimetry for surveillance of spatially constrained areas of interest such as: choke points (including most of the North West Passage); straits, channels and confined waterways; specific fishery zones; ports; and the Arctic Archipelago.

Estimated values of the ship Total RCS, especially at cross polarization, could be used to predict the ship detection performance of future SAR missions such as the proposed RADARSAT Constellation mission.

Future plans

The polarimetric signatures of other known vessels in the MARSIE data set remain to be analyzed and reported upon. In addition, the following polarimetric issues are relevant to the Polar Epsilon CONOPS and will be studied further:

- The effects of acquisition geometry, target motion, environmental conditions, etc. on the observed polarimetric signatures;
- The differences in the elemental scatterer distributions among the various polarimetric decomposition methods that offer the same set of target classes;
- The relationships between target features such as the ship superstructure, flight decks, and king posts, and the elemental scatterers;
- The feasibility of applying polarimetric decomposition methods to automatic target recognition (ATR) by using decomposition outputs as target features; and

- The simulation of RADARSAT-2 polarimetry signatures from CHASP products.

This page intentionally left blank.

Sommaire

Processing and Analysis of Polarimetric Ship Signatures from MARSIE: Report on Results for Polar Epsilon

Vachon, P.W.; Dragošević, M.; Kashyap, N.; Liu, C.; Schlingmeier, D.; Meek, A.; Potter, T.; Yue, B.; Kraft, J.; DRDC Ottawa TM 2006-202; R & D pour la défense Canada – Ottawa; octobre 2006.

Introduction

Un ensemble de données du radar à synthèse d'ouverture (SAR) polarimétrique a été recueilli durant l'expérience MARSIE (*Maritime Sensor Integration Experiment*, expérience conjointe sur l'intégration des capteurs). La participation de RDDC Ottawa à l'expérience MARSIE met à profit l'expérience antérieure réalisée avec le SAR polarimétrique du CV-580 d'Environnement Canada. Cette expérience a permis d'acquérir des connaissances sur les possibilités qu'offre la polarimétrie pour la détection et la classification des navires, et elle a mené directement au développement du processeur SAR adaptatif à puce (CHASP), qui permet d'adapter le traitement SAR aux navires cibles d'intérêt en mouvement.

L'expérience MARSIE est une activité menée dans le cadre du TTCP en vue d'explorer les avantages de la fusion des données des capteurs pour résoudre le problème de détection et de poursuite des cibles. Elle a été menée en octobre 2005 au large de la côte Est du Canada, et un grand nombre de capteurs y ont été utilisés pour recueillir des données relatives à un ensemble de navires cibles connus participant à un scénario d'incursion maritime simulée. Le SAR polarimétrique du CV-580 d'Environnement Canada a été utilisé comme détecteur de proximité pour la polarimétrie de RADARSAT-2. Quatre vols ont été effectués dans le cadre des événements de l'expérience MARSIE et ils ont permis de recueillir une grande quantité de données d'imagerie SAR polarimétrique de navires connus.

Dans le projet Polar Epsilon (PE), on utilisera le capteur SAR de RADARSAT-2 comme principal outil de surveillance maritime. Dans ce projet, on met actuellement l'accent sur l'utilisation des modes de fauchée large (ScanSAR) pour maximiser le taux de couverture de zone. Cependant, l'accroissement de la largeur de fauchée s'obtient au prix d'une réduction de résolution de l'image et, par conséquent, d'une réduction de la probabilité de détection des navires plus petits. En conséquence, les résultats de l'expérience de polarimétrie MARSIE pourraient avoir une incidence sur le concept des opérations (CONOPS) du projet PE. Afin d'illustrer l'importance de l'analyse MARSIE pour le projet Polar Epsilon, nous avons mis en évidence, dans le présent rapport, l'analyse des données d'imagerie du navire *Dominion Victory*, un navire d'une longueur de 25 mètres qui satisfait aux critères minimaux de détection établis dans l'énoncé de besoins du projet PE.

Le présent document décrit l'ensemble de données du SAR polarimétrique qui a été recueilli durant l'expérience MARSIE, le traitement des données qui a été effectué et l'analyse des produits images résultants.

Résultats

L’expérience MARSIE a permis de recueillir un ensemble de données polarimétriques volumineux et précieux qui a été et qui continuera d’être bénéfique pour l’étude des signatures polarimétriques des navires.

Il est prouvé que le traitement CHASP améliore toujours la netteté du navire observé et que ce traitement peut souvent être utilisé pour estimer la vitesse du navire dans le cas de la géométrie du SAR aéroporté.

La surface équivalente radar (SER) totale en fonction de l’état de polarisation linéaire a été calculée pour plusieurs navires. Les valeurs estimées de SER totale pour les canaux HV et VH étaient d’environ 10 dB inférieures aux valeurs estimées de SER totale pour les canaux HH et VV.

Le SAR polarimétrique peut être utilisé pour améliorer la détection des navires et pour fournir certaines données de classification. Dans le cas du *Dominion Victory*, on a observé que la probabilité de détection manquée était de six à onze fois moins grande lorsqu’on utilisait les données polarimétriques plutôt que les données d’un radar monocanal avec la même probabilité de fausse alarme.

Quatre méthodes de décomposition polarimétrique de cible ont été appliquées aux données MARSIE dans le but de caractériser les cibles d’intérêt quant aux diffuseurs élémentaires dont elles sont constituées. Certaines méthodes de décomposition semblent offrir des possibilités pour la classification des cibles, étant donné qu’il a été possible d’effectuer la décomposition en une variété de types de diffuseurs. D’autres permettent de détacher la signature de la cible par rapport au fond océanique.

Importance

L’ensemble de données de l’expérience MARSIE constitue une précieuse source d’information qui pourrait être utilisée dans le projet Polar Epsilon pour améliorer encore plus l’efficacité de détection et de classification des navires du système PE, notamment en réduisant le taux de fausse alarme. On a de bonnes raisons de croire que des améliorations importantes pourraient être réalisées par rapport aux modes d’acquisition en polarisation simple, à plus faible résolution. On recommande d’utiliser dans le projet Polar Epsilon la polarimétrie de RADARSAT-2 pour la surveillance des zones confinées d’intérêt, comme les points d’étranglement (y compris la plus grande partie du passage du Nord-Ouest); les détroits, les canaux et les voies de navigation confinées; les zones de pêche particulières; les ports; l’archipel Arctique.

Les valeurs estimées de SER totale du navire, particulièrement en polarisation croisée, pourraient être utilisées pour prévoir l’efficacité de détection des navires des futures missions SAR, comme la mission Constellation RADARSAT qui a été proposée.

Perspectives

Il reste encore à analyser les signatures polarimétriques d'autres navires connus de l'ensemble de données MARSIE et à en faire un compte rendu. De plus, les aspects suivants de la polarimétrie sont pertinents pour le CONOPS du projet Polar Epsilon et seront étudiés plus en profondeur :

- Effets de la géométrie d'acquisition, du mouvement des cibles, des conditions environnementales, etc. sur les signatures polarimétriques observées;
- Différences dans les distributions des diffuseurs élémentaires entre les diverses méthodes de décomposition polarimétrique qui offrent le même ensemble de classes de cibles;
- Relations entre les caractéristiques des cibles, par exemple superstructure du navire, ponts d'envol et mâtereaux, et les diffuseurs élémentaires;
- Faisabilité de l'application des méthodes de décomposition polarimétrique à la reconnaissance automatique de cibles (ATR) en utilisant les résultats de la décomposition comme caractéristiques des cibles;
- Simulation des signatures polarimétriques de RADARSAT-2 à partir des produits CHASP.

This page intentionally left blank.

Table of contents

List of figures

List of tables

Acknowledgements

The MARSIE trial was implemented as a TTCP SEN AG-7 activity with Gary Geling (DRDC Ottawa) and LCdr Anthony Cond (DRDC Ottawa) as the Chief Scientist and Experiment Coordinator, respectively. We thank Dr. J.K.E. (Jake) Tunaley (Polar Epsilon R&D Manager) for his interest in and support of this work. Dr. R. Sabry (DRDC Ottawa) provided insightful comments on an initial draft of this document.

1. Introduction

In this document we describe the polarimetric synthetic aperture radar (SAR) data set that was acquired during the Maritime Sensor Integration Experiment (MARSIE), the data processing that was carried out, and the analysis of the resulting image products. We summarize key findings to date of the benefits of polarimetry for maritime surveillance and make recommendations regarding how polarimetry could be introduced into the project Polar Epsilon (PE) Concept of Operations (CONOPS).

DRDC Ottawa has undertaken this polarimetric work because it has considerable experience with acquiring, processing, and analyzing polarimetric SAR data sets of known ships [7], [10], [11], [23] using data from the Environment Canada (EC) CV-580 polarimetric SAR [14]. These trials provided helpful insight into the potential of polarimetry for ship detection and classification and highlighted problems with the airborne SAR sensor that lead DRDC Ottawa to develop modifications to the airborne SAR hardware and to develop a new SAR processor (referred to as the Chip-based Adaptive SAR Processor – CHASP [21]), which permits adaptation of the processing to the moving ship targets of interest.

MARSIE is a TTCP-lead activity that is exploring the benefits of sensor fusion to solve the target detection and tracking problem. MARSIE, which included a live trial that was conducted in Oct. 2005, brought many sensors to bear on a set of known ship targets that were engaged in simulating a maritime incursion scenario (MIS). The MARSIE Trial occurred off the East Coast of Canada and consisted of a MIS that was conducted three times with one week intervals between each. In the scenario, a Freighter carried a simulated contraband package from Europe to Canada. This package was thrown overboard at the rendezvous point (nominally N45.5° W51° on the Grand Banks, see Figure 9) and was recovered by a Fishing Trawler which transported the package to Chedabucto Bay (see Figure 8). At this point, the contraband package was transferred by various smaller boats from the Fishing Trawler to a location ashore near Janvrin Point (N45.53° W61.20°). Key imaging opportunities included the three rendezvous events and the three Transfer events. The EC CV-580 SAR imaged the following events:

1. The second Transfer Event (17 and 18 Oct. 2005, the second date corresponded to an RCMP training exercise);

2. The third Rendezvous Event (20 Oct. 2005); and

3. The third Transfer Event (24 Oct. 2005).

Details of the EC CV-580 SAR data acquisition program are summarized in Annex A. Airborne photography was used for validation purposes and to provide the reader with a sense of the size and shape of the target vessels and the area of operations. These photographs are presented and summarized in Annex B.

As a significant component of the 2005 MARSIE trial, it was planned that the RADARSAT-2 SAR sensor would be used to augment other acquired sensor data sets. RADARSAT-2, which is currently scheduled for launch in 2007 and which will carry a very flexible C-band synthetic aperture radar (SAR) instrument, was unfortunately not available for MARSIE due to delays in its

launch schedule. In its place, the EC CV-580 C-band polarimetric SAR was configured to emulate certain RADARSAT-2 SAR characteristics and was flown as RADARSAT-2's replacement for MARSIE. Although there are differences in terms of resolution, noise floor, and geometry between RADARSAT-2 and the EC CV-580 C-band SAR, MARSIE provided a unique opportunity to collect polarimetric SAR data over a variety of known ship types and sizes.

1.1 Relevance of MARSIE to Polar Epsilon

RADARSAT-2 will offer the option of fully polarimetric SAR imagery for certain acquisition modes[1] that have a much narrower swath width than the modes preferred for PE. Since the area coverage rates of the narrow swath widths are low in comparison to those of the ScanSAR[2] modes, and polarimetric processing was not mature at the time that PE first developed its CONOPS, only the wide swath width modes are currently included in the PE CONOPS. However, with the rapid development of polarimetric data processing techniques, the opportunity for PE to achieve better vessel detection and classification performance exists for surveillance operations of constrained spatial extent for which narrower swath widths are appropriate. These operations might include: choke point surveillance (choke point examples are; straits, channels, confined waters, fishery zones and most of the North West Passage), port surveillance, and Arctic Archipelago surveillance.

Project Polar Epsilon has an interest in the results from the 2005 MARSIE trial because PE will use the RADARSAT-2 SAR sensor as its main maritime surveillance capability (once it deploys its capabilities in the 2007-2015 timeframe). PE's focus on the use of wide swath (i.e., ScanSAR) modes has been to maximize the area coverage rate and reduce the probability that a ship target of interest is missed. However, increased swath width comes at the expense of reduced image resolution, which in turn reduces the probability of detecting smaller vessels. This is where the MARSIE polarimetric experiments could have a beneficial impact on the PE CONOPS.

To better illustrate the significance of MARSIE to Project Polar Epsilon, in Table 1 we have cross referenced the MARSIE/Polarimetric SAR outcomes against the Polar Epsilon Statement of Operational Requirements (SOR) [1]. For example, in this report we have highlighted analysis of the imagery taken of the ship *Dominion Victory*, which, at 25 metres length, is a vessel that matches the minimum detection criteria laid out in the PE SOR.

1.2 Outline of this Document

In Section 2 we first describe the processing procedures for the available MARSIE data. The processing and analysis results are presented in Section 3. A summary of the results along with recommendations relevant to polarimetry and Polar Epsilon CONOPS are presented in Section 4. Many details have been relegated to Annexes including the EC CV-580 SAR data acquisition program (Annex A), supporting photographic data (Annex B), survey mode polarimetric data processing (Annex C), a catalogue of polarimetric decomposition results from MARSIE data (Annex D), a discussion of CHASP processing for RADARSAT data (Annex E), and a summary of Receiver Operating Characteristics from past trials (Annex F).

[1] The RADARSAT-2 Fine Quad-Pol and Standard Quad-Pole modes will have swath widths of 25 km.
[2] The RADARSAT-2 ScanSAR modes will have swath widths ranging from 300 km to 500 km.

Table 1: Relationship of MARSIE/Polarimetric SAR to the Polar Epsilon SOR (continued on next page).

PE SOR Ref	PE SOR Text	MARSIE/Polarimetric SAR relationship
PE Objective (e), page 6	optimize RADARSAT 2 for maritime surveillance, in particular for ship, wake, oil, and ice detection, and ship length, heading, and velocity extraction	Polarimetric SAR could help to meet this objective.
PE Objective (f), page 6	provide concept of operations and procedures to assist/advise the MSOCs/JIIFC in exploiting Polar Epsilon capabilities. Determine the personnel requirements with space expertise to execute the Polar Epsilon concept of operations and procedures in support of the MSOC/JIIFC.	This report addresses Polarimetric SAR CONOPS. Polarimetric SAR tools could operate automatically and would not require additional personnel to be employed in the PE capability.
PE Objective (h), page 6	develop exploitation tools in cooperation with Defence Research Development Canada (DRDC) (through a Service Level Agreement) for target extraction, tracking and manipulation of data from satellite sensors, including (but not limited to): i. advanced ship detection algorithms; ii. environmental assessment; iii. commercial satellite imagery acquisition planning system (CSIAPS); and iv. supporting trials – Maritime Cooperative Polarimetric Assessment (MARCO POLA III), Maritime Sensors Integration Experiment (MARSIE) and Submarine Vulnerability Assessment	This report explicitly addresses (h) i and (h) iv.
Para 2.4, page 14 (CONOPS section)	satellites, including RADARSAT 2, will be used on a case-by-case basis to support target classification and identification	Polarimetric SAR could provide ship classification characteristics such as length, breadth, and superstructure positioning, or less directly, from the distribution and orientation of discrete scattering elements.
Para 2.5.5, page 17 (Data processing tools section)	Polar Epsilon will provide tools for exploiting imagery data to accomplish target detection and determine some target characteristics. Data exploitation tools will comprise software and general-purpose hardware (including computers, data storage devices and peripherals)	Polarimetric SAR target detection tools are well developed, as are polarimetric decomposition tools. Classification tools still require development and demonstration.

Table 1: Concluded.

PE SOR Ref	PE SOR Text	MARSIE/Polarimetric SAR relationship
Para 2.7.2, page 18 and Para 4.2.1 (g), page 19 (Image processing section)	Where possible, Polar Epsilon will support MSOC staff in classifying and identifying vessels in all three maritime surveillance zones, and JIIFC staff in classifying and identifying land targets	Polarimetric SAR could support MSOC staff in classifying vessels; classification tools that operate automatically could be developed and demonstrated.
Para 6.1, Table 1	A trade-off exists between minimum detectable ship size and area coverage rate. Therefore, vessel detection will be dependent upon beam mode selection. The vessel sizes below do not limit the operator from selecting a finer resolution beam of RADARSAT-2 that could detect smaller sized vessels as small as 10 metres, depending upon environmentals. SOR calls for detection of vessels >25 m in seas up to Sea State 5[3].	RADARSAT-2's wide swath modes could miss smaller vessels. Use of higher resolution modes, which would be compatible with RADARSAT-2 polarimetry, may be required for PE to meet its requirement for detection of vessels as small as 25 m in length; this approach could be suitable for constrained areas of interest. MARSIE data were collected in seas of up to 2.3 m significant wave height with 9.3 s significant wave period, roughly translating to Sea State 4. This provides a good indication of the ability of polarimetric SAR to support PE, although further polarimetric data collection in Sea State 5 would still be beneficial.
Para 6.1, Table 1	Latency - All target reports to be generated within 15 minutes of target illumination for all frames in any given pass	It is anticipated that Polarimetric SAR software will not impact PE time latency requirements since decomposition and classification routines would only need to be run on candidate ship targets (for false alarm rate reduction or classification purposes, rather than across an entire image).
Staffing		Use of Polarimetric SAR software in PE should not have an impact on PE staffing requirements.
Training		Use of Polarimetric SAR software in PE would require some additional training of operators. The additional training should be marginal in comparison with the overall PE operator training requirements. The training requirement for Polarimetric SAR use by PE would require further examination.

[3] For a Pierson-Moskowitz ocean wave spectrum, Sea State 4 corresponds to a surface wind speed of roughly 9 m/s while Sea State 5 corresponds to a surface wind speed of roughly 12 m/s.

2. Processing Procedures

A data processing chain was implemented to permit a systematic processing and analysis of the acquired polarimetric ship signatures. The main elements of the processing chain are summarized in Figure 1. In a nutshell, there are two main processing streams: target detection and target analysis.

In the target detection stream, a strip-map image is first produced using the Configurable Airborne SAR processor (COASP) [21]. The COASP image product is fully compressed (i.e., fully focussed) in both range and azimuth under the assumption of static targets in the scene. This COASP image product is used to carryout data QC and target detection, to guide the preparation of the validation data, and to estimate the receiver operating characteristic (ROC) for the open ocean cases.

In the target analysis stream, target-adaptive processing is carried out using the Chip-based Adaptive SAR Processor (CHASP) [21]. CHASP is a highly adaptive SAR processor that contains several algorithms to facilitate the optimal processing of moving targets, such as vessels. The re-focussing provides estimates of the ship velocity which may be compared with available validation data. The refocused CHASP image products are used to estimate the target's Total RCS and form the input to the polarimetric decomposition analysis.

In Figure 1, the principle file types for each step in the processing chain are indicated by the file suffixes. Although it is beyond the scope of this document to expand upon the contents and format of each of the files, the figure is included to give an idea as to the complexity of the data processing and analysis that has been carried out.

An informal goal of the MARSIE data analysis project was to implement the processing chain such that it would run in an automated fashion on all of the MARSIE data sets. However, due to time constraints in delivering this report, a few of the steps had to be carried out manually. Therefore, only a representative sample of the acquired data has been processed and is reported upon here. The details of the steps in the processing chain and associated constraints are summarized in the following sub-sections, while the analysis results are presented in Section 3.

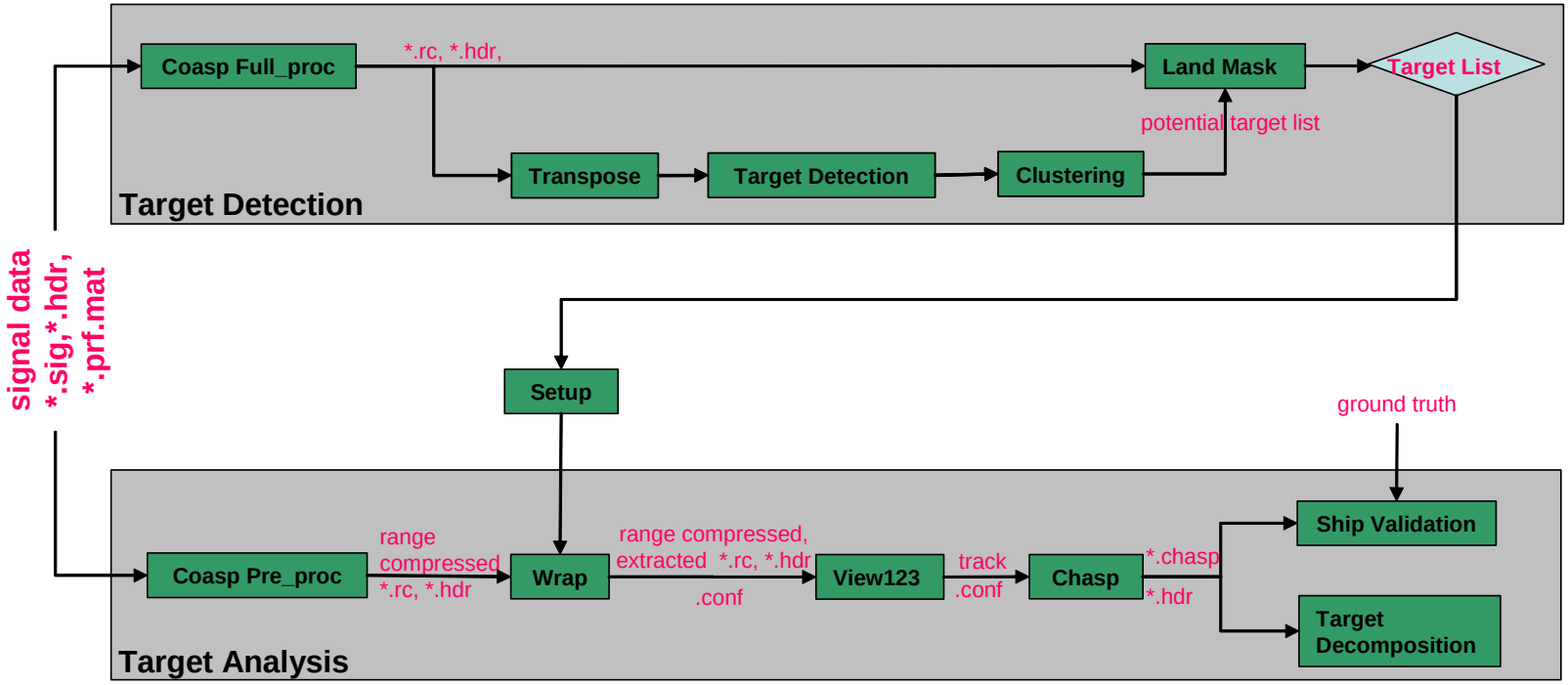

Figure 1: Data processing chain implemented for MARSIE polarimetry analysis.

2.1 COASP Processing

Survey mode strip-map images were produced for each data set using the COASP processor [21]. The processing procedures along with survey mode images for each flight line are presented in Annex C.

2.2 Use of ADSS

The Analysts' Detection Support System (ADSS) [16] is a set of tested and proven algorithms that provide a framework for automatic target detection and recognition. A demonstration processing chain involving COASP, CHASP, and PolSAR detection software run within an ADSS wrapper is being developed at DRDC Ottawa as part of another project. It was decided to use a portion of the available ADSS demonstration processing chain to carry out the target detection, clustering, and land masking operations on the MARSIE COASP products.

Using ADSS, the COASP data sets were ingested and the Adaptive Threshold algorithm (ATA) module was executed to perform point target detection; a custom module, *growing_clusterer*, performed point target clustering. The intention was to automatically apply a land mask to the clustered targets. Unfortunately, technical problems coupled with tight time constraints prevented this, such that the land mask had to be verified as a manual step.

ATA was run separately on each polarization channel of the COASP-processed image with the following settings:

- threshold-sd-over-mean 7.0
- outer-edge 30
- guard-size 10

These settings had previously been found to provide a balance between the probability of false alarm and the probability of missed detections when processing COASP data.

The *growing_clusterer* module clustered the resulting set of point targets using the following settings:

- x-cluster-proximity 4
- y-cluster-proximity 150
- min-cluster-size 10

Again, these settings had previously been found to work well with COASP data. The first two settings define the threshold distances (in both directions) for combining two clusters of point targets. Once clustering has finished, any clusters containing less than min-cluster-size point targets were removed.

The resulting target location file had to be filtered to remove any targets located over land. This was done by viewing the COASP image and detected targets using the Polarimetric Ship

Detection application [13] and manually stripping the target location file of land targets. Any ambiguous targets that could not be positively identified as land were kept (i.e., there could be some small islands in the filtered target location file).

2.3 CHASP Processing

The principal objective of CHASP processing [21] is to improve image focus; the secondary objective is to estimate the ship velocity.

If it is assumed that the ship of interest is moving uniformly at a constant velocity, then it is sufficient to estimate the Doppler centroid (DC) offset and the Doppler rate (DR) offset in order to correctly process the moving target image. These two processing parameters are used for subsequent image formation. They are also used for deriving cross-track and along-track components of the ship velocity.

In some cases, the uniform motion assumption is not appropriate; surge, sway and heave motion of the ship cannot be neglected. This tends to be the case for smaller vessels on open seas. In this case there is a variable acceleration along the line of sight (LOS) imparted on the ship by the underlying wave field that affects the phase history in an unpredictable way. In this case, the best strategy is to estimate and compensate for the motion-induced phase history via non-parametric methods (i.e., simply adjust the processing parameters in a systematic way in order to maximize the target contrast). However, as we shall see, surge, sway and heave motion, if present, make it impossible to estimate both the linear speed and the course of the vessel using CHASP.

The most difficult cases are vessels that exhibit yaw, pitch and roll motion. In this case, different parts of the ship follow different trajectories during the several second observation (i.e., coherent integration) interval; it is not possible to apply a unique compensation for each part of the ship. Under such conditions, CHASP processing is unsuccessful; a good focus cannot be achieved and the velocity of the ship cannot be estimated.

2.3.1 Theoretical Background

The phase history of a target in linear uniform motion can be represented very accurately by a hyperbolic model:

$$\varphi(t) = 2k\sqrt{R_o^2 + V^2(t - t_o)^2}\ , \tag{1}$$

where k is the radar wavenumber, R_o is the slant range at the point of closest approach, t is the "slow time" or time of platform flight measured from a given reference time, t_o is the time of closest approach, and V is the effective speed. The target speed is observable through this model because it impacts the effective speed via:

$$V^2 = V_r^2 + (V_e + V_a)^2\,, \tag{2}$$

where V_e is the aircraft speed, V_a is the projection of the target velocity anti-parallel to the ground track, and V_r is the projection of the target velocity along the LOS. The individual velocity components V_a and V_r cannot be uniquely derived from V. This ambiguity is known as "the blind angle" [17], referring to the arctangent of the ratio of V_r and V_a. Frequency-based imaging methods that adjust a single speed parameter have been known for over a decade. It has been suggested that stereo imaging must be used in order to resolve the blind angle, and effectively, to determine the direction of target motion.

If the antenna radiation pattern is known, it provides additional information that can be used to resolve the blind angle ambiguity. It has been shown that full velocity estimation becomes possible by exploiting the antenna gain pattern as well as the phase history [6]. This is achieved by estimating the LOS component of the velocity and the component parallel to the ground track. This velocity decomposition is relative to the target position, hence simultaneous estimation of target position and velocity components must be carried out. However, the proposed algorithm is derived for point targets, it is rather complicated, and it has not proven to be robust enough for targets with structure, such as ships.

To summarize, it is possible to estimate the velocity of ground moving targets under some conditions and with limited accuracy. This is possible by exploiting directly [6], or indirectly [9], the phase and amplitude modulation of the target response (TR). The LOS speed is related to the time when the target is at the beam center. Therefore, estimates of the target position and target LOS speed are tightly coupled and the respective estimation errors are correlated and may be large. Full velocity estimation is not possible when there is any acceleration along the LOS, since LOS acceleration modulates the TR phase in the same way as the along track speed. In this case:

$$V^2 = V_r^2 + (V_e + V_a)^2 + R_c A_r \,, \tag{3}$$

where R_c is the target range and A_r is the LOS component of the target acceleration when the target is at the beam centre. All of this places strong limitations on the accuracy of velocity estimates achievable with a single aperture SAR. It is also true that blind angle resolution is not a necessary condition to achieve good image focus. However, the DC must be estimated accurately enough to prevent aliasing.

The CHASP algorithms [21] are designed to estimate two components of ship velocity, both of which are assumed constant, which means that they must use the phase history, as well as the amplitude modulation that is a consequence of the antenna gain pattern. The CHASP algorithms are model-free, since there are no useful models of ships that could be used in an analytical derivation. In the case of point targets, we would expect the CHASP algorithms to be sub-optimal, but we do expect them to perform robustly under a variety of conditions.

The principle CHASP algorithms are:

- Ghost (i.e., azimuth ambiguity) minimization for DC and V_r estimation;
- Frequency tracking for V_a and DR estimation, ambiguity resolution, and DC and V_r correction;

- Inter-look cross-correlation (sometimes referred to as the map-drift algorithm) for V_a and DR estimation; and
- Contrast maximization for V_a and DR estimation, ambiguity resolution, and DC and V_r correction.

In this sub-section, we quantify the performance of the implemented CHASP algorithms. We also try to explain what disturbs these algorithms and the conditions under which we can expect to achieve reliable results.

The CHASP estimation algorithms were further analysed by simulation and by comparison with the theoretical limits for the estimation error variance, known as the Cramer-Rao lower bound (CRB). An unbiased estimator that achieves the CRB does not always exist, but if one does exist, it corresponds to the maximum-likelihood estimator.

Figure 2 shows the CRB and the measured standard deviation (SD) of the tracking algorithm for a simulated moving point target for various signal-to-clutter and noise ratios (SCNRs). Note that the CHASP algorithms are not derived according to a maximum-likelihood methodology, but we shall see that their performance is similar.

In these comparisons, the CRB is computed for simultaneous estimation of the signal amplitude, phase, along-track speed, cross-track speed, and azimuth position, by assuming, for simplicity, a raised Cosine-shaped antenna pattern with white additive noise. It is interesting to note that the CRB for the position estimation error is practically the same as that for the case of independent estimation of position only. This justifies our approach ofo estimating the target position in slow time, independent of other parameters. Another analytical result is that the cross-track estimation error is strongly coupled to the position estimation error.

In Figure 2, the SCNR is defined as the ratio of the maximum target amplitude in slow time and the SD of the additive noise. A mixture of white and coloured noise was simulated to represent both system noise and static clutter, as shaped by the antenna radiation pattern. The CHASP tracking results, in both white and coloured noise, are presented. In the case of coloured noise, there is an increase in the SD compared to the white noise case for the same SCNR.

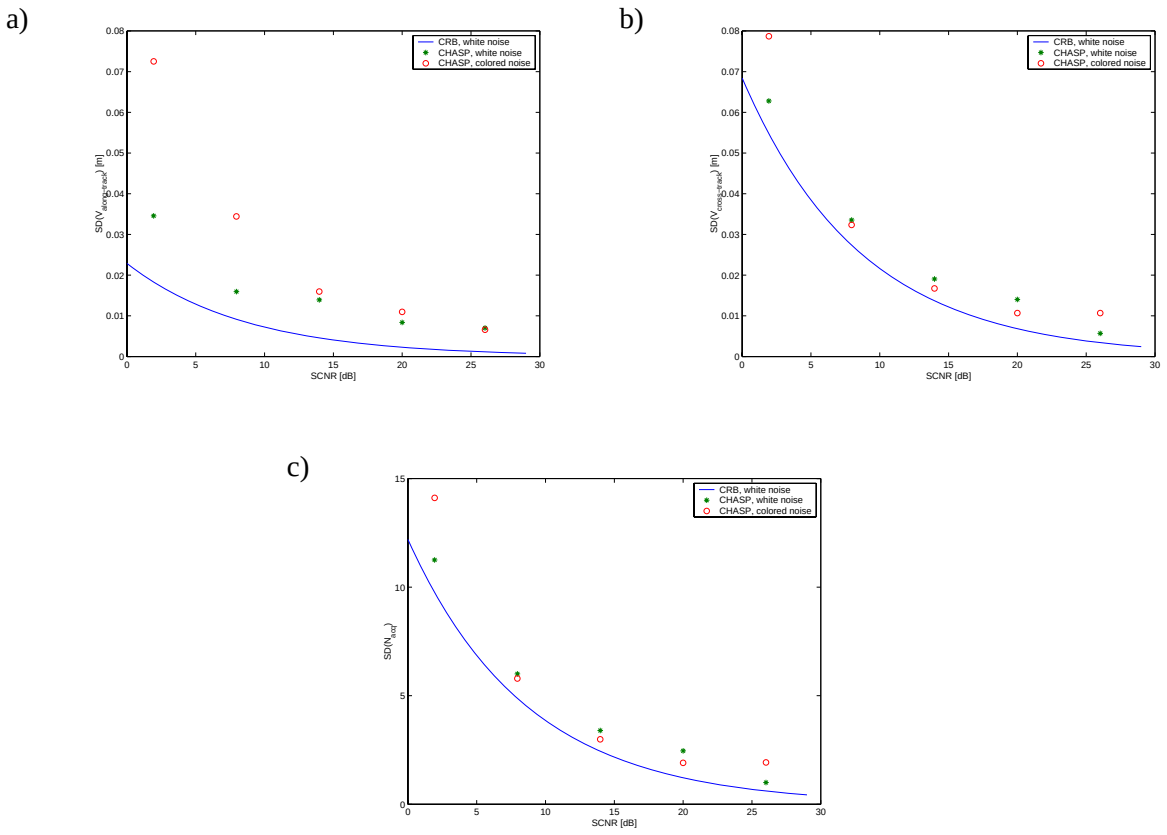

Figure 2: Standard deviation of: a) the along-track speed estimation error; b) the cross-track speed estimation error; and c) the along track position estimation error. The CRB was computed assuming simultaneous estimation of along and cross track speed, along track position, amplitude and phase of a moving point target in white additive noise. Experimental SD was found from 20 simulated cases, both for white noise and for a mixture of additive white noise and coloured clutter, processed by CHASP's tracking algorithms. CHASP was run iteratively to generate these results

Table 2 shows a comparison between three CHASP algorithms, namely the tracking, multi-look (map-drift), and contrast algorithms for the case of a more complex moving structure. In this table, $V_a = V_r / \sin\alpha$ is the cross-track speed, which is related to the LOS velocity component V_r via the incidence angle α, and "pos" refers to the azimuth position as a pulse index. The moving object was composed of 5 point targets in a "V-shaped" formation. All of the point targets are of equal radar cross section (RCS), but have random phases. Their interference deforms the target envelope in slow time and modulates the phase. This interference, rather than noise, is responsible for higher estimation errors than in the case of isolated point targets with the same SNCR. This example shows that LOS speed estimates are more affected than the along-track estimates. This is one of the effects that CHASP faces when working on ships, since ship structure results in signficant interference, especially at aspect angles close to 90° (i.e., broadside, for the ship oriented parallel to the ground track). This also means that the RCS estimated by sub-aperture processing may vary, even for slight variations of the ship's orientation.

Table 2: CHASP algorithm results for a simulated complex moving structure.

SD	Tracking	Multi-look	Contrast
V_r [m/s]	0.0283	0.0377	0.0029
V_a [m/s]	0.2646	0.7150	0.2422
pos	46		

Figure 3 illustrates the impact of non-uniform motion on the target phase history. Similar frequency tracking curves are often seen in CHASP ship processing. In the first case, the object, composed of 5 point targets, is moving parallel to the ground track at a cruising speed of 1 m/s. The slope of the frequency curve is proportional to the along track speed. In the second case, the same object, with the same cruising speed, is also slowly translating circularly about an axis parallel to the ground track. The radius of the circular movement was chosen to be 0.25 m, and the period was chosen to be 6.7 s, which is consistent with vessel movements due to sway or heave. The aperture time was 4.1 s. Surge movements can produce similar effects. It is clearly shown that such movements significantly disrupt the phase history and can overshadow the phase contribution from the cruising velocity of the ship. The slope of the frequency curve is mostly related to the variable LOS acceleration. It is demonstrated that focusing is possible, but velocity estimation is not. Table 3 shows velocity estimation results for two cases: first for linear uniform motion and second when circular motion is combined with linear uniform motion.

Table 3: CHASP velocity estimation results uniform/uniform with circular motion.

	Motion	Linear Uniform		Combined Linear and Circular	
Speed	true	estimate	nonlinearity	estimate	nonlinearity
V_r [m/s]	0	-0.0313		-0.3472	
V_a [m/s]	1	0.9480	0.0688	-4.9828	3.2808

a)

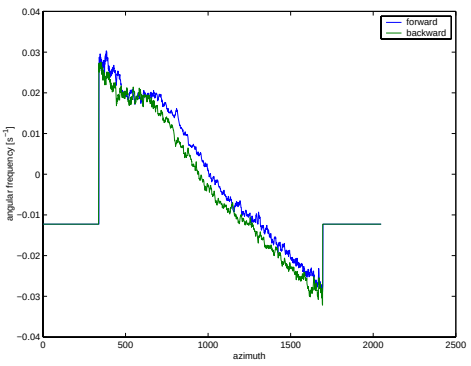

b)

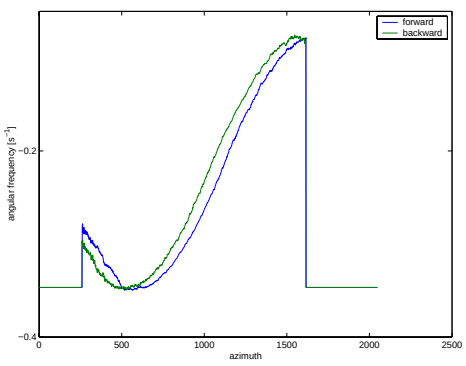

Figure 3: Illustration of the CHASP tracking algorithms for simulated moving object composed of five point targets in coloured noise with SCNR = 14 dB : a), Uniformly moving along track at 1 m/s; and b) Moving along track at 1 m/s with combined sway and heave circulation motion of 0.25 m amplitude with a period of 6.7 s.

Even though velocity estimation may be inaccurate or ambiguous, it may still be possible to improve the image resolution. CHASP is equipped with methods for higher order polynomial fitting of the TR phase history; these methods are used in conjunction with the tracking and multi-look methods. Evaluation of the higher order model is used to assess the nonlinearity of the frequency modulation. If the azimuth chirp turns out to be nonlinear, then it is not always straightforward to determine the proper order of the modulation. Because of this problem, a non-parametric phase correction, similar to motion compensation, is applied. Figure 4 illustrates the operation of this approach on a synthetic signal. Parts a) and b) of the figure show an image of a simulated object moving at uniform speed. It was first processed using the true constant DC and DR parameters, and then using the adaptive non-parametric method. Parts c) and d) of the figure show an image of the same object moving at the same cruising speed, but with additional circular motion perturbations imparted on the object. The data were first processed with the constant DC and DR parameters derived from the constant velocity case, and were then processed using the adaptive non-parametric method. The benefits of this method are made clear in Table 4, which shows the velocity metric computed for the four images. We see that the target contrast can be improved although velocity estimation failed. As expected, the estimates of target Total RCS and the ocean clutter (i.e., the normalized radar cross section, σ°) are essentially invariant.

Table 4: Impact of the CHASP parametric motion estimation algorithm.

	Linear Uniform		Combined Linear and Circular	
	DC & DR adjustment	non-parametric	DC & DR adjustment	non-parametric
Contrast	269.44	260.89	12.95	226.98
σ° [dB]	−16.65	−16.58	−16.60	−16.57
RCS [dB-m^2]	38.00	37.96	37.85	37.73

It can also be demonstrated that even much smaller target oscillations have a large impact on the accuracy of the along-track speed estimation. The effect is more pronounced when the sway and heave radii are larger and when the oscillation period is shorter, because the effect depends on the acceleration along the radar LOS.

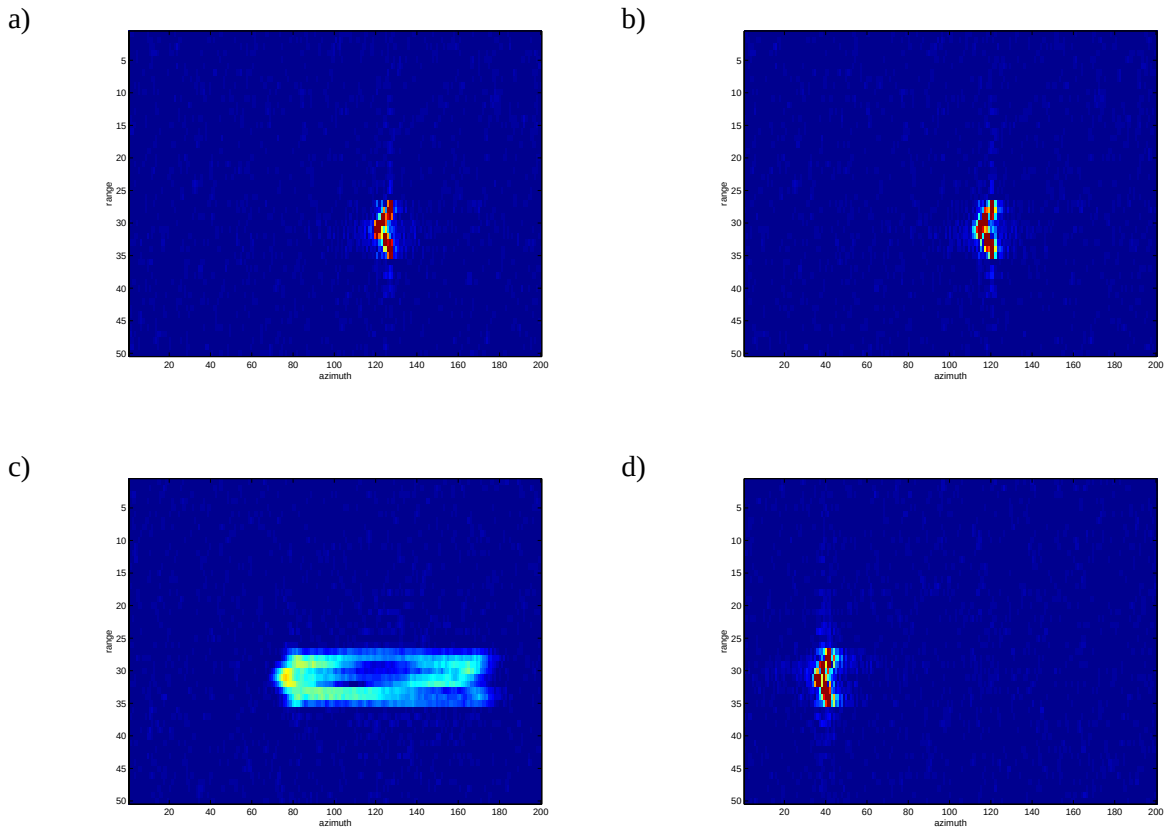

Figure 4: CHASP processed images of a moving object composed of five point targets in coloured noise with SCNR = 14 dB: a) Moving uniformly along track at 1 m/s and processed using the correct DC and DR parameters; b) Moving along track at 1 m/s and processed using adaptive non-parametric phase corrections based on Figure 3a; c) Moving along track at 1 m/s with a combined sway and heave of 0.25 m with a period of 6.7 s processed using the same DC and DR that was used for the uniformly moving target at the same along track speed; and d) the same object as c) but processed using adaptive non-parametric phase corrections based on Figure 3b. Warmer colours represent increasing intensity.

2.3.2 Adopted Processing Procedure

Following target detection, there is an automated CHASP-based procedure that works from the list of potential targets. The role of CHASP in this procedure is to georeference the target candidates, to provide time information for them, and to do preliminary coarse estimates of the RCS, σ°, and incidence angle. This module does not re-focus data; it only appends some basic attributes to the list of ship candidates. Time information can then be used to look up ground truth data, as described in the subsequent sub-section. The other information, especially the geographical coordinates and RCS, can be used for early identification of known ships and for

selection of target candidates for further processing. Final ship identification is done only after full CHASP processing.

CHASP processing is semi-automated. The analyst is guided by the software, but there are interactive parts, which give an opportunity to the analyst to override the automatic settings or decisions. There are two programs that streamline CHASP processing and serve as an interface. The first one is called "wrap", and the second one is called "view123" (see Figure 1).

The first step is to choose a suitable chip of signal data associated with a detected ship candidate. Signal (acquisition) coordinates of a ship do not necessarily coincide with the image (detection) coordinates. The analyst can modify the chip coordinates interactively while viewing the ship signature in slow time (uncompressed). Ideally, the chip is centered on a single ship signature. There are cases when this is not strictly possible because of other nearby ships or land, which makes the subsequent analysis more complicated.

The second step is to choose a suitable DC offset for processing. Once chosen, it is not modified during the analysis, though correction terms may be estimated. The theoretical analysis shows that the estimation of the along-track speed is not very sensitive to the DC setting or, in other words, the LOS speed and the along-track speed errors are weakly coupled. The main objective of this step is to select a DC value such that the major part of the ship energy is used in processing and to avoid aliasing. This is routinely achieved by ghost minimization, since ghosts (i.e., azimuth ambiguities) are caused by aliasing. The software varies the value of DC, generates an image, and then measures the ratio between the ghost power and the main ship image power. At the same time, the images and the power profile plots are presented to the analyst, who can visually check that the ghosts are symmetric or completely absent. The analyst can optionally override the automatic selection of the optimum DC. Since high DC precision is not necessary and not even possible, the resolution of the DC selection is 0.05 in terms of the pulse repetition frequency (PRF). The search interval for DC is from −0.5 to +0.5 of the PRF, and the PRF ambiguity is resolved by further iterations.

The balance of the CHASP analysis has two goals. The first goal is to determine the ambiguity number. The second goal is to estimate the along-track speed of the ship. Also, possible DC corrections are estimated in the process. The ambiguity number is resolved by testing three hypotheses for ambiguity values of −1, 0, and +1 relative to the DC value obtained by ghost minimization. Higher ambiguity numbers are not expected for ships acquired by EC CV-580 SAR. Three auto-focusing algorithms are then run for each hypothesis and the results are compared at the end. The three algorithms are: tracking, multi-look, and contrast enhancement.

The tracking algorithm is applied first. Its outputs include target position in slow (acquisition) time, residual frequency modulation, residual range migration curve, and an estimate of the target-to-clutter ratio. The estimated target position in slow time, in relationship to the target image position, is used for DC and LOS speed corrections. The residual frequency modulation is used for phase history modeling and for estimation of the along-track speed. The residual range migration curve is used for selecting the correct ambiguity number. The estimated target to clutter ratio is a good indicator of target detectability in the individual polarimetric channels. Typically, ships with a significant along-track speed have a linear residual frequency modulation and the slope is proportional to the along-track speed. Often, residual frequency modulation

follows a pseudo-periodic pattern. This is especially the case for slow-moving small vessels. As was shown, even a small amount of sway, heave, or surge can cause such patterns.

The multi-look algorithm is applied next. Five pairs of azimuth looks are created and mutually correlated to estimate relative look displacement. If a ship is really moving at a constant along-track speed and with no LOS acceleration, all look pairs should reveal the same displacement, which is proportional to the along-track speed. In this case the correlation peaks should be aligned. This is often the case for ships moving at a significant constant along-track speed, especially for large ships. Vessels subjected to sway, heave or surge do not have this feature. In this latter case, the output of the multi-look algorithm is a set of inter-look displacements and the magnitude of the cross-look correlation peaks. The displacements are used for estimating the along-track speed and its linearity. The magnitude of the correlation peaks is used for selecting between the three ambiguity hypotheses. Additionally, the integrated target response for each look is computed and can be used to verify the DC value.

The tracking algorithm and the multi-look algorithm each provide an estimate of the along-track speed and an associated error bound, which is based on higher order modeling. Each of these values is used to set an interval of along-track speeds to be tested by the contrast algorithm. CHASP is run for equally-spaced speed adjustments from this interval and the contrast is evaluated for each of the images. The value of the speed adjustment corresponding to the highest contrast is recorded. Another metric for image focusing is entropy, which is also computed. The speed adjustment corresponding to the minimum entropy is recorded.

At the end of this procedure, the scores for the three hypotheses are evaluated. Scores are composite and take into account: slope of the residual range migration as estimated by the tracking algorithm, magnitude of the inter-look correlation as estimated by the multi-look algorithm, target contrast, and entropy. The final along-track speed estimate depends on all three algorithms. If residual frequency modulation of the tracking algorithm is roughly linear, then this algorithm is given a higher weight. If multi-look displacement is consistent, then this algorithm is favoured. If neither of these algorithms offers these expected features, then the results of the contrast algorithm are used.

In this way the optimal processing parameters DC and DR are determined for image focusing. The corresponding velocity estimates are also made available.

Finally, there is a procedure to choose the appropriate strategy for focusing. This procedure is interactive and semi-automated. The analyst can select between three images for the analyzed chip. The first image is produced with nominal parameters and is the same as the COASP image of the target. The second image is the image produced using the optimized DC and DR parameters. The third image is the image formed by the non-parametric motion compensation using the phase history extracted by the tracking algorithm. For each option, the software computes the contrast and the entropy as objective criteria for choosing the most successful processing strategy. The final choice, however, is made by the analyst.

This whole procedure may take up to 30 minutes to complete since all of the steps are supervised by an image analyst. CHASP execution itself is fully automated and very fast. Automatically derived results are written to header files and logged automatically, but they are also displayed, monitored and reviewed by the analyst interactively. In this way, we are developing a level of

confidence in the various algorithms. A fast and fully operational processing procedure for EC CV-580 SAR refocusing will not be pursued until confidence in the level of performance is deemed to be acceptable.

Several fully automated processing chains based on CHASP, have been implemented as needed to facilitate systematic processing. Examples include: georeferencing of detected target candidates (presented in several tables in Section 3), processing of simulated data by the same algorithm (as shown in Figure 2), and processing a list of RADARSAT-1 ships using the same algorithms (as discussed in Annex E).

2.3.3 Relevance of CHASP Products to RADARSAT-2

The processing of RADARSAT-1 data using CHASP is discussed in detail in Annex E. CHASP-processed EC CV-580 SAR images of ships are expected to be much closer to RADARSAT-2 images of the same ship than the corresponding COASP-processed EC CV-580 SAR images, although the differences in image resolution and noise floor remain the same. Due to the higher PRF of RADARSAT-2 acquisitions, relative DC variations of ships in RADARSAT-2 data will not be significant and ambiguities are less likely. A similar condition is achieved by CHASP processing of EC CV-580 SAR data because the DC is adjusted to the estimated DC of the ship. On the other hand, the along-track speed of the ship will always be relatively insignificant compared to the RADARSAT-2 ground speed. This condition is not met by the CV-580 SAR due to its considerably lower speed, but effectively, this is achieved through CHASP processing.

Some differences still remain between CHASP and RADARSAT-2 products, but some of these can be mitigated by starting from a CHASP-processed image. For example, modification (i.e., degradation) of the resolution and the signal-to-noise ratio can be done relatively easily starting from a CHASP product. Furthermore, CHASP allows use of sub-aperture processing, if so desired. Some cases could force the use of this technique, especially when a ship is moving non-uniformly during synthetic aperture formation. Finally, it is possible to reduce the aperture (i.e., the bandwidth processed) to study the case of a lower azimuth resolution.

2.4 Validation Data

The ship validation task encompassed the following requirements:

- Provide location, course, and speed for *Atlantic Concert*, *Toronto*, and *Dominion Victory* on 20 Oct. 2005 (Rendezvous event 3) for each of the CV-580 pass times;
- Provide location, course, and speed of nearby and player vessels in Chedabucto Bay on 17/18 Oct 2005 (Transfer event 2) and 24 Oct. 2005 (Transfer event 3) for each of the CV-580 pass times;
- Incorporate as many sensor detections as possible from the MARSIE dataset by using the available ground truth contact data (i.e., various AIS and GPS sources) as a means of identifying the extrapolated or interpolated lat/long values for the ship tracks; and
- Use the Common Operating Environment (COE) for the data analysis.

A number of data sources were used to compile the validation data for the ships of interest, including:

- Raw AIS Vessel Management System (AVMS) data (it was discovered that the OTH messages that were received through the Canadian Maritime Network were not correct since the time tags for the detections had not been set properly);
- GPS data recorded on certain vessels;
- AIS data recorded onboard the EC CV-580 (see Annex A); and
- AIS data recorded at Canso lighthouse.

The COE is an environment for sharing data between applications and systems with an architecture approach for building interoperable systems (see https://coe.mont.disa.mil). The Canadian Navy has adopted this system in its daily operations to meet its need for a common operating environment and to ensure interoperability with the US Navy. Operators in the Joint Information Operations Centre (JIOC) use this system on a routine basis for maintaining the Recognized Maritime Picture (RMP).

In this project, the COE was used to analyze previously-recorded vessel track data in order to identify the locations of ships of interest at specific instants of time. This information was used as ground truth for validation of EC CV-580 SAR polarimetric signatures.

The validation data were prepared using the following steps.

1. Combine vessel messages from available sources including:

    a. CV-580 AIS data consisting of separate log files in the ShipPlotter (a specific AIS reception and display software) format for each of the four flight dates. Each file was converted into OTH messages that could be read by COE;

    b. AVMS messages from ships outfitted with AVMS packages including *Dominion Victory*, *Toronto*, *E. Cornwallis*, *Atlantic Beech*, *Ambassador*, and *Eagle Boston*. The data were recorded in the ShipPlotter file format. Each file was converted into OTH messages that could be read by COE;

    c. GPS data recorded onboard ships including *Dominion Victory*, *Toronto*, *Cajun Spirit*, *Preventer*, *J. Franklin Wright*, and *Strait Signet*. The GPS data were recorded in Fugawi (a specific GPS processing software) format and were converted to ASCII format and then to OTH messages that could be read by COE;

    d. AIS data recorded at Canso lighthouse from 16 to 19 Oct. 2005. The data were recorded in the ShipPlotter file format. Each file was converted into OTH messages that could be read by COE.

2. Partition the data by date of interest, specifically, 17, 18, 20 and 24 Oct. 2005.
3. The program REPEAT (Repeat Performance Evaluation and Analysis Tool) was used to read the OTH messages into COE. In a batch process, the messages were sent to COE, which populated the COE Track Management Server Database with ship tracks.

4. Once all tracks were in the system for a specific date (Figure 5), they were highlighted and a function called GeoSit within COE was used to dead reckon the tracks to the specified time (Figure 6), providing the ship location at that time based upon interpolation or extrapolation.
5. The player vessels were located on the COE chart display (Figure 7).
6. The zoom tool within COE was used to inspect the ship track of interest. Examples are shown in Figure 8 and Figure 9.
7. The following ship track attributes were recorded in an Excel spreadsheet for the ship track of interest:
   - date/time;
   - ship name;
   - latitude;
   - longitude;
   - speed (knots);
   - course;
   - the time over which the track was dead-reckoned in determining the lat/long coordinates (this is an important parameter since the higher this value, the higher the probability that the ship may have changed course or speed, rendering the dead reckoning process invalid);
   - comments that might be of interest that are provided in the dataset, such as a ship is moored or anchored; and
   - the source of the closest contact that was dead-reckoned.
8. All validation data were saved in an Excel spreadsheet that was made available for validation purposes.

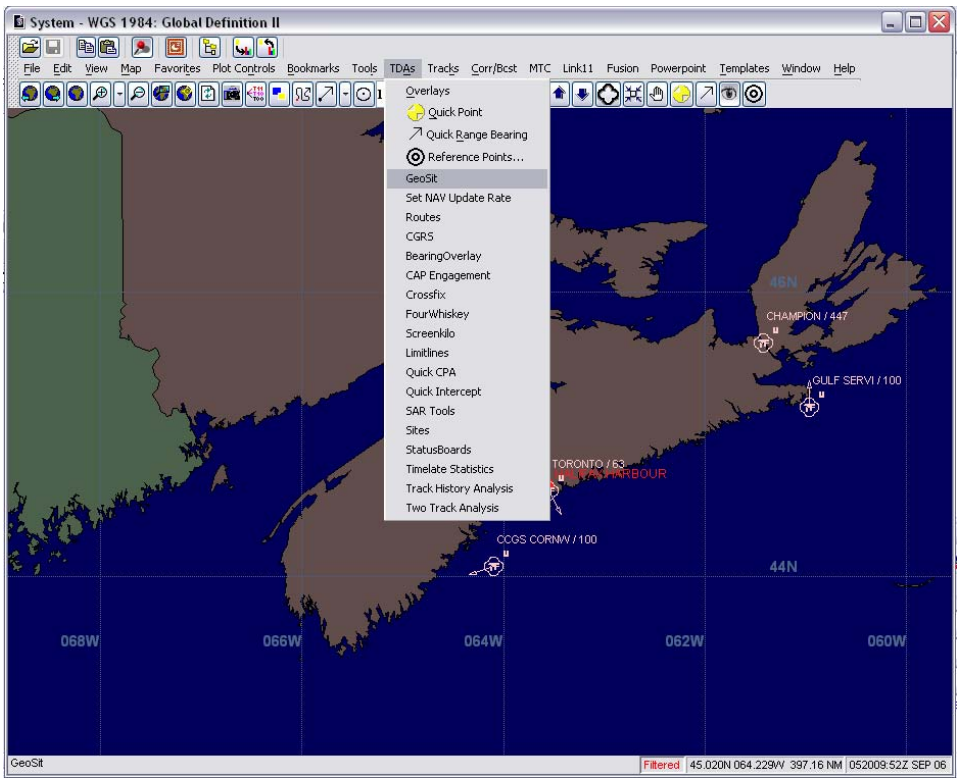

Figure 5: COE – Selecting tracks for GeoSit.

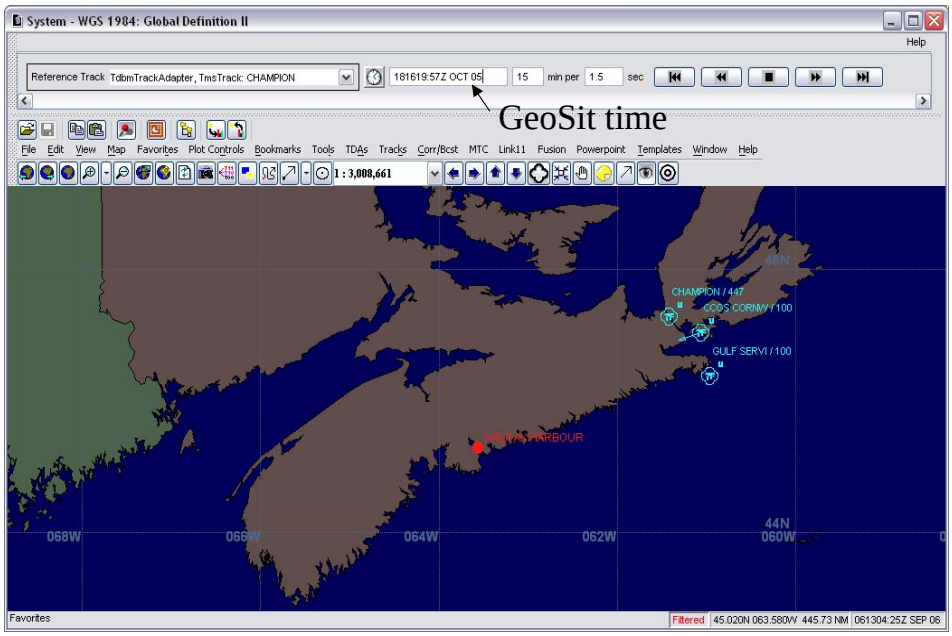

Figure 6: COE – Setting the GeoSit time.

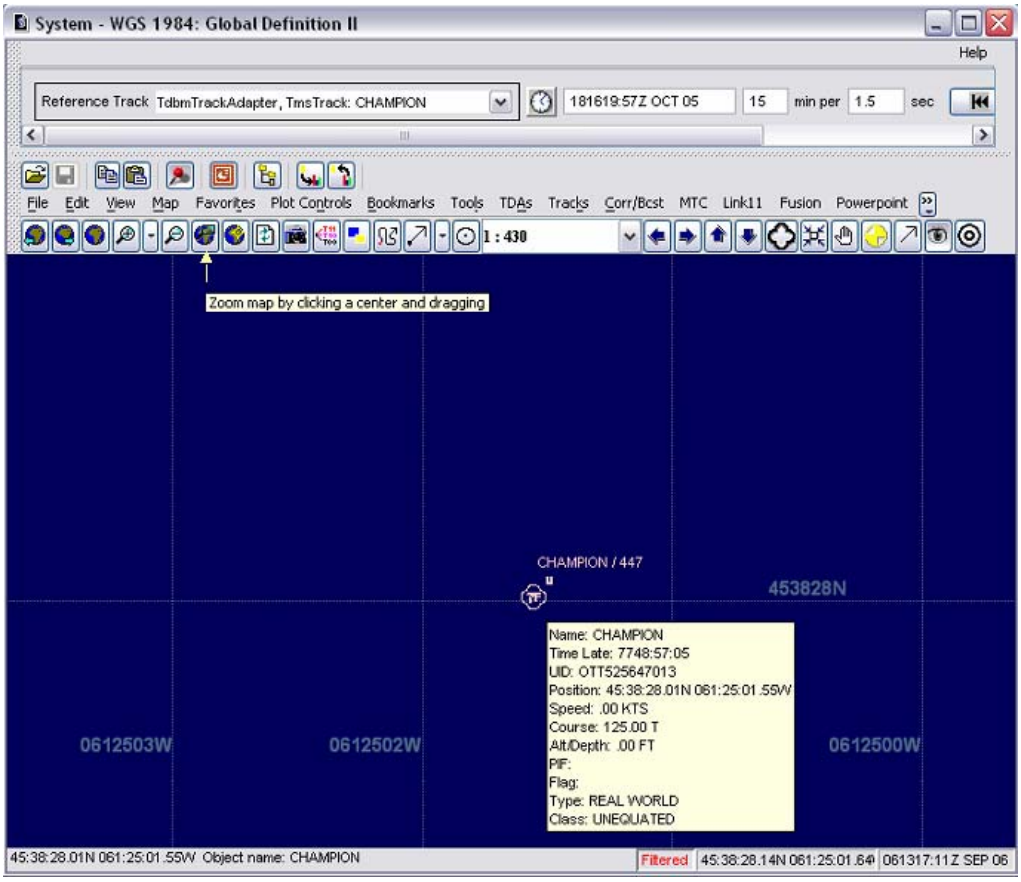

Figure 7: COE – Locate player vessel.

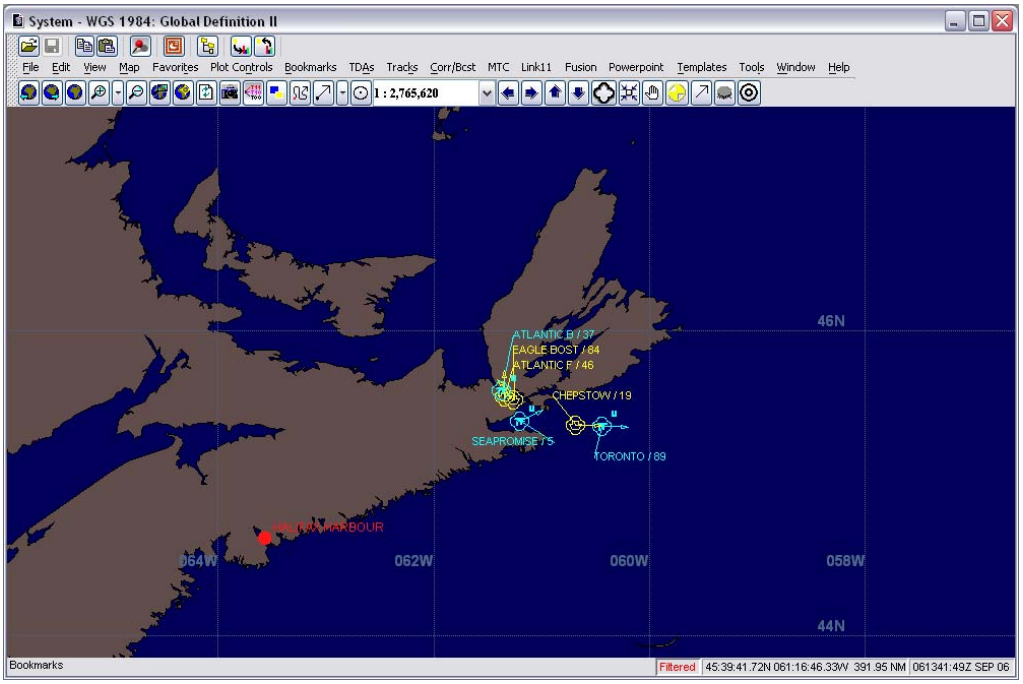

Figure 8: COE – Chedabucto Bay, 18 Oct. 2005.

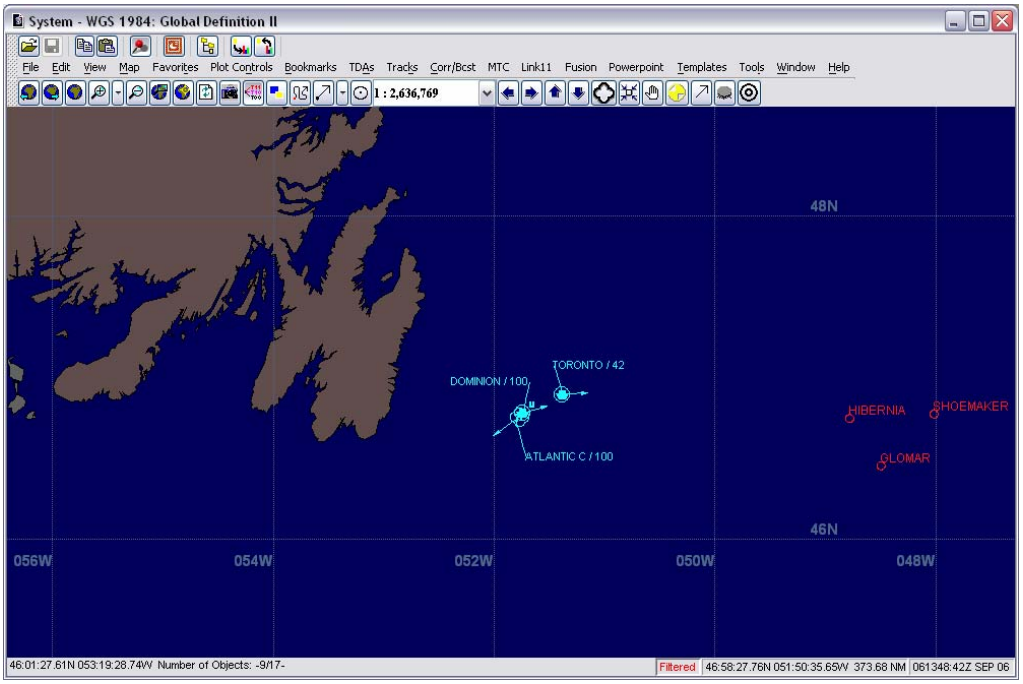

Figure 9: COE – Grand Banks, 20 Oct. 2005.

2.5 Polarimetric Analysis

The polarimetric SAR (PolSAR) data analysis includes ship detection and target classification assessment. For ship detection, we studied the detection performance of various PolSAR systems and estimated the receiver operating characteristic (ROC). The performance of three PolSAR system configurations was compared: polarimetric, dual co-polarization (i.e., HH and VV) with relative phase, and single polarization HH.

For target classification, four polarimetric decomposition methods were used: Pauli, Cameron, symmetric scattering characterization method (SSCM), and an entropy based classification method, H/α. The software for the Pauli and the Cameron methods were developed at DRDC Ottawa, while the SSCM and H/α methods were implemented in a PolSAR workstation that was developed at the Canada Centre for Remote Sensing and was made available to DRDC Ottawa by the Canadian Space Agency.

2.5.1 ROC

The receiver operating characteristic is plotted as the probability of missed detection (P_{MD}) versus probability of false alarm (P_{FA}). Measured data processed by COASP was used to calculate these probabilities using a well-known statistics-based methodology based upon likelihood ratio tests with the Neyman-Pearson criterion [12].

A polarimetric SAR system provides observations of the scattering matrix $\mathbf{X}(i, j)$ for each pixel (i, j) in the image. The matrix components S_{HH}, S_{HV}, S_{VH}, and S_{VV} are complex valued elements obtained from the amplitude and phase of the four channels in the polarimetric data, the possibilities being horizontal (H) or vertical (V) polarization for transmit and receive. The components of $\mathbf{X}(i, j)$ can be written as a vector:

$$\mathbf{X}(i, j) = \left[S_{HH}(i, j)\ S_{HV}(i, j)\ S_{VH}(i, j)\ S_{VV}(i, j) \right]^T \tag{4}$$

where the superscript T is the transpose operator.

Ship detection is a binary decision problem. The fundamental algorithms of polarimetric SAR ship detection are that statistical decision theory is applied directly to the components of the scattering matrix to obtain a decision variable. A likelihood ratio test with the Neyman-Pearson criterion is used to define a pixel-based detection criterion. The Gaussian distributions for the scattering matrix components are assumed to derive an approximate decision variable while the measured data were used to calculate the detection variables.

Following [12], the decision variable is approximately given by:

$$\mathbf{X}^H (C_o^{-1})\mathbf{X} = \begin{cases} > \eta & \text{for a ship} \\ \\ \leq \eta & \text{for ocean} \end{cases} \tag{5}$$

where C_o is the covariance matrix of ocean and *H* is the Hermitian transpose operator.

For a polarimetric system, $\mathbf{X}$ is given by equation (4); for a dual co-polarization system (i.e., HH and VV with both amplitude and phase), $\mathbf{X}$ is given by:

$$\mathbf{X}(i, j) = [S_{HH}(i, j) \quad S_{VV}(i, j)]^T \tag{6}$$

For a single polarization system, the decision variable is given simply by the amplitude as:

$$|X|^2 \left(\frac{1}{\sigma_o^2} \right) = \begin{cases} > \eta & \text{for a ship} \\ \\ \leq \eta & \text{for ocean} \end{cases} \tag{7}$$

From these algorithms, we see that a polarimetric system contains both amplitude and phase information from four channels. As such, more information is available so such a system is expected to provide the best detection performance compared to systems with fewer channels. A dual co-polarization system with amplitude and phase contains information from two channels, so it provides better detection performance than a single channel which contains only amplitude information.

For this study, there are two issues to be addressed with regard to the probability of false alarm. The first is whether or not the ROC can be computed from the measured data to a certain probability of false alarm, for example $P_{FA} = 10^{-9}$. The second is whether or not the detection algorithm can achieve this probability of false alarm in operation.

The algorithms for calculation of the ROC can be applied to any designed probability of false alarm, provided there are enough ocean samples available. The algorithms are independent of the environmental conditions; in principle they can be applied to any sea state condition, for example Sea State 5, if supporting data are available.

The ROC provides the probability of missed detection (P_{MD}) versus the probability of false alarm (P_{FA}). Measured data is used to calculate these probabilities as the detection threshold η is varied.

The accuracy of the estimated values of P_{MD} and P_{FA} may be determined from the number of missed detection and false alarm events. Let N_s be the number of ship samples, N_o be the number of ocean samples, P'_{MD} be the true probability of missed detection, and P'_{FA} be the true probability of false alarm. Assuming that both the ship and ocean samples are independent, then the number of missed detection events counted and the number of false alarm events counted during the estimation procedure follow binomial distributions. Therefore, the average number of missed detection events is $N_s P'_{MD}$ and the standard deviation is $\sqrt{N_s P'_{MD}(1 - P'_{MD})}$. Similarly, the average number of false alarms is $N_o P'_{FA}$ and the standard deviation is $\sqrt{N_o P'_{FA}(1 - P'_{FA})}$.

Usually, $P'_{MD} \ll 1$ and $P'_{FA} \ll 1$, so the standard deviations are approximately $\sqrt{N_s P'_{MD}}$ and $\sqrt{N_o P'_{FA}}$.

For a $P_{FA} = 10^{-9}$, to obtain an error of about 30% in the estimate of P_{FA}, roughly 10^{10} independent ocean samples, acquired at nominally the same acquisition geometry (i.e., incidence angle) and under the same environmental conditions, are required; to obtain an error of about 10%, roughly 10^{11} independent ocean samples are required. Since these numbers are rather large, especially consider the rate of change of incidence angle for airborne SAR geometry, $P_{FA} = 10^{-5}$ was used to estimate the relative performance. In general, 2×10^6 ocean samples are used, giving an error bar of about 22% at this P_{FA}.

Several steps are required for target detection. In the present work, we set $P_{FA} = 10^{-5}$ in considerations of:

- Obtaining a lower P_{MD}; and
- Constraining the estimation accuracy due to the limited number of available samples.

There is a trade-off between P_{FA} and P_{MD}. In general, the lower P_{FA} is set for detection, the higher P_{MD} becomes. To obtain a lower P_{FA} with a low P_{MD}, a combination of pixel detection with other algorithms must be employed. Following pixel-based detection, other algorithms such as target clustering, sub-aperture coherence analysis, or polarimetric signature analysis may be applied to achieve a lower P_{FA} with a low P_{MD}. For clustering, the detected pixels must be grouped and a decision made as to whether or not there are sufficient pixels in the group to represent a target. Such a procedure will improve P_{FA} and P_{MD}, but at the cost of increasing the minimum size of target that can be detected.

In previous studies (see Annex F), ROC analysis has been applied to various types of ships (lengths from 18.3 m to 135 m), in wind speeds up to 35 knots, and in wave heights up to 4 m. For all of the cases studied, polarimetric systems always provide the best detection compared to other systems with fewer channels, especially, for the detection of small ships.

2.5.2 Pauli

The Pauli method permits the extraction of physical information from a 2 by 2 coherent scattering matrix **X** that includes the four possible linear polarization scattering components S_{HH}, S_{HV}, S_{VH}, and S_{VV}. Under the reciprocity assumption (i.e., that the HV and VH channels are identical), the Pauli vector is described by three components of the scattering matrix [4]. The $(S_{HH} + S_{VV})$ component tends to be large for single or odd bounce scattering; the $(S_{HH} - S_{VV})$ component tends to be large for double or even bounce scattering; and the $(S_{HV} + S_{VH})$ component represents volume scattering.

2.5.3 Cameron

In the Cameron method, the measured scattering matrix is decomposed into one of six types of elementary scatterers. These symmetric scattering components include trihedral, diplane, dipole, cylinder, narrow diplane, and quarter-wave devices [1].

2.5.4 SSCM

The symmetric scattering characterization method (SSCM) is an alternate approach to exploiting the information from the largest coherent symmetric scattering components [18] and appears to have some value for ship classification [19]. These scattering components are as defined in the Cameron method. However, the symmetric scattering vectors are represented in terms of the latitude 2ψ and longitude 2χ on the surface of the target Poincaré unit sphere. The elemental scatterer coordinates on the Poincaré sphere are summarized in Table 5.

Table 5: Elemental scatterer coordinates on the Poincaré sphere.

scattering	trihedral	dihedral	dipole	cylinder	narrow diplane	¼-wave
(ψ, χ)	(0°, 0°)	(90°, 0°)	(45°, 0°)	(18.43°, 0°)	(81.88°, 0°)	(0°, 45°)

Based upon the symmetric scatterer centres on the Poincaré sphere [18], the six types of symmetric scatterers can be generated by using the thresholds shown in Table 6. For example, a symmetric scatterer is classified as a trihedral scatterer if its Poincaré sphere longitude angle ψ is between 0° and 9.22°, and its Poincaré sphere latitude angle χ is between −10° to 10°.

Table 6: SSCM thresholds.

Symmetric Scatterer	ψ [deg]		χ [deg]
trihedral	0 to 9.22	and	−10 to 10
cylinder	9.22 to 31.72		
dipole	31.72 to 63.44		
narrow diplane	63.44 to 85.94		
dihedral	85.94 to 90		
¼-wave	0 to 90	and	<−10 or >10

2.5.5 *H*/α

The H/α method is an entropy-based classification scheme which is based on an Eigen value analysis of the coherency matrix, and uses a statistical model to estimate the average target scattering parameters from the measured data [5]. The scattering entropy H is a key parameter to measure the randomness of the scattering mechanism, while the α angle characterizes the scattering mechanism. The H and α plane is divided into 9 distinct zones, as illustrated in Figure 10; the interpretation of the physical scattering characteristics of each of the nine zones is summarized in Table 7.

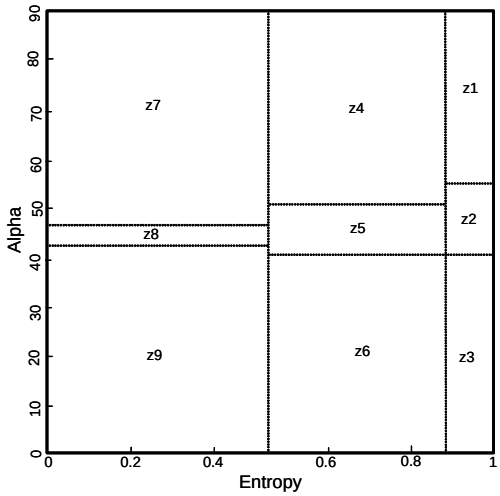

Figure 10: Distinct zones in the H/α plane.

Table 7: Physical scattering characteristics of the nine H/α analysis zones.

Zone	Physical Scattering Characteristics
1	High entropy multiple scattering
2	High entropy scattering
3	Not a feasible region (not used)
4	Medium entropy multiple scattering
5	Medium entropy scattering
6	Medium entropy surface scattering
7	Low entropy multiple scattering
8	Low entropy dipole scattering
9	Low entropy surface scattering

3. Analysis Results

While the hope had been to systematically process the polarimetric signature of all known targets in the MARSIE data set, this goal had to be scaled back due to the enormity of the undertaking and the requirement to report results to the Polar Epsilon Project within a useful timeframe. As such, the data analysis activity was scoped-down to focus primarily on the ship *Dominion Victory* (Figure 29), a multi-purpose diving support vessel of 25 m length that was hired to play the role of the fishing trawler in the MARSIE MIS. Representative results have been drawn from the available flight dates. Other vessels have also been considered; some were trial participants and some were vessels of opportunity. The vessels that were present and imaged on each date, including links to additional information concerning the known vessels, are available in Annex A. Airborne photographs of some of the participating vessels are contained in Annex B.

Of course, in the process of carrying out the analysis, certain problems with the data were uncovered, not all of which could be dealt with in the timeframe available to complete the analysis. It is anticipated that further results will come out of other MARSIE data sets. This analysis section could be augmented if warranted.

The analysis results have been organized as follows. We first consider the availability of validation data for the CHASP-processed imagery. From these, we proceed, on a case study basis, to estimate the Total RCS of some known vessels. These results are thought to be unique since the RCS is available for all four linear transmit/receive polarizations. We then derive ROCs for the *Dominion Victory* for the open ocean images of 20 Oct. 2006. Finally, polarimetric decompositions are considered for the *Dominion Victory* and for several other vessels in a Chedabucto Bay data set.

3.1 CHASP Results and Comparisons with Validation Data

Open ocean passes l41p1, l41p2, l41p3 and l42p4 acquired on 20 Oct. 2005 have only three or fewer ships and it was straightforward to find them and identify them, since ground truth data are available for each. *Dominion Victory* was identified in four passes. On this date, a waverider buoy was deployed from *Dominion Victory* in the vicinity of the Rendezvous point, and indicated a wave field with a 2.3 metre significant wave height and a 9.3 second significant wave period, corresponding roughly to Sea State 4. The buoy was recovered prior to completion of the CV-580 flight program since a gale warning was in effect and haste was necessary for the vessel to safely reach St. John's harbour following the Rendezvous event activities. Wind observations are not available for this event.

Passes over Chedabucto Bay had many ships and smaller vessels, some of them in close proximity of each other or land. Chedabucto Bay is rather sheltered; the sea state was rather calm during each of the CV-580 flight programs. Based upon shored-based met station measurements made at Janvrin Point, the measured wind speed was roughly 14, 9, and 3 knots at the start of the flight programs on 17, 18, and 24 Oct. 2005, respectively.

Preliminary detection was done for all Chedabucto Bay passes creating lists of target candidates given by image coordinates. All of these lists were run through a CHASP-based fully automated

processing module which associates geographical coordinates and acquisition time with each target candidate. Besides geo-referencing, this module also computes a preliminary estimate of the Total RCS, σ°, and the incidence angle at the target position. It also checks the geographic location of each target against a coarse land mask database. Table 8 provides the target candidate list for 17 Oct. 2005, l22p2 (a342). This list includes all vessels in the Chedabucto Bay region of interest (ROI) with all information available after detection and after geo-referencing. "Ocean" is a flag that is set by the land-masking operation and is "0" for land and "1" for ocean.

Table 8: Candidate targets for 17 Oct. 2005, l22p2 (a342).

#	Azimuth [pixel]	Range [pixel]	Latitude [deg]	Longitude [deg]	Time [hh:mm:ss.s]	RCS [dB-m^2]	σ° [dB]	sin(inc)	Ocean
1	7703	292	45.502690	-61.212244	13:09:36.63552	18.132580	-22.278009	0.690336	1
2	8026	375	45.506545	-61.215290	13:09:37.59550	34.356945	-23.586973	0.715683	1
3	9110	291	45.506460	-61.206746	13:09:40.81255	27.204214	-22.274660	0.690013	1
4	9326	368	45.509813	-61.209915	13:09:41.45261	47.045170	-24.433859	0.713703	1
5	10183	350	45.511518	-61.205639	13:09:43.99212	24.839727	-23.177179	0.708439	1
6	12544	776	45.532203	-61.216786	13:09:50.98833	33.200798	-29.114510	0.801196	1
7	12705	835	45.534494	-61.218815	13:09:51.46542	33.227711	-29.889580	0.810281	1
8	12986	515	45.524843	-61.202928	13:09:52.29809	13.741380	-25.724087	0.751147	0
9	7722	950	45.524645	-61.243130	13:09:36.69199	5.719216	-33.312965	0.826394	1
10	9417	990	45.530406	-61.238404	13:09:41.72227	15.379671	-32.186028	0.831462	1
11	5107	1329	45.528859	-61.269590	13:09:28.92004	7.401902	-34.805408	0.866579	1
12	8774	1438	45.542045	-61.259803	13:09:39.81690	13.004142	-33.278973	0.875369	1
13	8747	1509	45.544029	-61.262835	13:09:39.73689	16.744814	-33.659096	0.880687	1
14	8245	1356	45.538169	-61.258512	13:09:38.24638	26.308144	-33.980373	0.868758	1
15	11069	1442	45.548366	-61.251094	13:09:46.61755	8.641609	-33.474102	0.875655	1
16	10254	1352	45.543578	-61.250452	13:09:44.20250	36.674061	-33.605145	0.868428	1
17	13082	1441	45.553779	-61.243246	13:09:52.58256	41.180847	-33.570122	0.875474	1
18	4684	1836	45.542189	-61.292116	13:09:27.66285	18.782265	-32.138046	0.901309	1
19	5644	1978	45.548916	-61.293885	13:09:30.51604	26.863464	-31.335672	0.908538	1

Table 9 shows the CHASP processing status for 17 Oct. 2005, l22p2 (a342). Some of the ships appear as ambiguities in the COASP image due to their LOS speed. When they appear, both ambiguities are equally viable and there is nothing to distinguish between a ship and its ghost before the LOS speed becomes available. In spite of image ambiguities, it is clear that all of these ships are processed only once by CHASP, since raw data chip selection is based on azimuth uncompressed signatures, which are unambiguous.

Table 9: Status of CHASP processing for 17 Oct. 2005, l22p2 (a342).

#	Processed	Identified	Comment
1	Yes	*Gulf Service*	one of two ambiguities
2	Yes	No	ambiguous to target 4
3	Yes	*Gulf Service*	one of two ambiguities
4	Yes	No	ambiguous to target 2
5	Yes	No	
6	Yes	No	guess: *Preventer*
7	Yes	No	
8	No		too close to coast
9	No		
10	Yes	No	
11	No		
12	Yes	No	
13	Yes	No	
14	Yes	*E. Cornwallis*	one of two ambiguities
15	No		
16	Yes	*E. Cornwallis*	one of two ambiguities
17	Yes	*Toronto*	
18	No		
19	No		

Table 10 shows detection and geo-referencing results for 17 Oct. 2005, l23p3 (a343).

Table 10: Candidate targets for 17 Oct. 2005, l23p3 (a343).

#	Azimuth [pixel]	Range [pixel]	Latitude [deg]	Longitude [deg]	Time [hh:mm:ss.s]	RCS [dB-m^2]	$\sigma°$ [dB]	sin(inc)	Ocean
1	50384	287	45.550904	-61.220714	13:29:00.06635	45.583748	-17.795862	0.683946	1
2	254753	219	45.554503	-61.242406	13:29:14.09296	37.244328	-14.709577	0.659934	1
3	47224	1147	45.511142	-61.205086	13:28:49.92122	0.000000	-27.275620	0.846504	1
4	49674	599	45.535471	-61.217162	13:28:57.78690	33.764244	-22.610361	0.765768	1
5	49951	628	45.534112	-61.218507	13:28:58.67621	33.690285	-23.054100	0.771614	1
6	50522	662	45.532531	-61.221383	13:29:00.50940	13.433002	-22.587166	0.778186	1
7	53928	716	45.530017	-61.238274	13:29:11.44431	24.169855	-23.399485	0.788105	1
8	58822	430	45.543548	-61.262631	13:29:27.15642	17.136108	-18.776947	0.726747	1
9	57881	540	45.538207	-61.258000	13:29:24.13535	18.326778	-20.600925	0.753394	1

Table 11 shows detection and geo-referencing results for 17 Oct. 2005, l24p4 (a344). Several ships have been processed with CHASP including targets 3 and 4 identified as *Champion* (238 m), targets 8 and 10 identified as *Gulf Service* (42 m), and target 16 identified as *E. Cornwallis* (83 m).

Table 11: Candidate targets for 17 Oct. 2005, l24p4 (a344).

#	Azimuth [pixel]	Range [pixel]	Latitude [deg]	Longitude [deg]	Time [hh:mm:ss.s]	RCS [dB-m^2]	σ° [dB]	sin(inc)	Ocean
1	87403	623	45.533429	-60.957663	13:48:10.90611	38.836327	-22.833834	0.771041	1
2	77380	3638	45.412408	-61.012304	13:47:39.91612	20.701950	-19.407623	0.955080	1
3	73972	3631	45.412634	-61.030664	13:47:29.37821	59.536129	-18.602777	0.954983	1
4	70647	3633	45.412500	-61.048654	13:47:19.09694	20.711082	-19.272177	0.955038	1
5	69805	1769	45.484501	-61.053797	13:47:16.49339	0.000000	-25.547300	0.896298	1
6	61326	2377	45.460353	-61.101725	13:46:50.29730	16.073578	-24.905582	0.924291	1
7	59984	3340	45.423432	-61.110147	13:46:46.15103	24.092445	-21.006809	0.949865	1
8	57031	2776	45.445063	-61.129134	13:46:37.02003	23.313608	-23.513098	0.936881	1
9	56428	2654	45.449810	-61.133116	13:46:35.15219	32.560387	-24.059938	0.933392	1
10	54063	2775	45.445436	-61.148641	13:46:27.81542	28.641167	-23.718506	0.936856	1
11	53631	2664	45.449752	-61.150793	13:46:26.47479	36.584557	-24.285257	0.933701	1
12	50413	1941	45.478347	-61.167110	13:46:16.49350	14.520850	-25.053028	0.905786	1
13	42700	1759	45.486345	-61.208303	13:45:52.58712	15.355786	-25.792406	0.895921	1
14	40371	641	45.534054	-61.219614	13:45:45.38559	33.190189	-21.307447	0.775697	1
15	39885	295	45.551023	-61.221765	13:45:43.88283	42.102158	-17.533268	0.688357	1
16	35956	235	45.554442	-61.243021	13:45:31.76724	36.155922	-16.006256	0.667487	1
17	33144	561	45.538200	-61.258512	13:45:23.10573	27.619240	-20.520102	0.759289	1

Table 12 shows detection and geo-referencing results for 17 Oct. 2005, l26p6 (a345). As for other passes, this table only includes ships within the MARSIE trial ROI within Chedabucto Bay. Other targets outside of the ROI have also been considered on a case-by-case basis. For example, *Champion* (238 m) was processed by CHASP for the purpose of velocity validation.

Table 12: Candidate targets for 17 Oct. 2005, l26p6 (a345).

#	Azimuth [pixel]	Range [pixel]	Latitude [deg]	Longitude [deg]	Time [hh:mm:ss.s]	RCS [dB-m^2]	σ° [dB]	sin(inc)	Ocean
1	33600	843	45.486208	-61.204280	14:26:20.30718	0.000000	-25.100637	0.810260	1
2	30518	1383	45.474204	-61.171509	14:26:10.74810	12.818768	-27.553366	0.870027	1
3	31577	1494	45.478323	-61.165007	14:26:14.03231	19.454998	-28.077164	0.878684	1
4	40118	832	45.511487	-61.204936	14:26:40.52449	9.265054	-27.140400	0.808666	1
5	44958	340	45.530301	-61.238021	14:26:55.57316	21.616531	-24.259457	0.703456	1
6	45424	634	45.532114	-61.217708	14:26:57.02309	32.660027	-26.525108	0.774852	1
7	47028	86	45.538343	-61.257822	14:27:02.01147	0.000000	-17.989491	0.604974	1
8	47274	598	45.539293	-61.220099	14:27:02.77628	0.000000	-25.709154	0.767667	1
9	46686	673	45.537004	-61.215147	14:27:00.94736	19.515991	-27.242159	0.782203	1
10	48775	603	45.545078	-61.219751	14:27:07.43203	14.360510	-27.288847	0.768719	1
11	50215	597	45.550661	-61.220147	14:27:11.89857	39.849228	-26.875757	0.767496	1
12	50602	587	45.552157	-61.220816	14:27:13.09896	39.855118	-26.532286	0.765428	1
13	51178	291	45.554425	-61.241607	14:27:14.88558	38.376266	-22.959627	0.687946	1
14	50930	382	45.553448	-61.234975	14:27:14.11634	0.000000	-24.568712	0.715766	1
15	51001	460	45.553728	-61.229470	14:27:14.33656	16.536274	-25.464481	0.736518	1
16	62318	681	45.597581	-61.214485	14:27:49.51397	33.317467	-26.180887	0.783865	1
17	62191	837	45.597076	-61.204451	14:27:49.11882	32.204529	-30.813780	0.809550	1
18	53579	968	45.563680	-61.196337	14:27:22.33292	30.503305	-30.874060	0.827565	1
19	53680	998	45.564093	-61.194479	14:27:22.64619	0.000000	-25.257969	0.831322	1
20	54487	737	45.567197	-61.210919	14:27:25.14932	0.000000	-22.896936	0.793633	1
21	54628	804	45.567798	-61.206623	14:27:25.58713	29.493183	-31.432320	0.804485	1
22	54832	786	45.568526	-61.207770	14:27:26.22186	37.427917	-30.791607	0.801663	1
23	54828	861	45.568505	-61.203010	14:27:26.20942	33.991863	-24.067167	0.813028	1

Table 13 shows detection and geo-referencing results for 18 Oct. 2005, l31p2 (a349).

Table 13: Candidate targets for 18 Oct. 2005, l31p2 (a349).

#	Azimuth [pixel]	Range [pixel]	Latitude [deg]	Longitude [deg]	Time [hh:mm:ss.s]	RCS [dB-m^2]	σ° [dB]	sin(inc)	Ocean
1	52642	102	45.540870	-61.258321	12:42:33.80485	31.760284	-17.548424	0.589866	1
2	49108	315	45.553209	-61.241170	12:42:22.38094	39.654850	-22.404160	0.678911	1
3	49860	315	45.550590	-61.241163	12:42:24.81118	39.670532	-23.104189	0.678988	1
4	55735	358	45.530048	-61.237987	12:42:43.84792	10.496686	-24.151836	0.693153	1
5	55356	649	45.531393	-61.217633	12:42:42.61512	31.587011	-28.475439	0.766385	1
6	55384	659	45.531284	-61.216964	12:42:42.70620	31.744404	-29.415600	0.768386	1
7	61120	844	45.511200	-61.204977	12:43:01.44221	14.261165	-35.240005	0.800742	1
8	46074	1010	45.563833	-61.194370	12:42:12.60912	17.262239	-28.853922	0.824402	1
9	45499	1058	45.565855	-61.191392	12:42:10.76286	37.606087	-27.642113	0.830394	1
10	44736	799	45.568533	-61.207723	12:42:08.31294	37.272739	-22.766047	0.793644	1
11	44976	816	45.567706	-61.206623	12:42:09.08355	0.000000	-22.947792	0.796439	1
12	44745	874	45.568495	-61.202914	12:42:08.34184	32.733208	-22.394207	0.805476	1
13	36454	696	45.597476	-61.214423	12:41:41.87812	30.968227	-26.230034	0.775561	1
14	46186	675	45.563468	-61.215837	12:42:12.96875	40.950405	-21.232691	0.771444	1

Table 14 shows detection and geo-referencing results for 18 Oct. 2005, l32p3 (a350). Unfortunately, missing range lines of data have been discovered in both l31p2 and l32p3. The impact is not noticeable via visual inspection of the COASP image product following azimuth compression, but the dropped lines are visible in the first stage of CHASP processing. Due to the potential of phase distortion, further analysis of the 18 Oct. 2005 data sets was not pursued.

Table 14: Candidate targets for 18 Oct. 2005, l32p3 (a350).

#	Azimuth [pixel]	Range [pixel]	Latitude [deg]	Longitude [deg]	Time [hh:mm:ss.s]	RCS [dB-m^2]	σ° [dB]	sin(inc)	Ocean
1	80128	374	45.511449	-61.205380	13:04:57.95236	0.000000	-25.674944	0.696823	1
2	77616	971	45.524505	-61.243390	13:04:50.10355	0.000000	-31.287275	0.819147	1
3	79205	1008	45.529986	-61.238834	13:04:55.07221	25.160183	-32.919456	0.824070	1
4	82247	766	45.530628	-61.216090	13:05:04.56453	33.320175	-31.966629	0.787550	1
5	82137	790	45.531107	-61.217606	13:05:04.22129	33.339081	-32.037560	0.791632	1
6	84068	669	45.532541	-61.204342	13:05:10.23174	19.684208	-29.440237	0.769779	1
7	83517	1146	45.546133	-61.227762	13:05:08.51774	15.418204	-33.538780	0.840442	1
8	85420	1144	45.551283	-61.220201	13:05:14.43189	41.837261	-33.307571	0.840174	1
9	87362	1148	45.556686	-61.212736	13:05:20.45413	0.000000	-30.013893	0.840353	1
10	78186	1375	45.538306	-61.258478	13:04:51.88777	18.022058	-34.946518	0.863106	1
11	78629	1524	45.543906	-61.262924	13:04:53.27444	11.649947	-34.286945	0.875245	1
12	79615	1459	45.544647	-61.256449	13:04:56.35158	16.627775	-34.748837	0.870103	1
13	80839	1407	45.546676	-61.249155	13:05:00.17098	10.253681	-34.056442	0.865638	1
14	82845	1405	45.551983	-61.241430	13:05:06.42735	38.575317	-34.993683	0.865543	1
15	85041	1406	45.558096	-61.232762	13:05:13.25659	0.000000	-32.757599	0.865658	1
16	84927	1413	45.557990	-61.233500	13:05:12.90307	8.824917	-33.514645	0.866256	1
17	74507	1850	45.542076	-61.292226	13:04:40.37177	16.217081	-35.175900	0.896688	1
18	72955	2083	45.544402	-61.307594	13:04:35.51370	11.200048	-32.335762	0.908615	1
19	75558	1992	45.548865	-61.293961	13:04:43.66161	29.103413	-30.389193	0.904237	1
20	76378	1156	45.526954	-61.256026	13:04:46.22837	12.667133	-33.577248	0.841562	1
21	75441	1153	45.524150	-61.259803	13:04:43.29538	18.019711	-30.969227	0.841342	1
22	74136	1347	45.526428	-61.273094	13:04:39.21046	20.646759	-30.555288	0.860675	1
23	75015	1347	45.528842	-61.269645	13:04:41.96191	8.421835	-33.688221	0.860670	1
24	74836	1408	45.530181	-61.272862	13:04:41.40160	12.254995	-34.001343	0.866000	1
25	73927	1405	45.527548	-61.276366	13:04:38.55626	23.794483	-32.642696	0.865720	1
26	93131	1737	45.589730	-61.214840	13:05:38.27547	30.004745	-32.772186	0.889720	1
27	91076	1065	45.564236	-61.194807	13:05:31.94213	0.000000	-26.514389	0.831096	1
28	91103	1271	45.570551	-61.203529	13:05:32.02534	0.000000	-11.410457	0.853436	1
29	90745	1237	45.568553	-61.203495	13:05:30.92012	21.120056	-21.638590	0.850077	1
30	90146	1270	45.567901	-61.207231	13:05:29.06834	35.024864	-28.826851	0.853300	1
31	88566	1348	45.565923	-61.216602	13:05:24.18384	33.748093	-28.038275	0.860358	1

Table 15 shows detection and geo-referencing results for 18 Oct. 2005, l31p7 (a354). A large ship identified as *Gemini Voyager* (333 m), corresponding to targets 8 to 12, has been processed with CHASP. Also, *Champion* (238 m), which was outside of the ROI, was processed to provide additional data for velocity validation.

Table 15: Candidate targets for 18 Oct. 2005, l31p7 (a354).

#	Azimuth [pixel]	Range [pixel]	Latitude [deg]	Longitude [deg]	Time [hh:mm:ss.s]	RCS [dB-m^2]	σ° [dB]	sin(inc)	Ocean
1	17500	75	45.54367	-61.2627	14:21:16.80321	9.321889	-16.8531	0.605308	1
2	16103	135	45.53829	-61.2578	14:21:12.56288	14.53022	-18.891	0.636413	1
3	19631	357	45.5519	-61.2411	14:21:23.28443	38.76648	-22.6984	0.722246	1
4	18391	360	45.54708	-61.2409	14:21:19.50919	16.63836	-23.04	0.723115	1
5	14015	402	45.5302	-61.238	14:21:06.23735	19.1244	-24.188	0.735256	1
6	19946	420	45.55311	-61.2366	14:21:24.24346	35.74039	-24.8328	0.740606	1
7	2774	924	45.48676	-61.2043	14:20:32.26092	18.49885	-30.586	0.836526	1
8	6335	1108	45.50049	-61.1932	14:20:43.03696	48.6794	-29.9127	0.858359	1
9	4336	1125	45.49278	-61.1922	14:20:36.98773	40.01544	-30.6118	0.860091	1
10	4934	1135	45.49505	-61.1916	14:20:38.79735	31.33226	-26.5821	0.861134	1
11	5826	1135	45.49854	-61.1916	14:20:41.49666	48.79449	-28.1514	0.861161	1
12	6255	1146	45.50019	-61.1909	14:20:42.79487	48.90122	-29.9824	0.862293	1
13	9192	913	45.51156	-61.205	14:20:51.66429	13.05181	-31.4816	0.835132	1
14	12669	715	45.52499	-61.2173	14:21:02.16418	-999	-27.4106	0.804967	1
15	14291	710	45.53124	-61.2176	14:21:07.07256	29.73966	-27.9564	0.804167	1
16	19376	672	45.55085	-61.2199	14:21:22.50807	46.46561	-28.6796	0.7975	1
17	20919	677	45.55686	-61.2196	14:21:27.20679	4.866098	-28.1985	0.798481	1
18	19705	703	45.55212	-61.2179	14:21:23.50972	46.46635	-30.3586	0.803129	1
19	23706	884	45.56762	-61.2065	14:21:35.72351	29.0545	-32.2543	0.831499	1
20	23901	940	45.56836	-61.2031	14:21:36.32084	34.56483	-23.3415	0.838995	1
21	15085	899	45.53426	-61.2057	14:21:09.47531	15.3595	-29.3864	0.833441	1
22	12624	953	45.52477	-61.2025	14:21:02.02801	-999	-24.6551	0.840457	0
23	14843	1110	45.53331	-61.193	14:21:08.74298	18.79015	-29.0632	0.858735	0
24	15066	1138	45.53416	-61.1913	14:21:09.41781	36.44358	-27.8744	0.861648	0
25	22653	1053	45.5635	-61.1962	14:21:32.50215	29.72098	-33.0291	0.852649	1
26	22770	1087	45.56395	-61.1942	14:21:32.85945	16.30173	-29.4485	0.856399	1
27	28846	3079	45.58722	-61.0827	14:21:51.48854	23.56247	-29.2933	0.952511	1
28	13055	1629	45.52635	-61.1629	14:21:03.33227	32.14629	-32.5223	0.900604	1
29	6614	2367	45.50151	-61.1218	14:20:43.88125	-999	-31.0052	0.93397	1
30	12400	2169	45.52381	-61.1327	14:21:01.35015	13.64874	-31.4688	0.926943	1
31	15143	2265	45.53434	-61.1273	14:21:09.65082	34.66275	-14.7483	0.930546	1
32	12752	2658	45.52509	-61.1059	14:21:02.41535	23.35015	-25.1585	0.942663	1
33	13271	2801	45.52704	-61.0981	14:21:03.98591	30.15843	-25.4539	0.946308	1
34	13507	2935	45.52796	-61.0909	14:21:04.70008	-999	-17.1105	0.949414	1
35	16084	3042	45.53788	-61.085	14:21:12.50521	-999	-12.8267	0.95173	0
36	7793	3498	45.50598	-61.0608	14:20:47.44358	29.77239	-23.3391	0.959874	0
37	8199	3531	45.50751	-61.059	14:20:48.66846	30.15881	-22.5222	0.960385	0

As representative results, Table 16 throughTable 19 summarize CHASP results in comparison with validation data for the identified vessels observed on 17 Oct. 2005, l22p2 (a342). In these tables, the ground truth time refers to the time for which ground coordinates were found by dead reckoning using the available data sources. The CHASP time is the estimated acquisition time, which may differ from the zero-Doppler time of a ship. The CHASP coordinates refer to the zero-Doppler coordinates of the ship. The ship reaches the CHASP coordinates at the zero-Doppler time, which may be slightly different from the acquisition time. Speed estimates include error intervals based upon nonlinearity of the along-track speed estimates of the tracking or multi-look algorithm. When such error intervals are too large, speed estimation has no physical sense. Similarly, if the estimated speed is very low, course estimates are not meaningful. The error interval for the contrast algorithm reflects the difference between polarimetric channels. Contrast is maximized separately for each of the four channels and any discrepancies between the channels are used to define the error interval. These examples point out possible differences among the

estimates made by the various available CHASP algorithms, justifying the use of a decision rule based upon scores as described in Section 2.3.2.

Since most of the known ships in Chedabucto Bay are moving at a low speed, or perhaps not moving at all, several other ships were processed to allow better comparison between the ground truth data and the CHASP-derived velocity estimates. Example results from the tracking algorithm and the multi-look algorithm are plotted in Figure 11 for *E. Cornwallis* (83 m), Figure 12 for *Gemini Voyager* (333 m), and in Figure 13 for *Champion* (238 m).

A summary of the velocity estimation results are presented in Figure 14. The plotted data include ships that were moving with speeds up to 8 m/s and in various directions. In general, the accuracy of the speed estimation tends to improve for larger ships (i.e., having a larger signal-to-noise ratio). The course estimation results have been plotted only for cases with a speed that is larger than 2 m/s.

a) b)

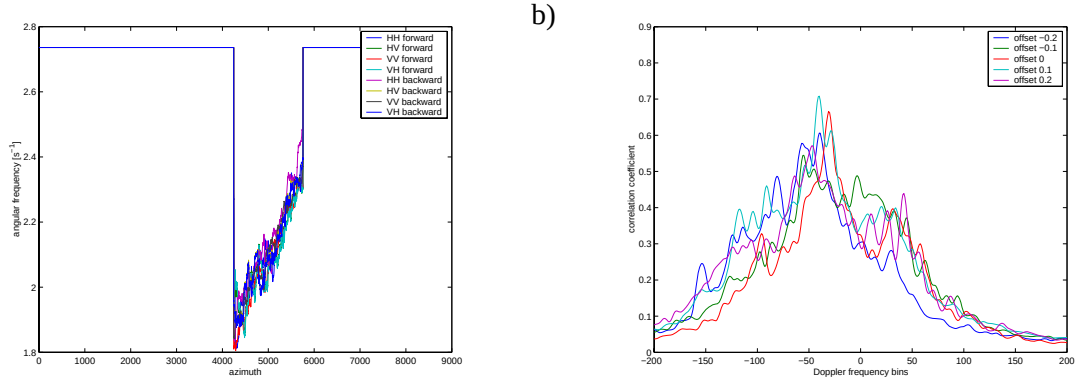

Figure 11: a) Frequency tracking; and b) cross-correlation for 5 azimuth looks for 17 Oct. 2005, l22p2 (a342), E. Cornwallis.

a) b)

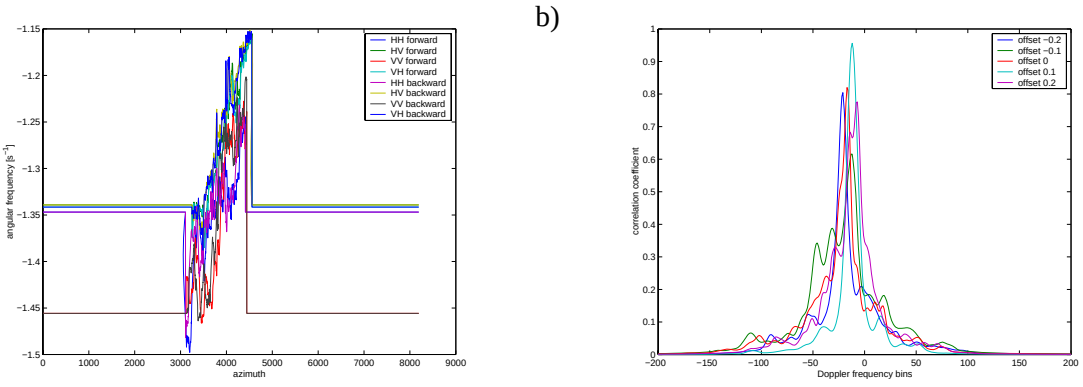

Figure 12: a) Frequency tracking; and b) cross-correlation for 5 azimuth looks for 18 Oct. 2005, l31p7 (a354), Gemini Voyager.

a)

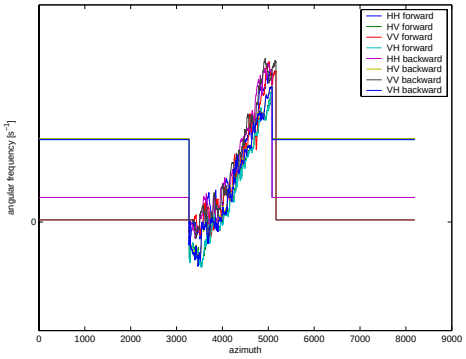

b)

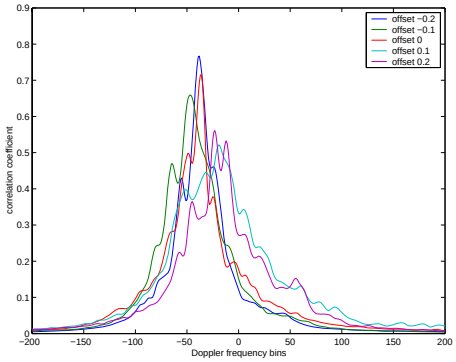

Figure 13: a) Frequency tracking; and b) cross-correlation for 5 azimuth looks for 18 Oct. 2005, l31p7 (a354), Champion.

Table 16: CHASP velocity for 17 Oct. 2005, l22p2 (a342), E. Cornwallis.

	Ground Truth	CHASP	Comments
Identity	*E. Cornwallis*	l22p2	
Time [hh:mm:ss.s]	13:09:42	13:09:41.91	dead-reckon 50 s
Latitude [deg]	45.5428	45.5414	
Longitude [deg]	-61.2488	-61.2535	
Speed [m/s]	7.46		
		8.3±1.2	tracking
		9.7±1.3	multi-look
		8.2	contrast
Course [deg]	70		
		70	tracking
		76	multi-look
		80	contrast

Table 17: CHASP velocity for 17 Oct. 2005, l22p2 (a342), Toronto.

	Ground Truth	CHASP	Comments
Identity	*Toronto*	l22p2	
Time [hh:mm:ss.s]	13:09:53	13:09:52.47	dead-reckon 10 min
Latitude [deg]	45.5539	45.5536	
Longitude [deg]	-61.2423	-61.2433	
Speed [m/s]	0	1.5±2.7	tracking
		0.8±1.7	multi-look
		0.6±1.3	contrast
	N/A	N/A	speed too low

Table 18: CHASP velocity for 17 Oct. 2005, l22p2 (a342), Gulf Service.

	Ground Truth	CHASP	Comment
Identity	*Gulf Service*	l22p2	
Time [hh:mm:ss.s]	13:09:40	13:09:39.82	dead-reckon 41 s
Latitude [deg]	45.5046	45.5055	
Longitude [deg]	-61.2064	-61.2080	
Speed [m/s]	2.5		
		5.1±1.9	tracking
		3.7±1.8	multi-look
		3.6	contrast
Course [deg]	138		
		138	tracking
		149	multi-look
		150	contrast

Table 19: CHASP velocity for 17 Oct. 2005, l22p2 (a342), Preventer.

	Ground Truth	CHASP	Comments
Identity	*Preventer*	l22p2	TBC
Time [hh:mm:ss.s]	13:09:51	13:09:50.99	
Latitude [deg]	45.52930	45.5322	
Longitude [deg]	-61.2158	-61.2168	
Speed [m/s]	0.28		
		1±1.4	tracking
		2.2±6.1	multi-look
		2.2±7	contrast
Course [deg]	33	N/A	speed too low

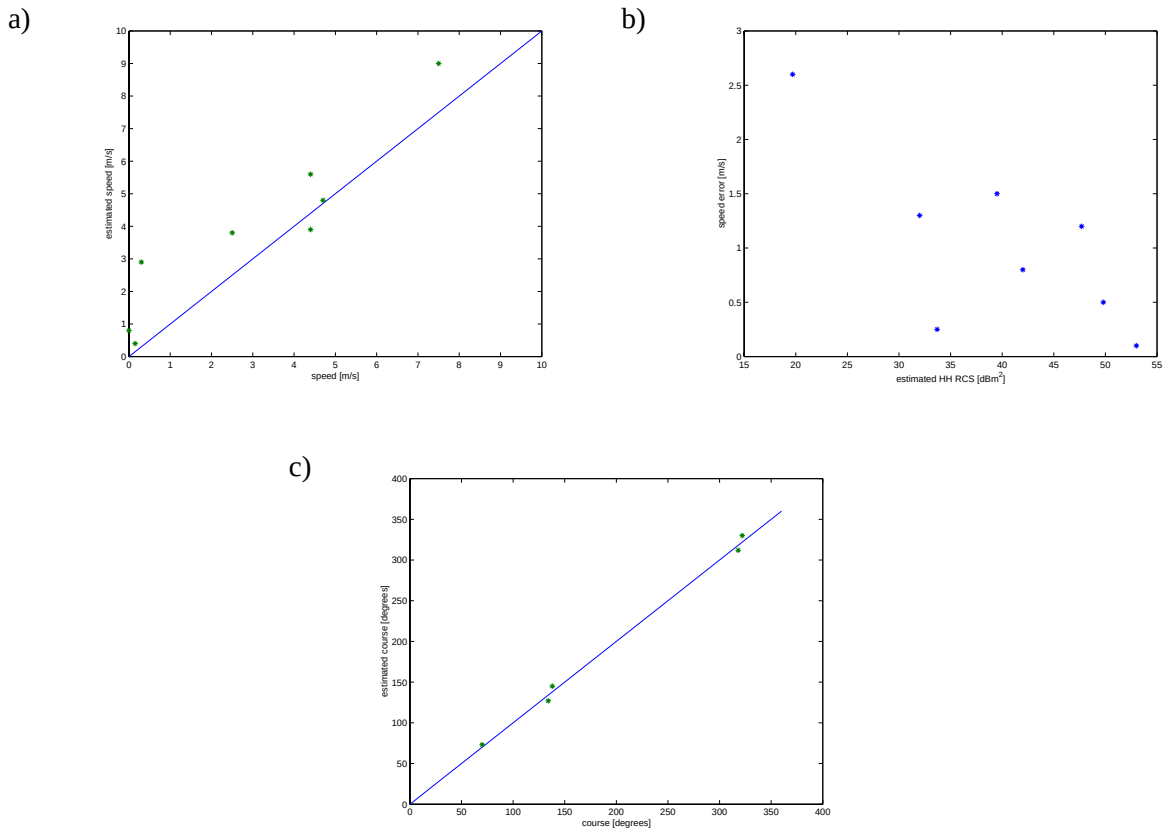

Figure 14: Velocity estimation scatter plots: a) Estimated vs. validation data speed; b) Speed error vs. estimated Total RCS; and c) Estimated vs. validation data course. The blue-line represents unity slope.

Dominion Victory (25 m) was analysed for four open ocean passes of 20 Oct. 2005. Due to the low signal-to-noise ratio, velocity estimation was not possible in any of these cases. Figure 15 shows the outcome of target tracking for *Dominion Victory* in passes l41p1 (a358), l41p2 (a359), l41p3 (a360) and l42p4 (a361). The waveforms resemble the effect shown in Figure 3b in which a moving target with oscillation was simulated. Figure 16 shows the outcome of the multi-look algorithms for the same passes for the HH channel. The azimuth looks were processed and cross-correlated in pairs covering the entire Doppler bandwidth. These tracking and multi-look plots illustrate the non-linear nature of the Doppler chirp. The non-parametric focusing method had to be used in all four of these cases.

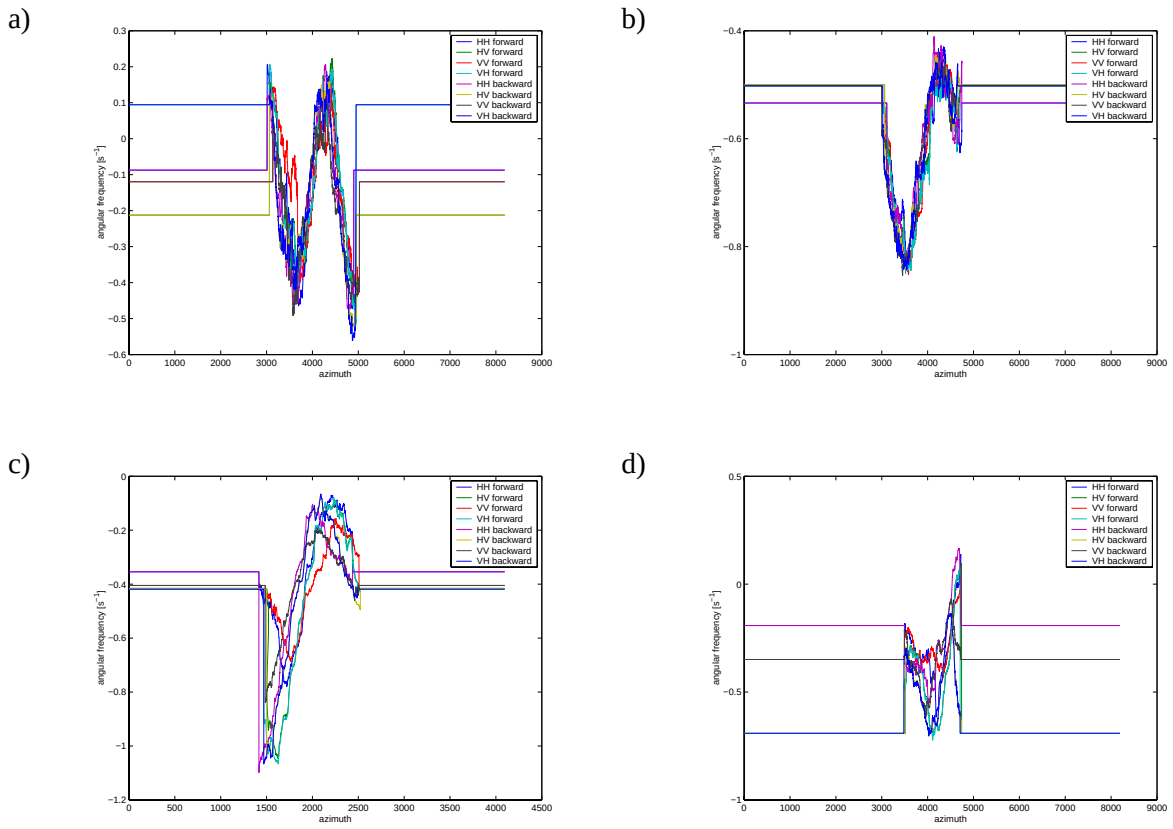

Figure 15: Frequency tracking for Dominion Victory *on 20 Oct. 2005: a) l41p1 (a358); b) l41p2 (a359); c) l41p3 (a360); and d) l42p4 (a361).*

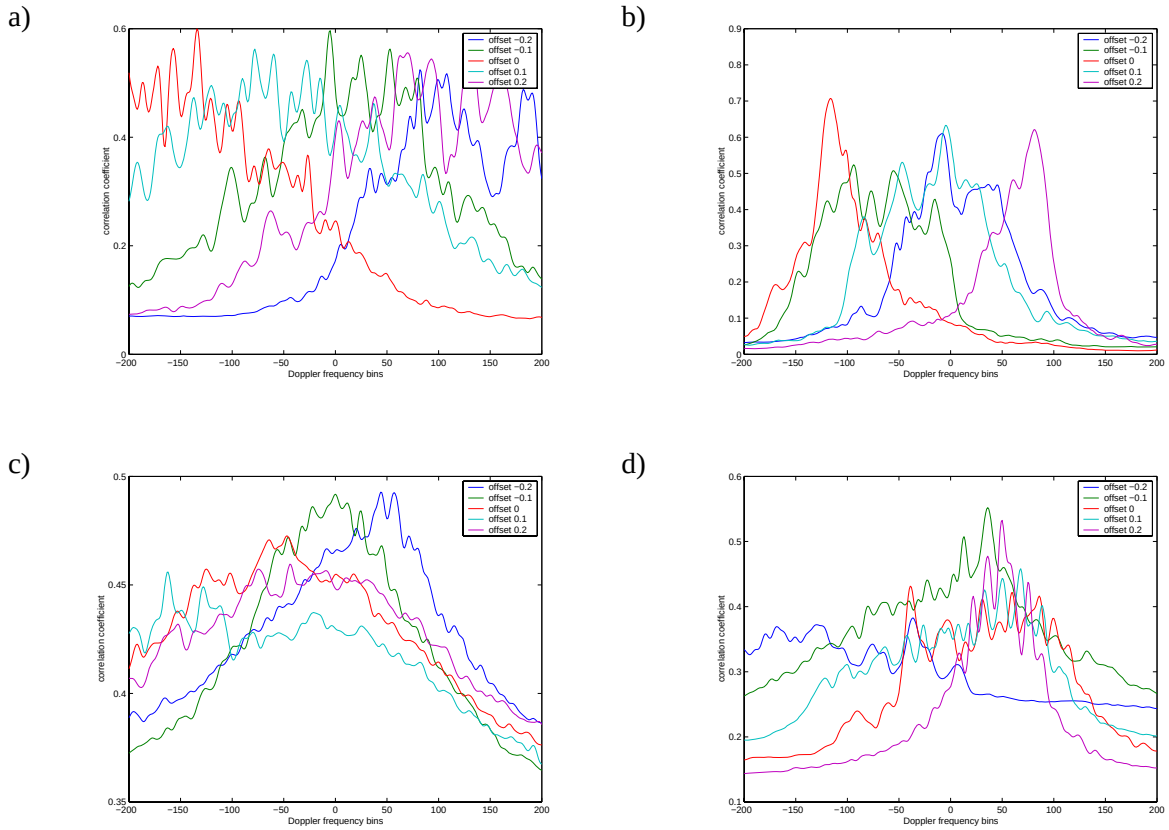

Figure 16: Cross-correlation coefficients for 5 azimuth looks for Dominion Victory *on 20 Oct. 2005: a) l41p1 (a358); b) l41p2 (a359); c) l41p3 (a360); and d) l42p4 (a361).*

For completeness, representative image chips from before and after CHASP processing are shown in Figure 17. In each case, the image is shown in terms of its Pauli decomposition with (S_{HH} + S_{VV}) displayed as Blue (single bounce scattering), ($S_{HH} - S_{VV}$) displayed as Red (double bounce scattering), and (S_{HV} + S_{VH}) displayed as Green (volume scattering). The before CHASP processing chip is the COASP product while the CHASP result is the best/optimized result that was obtained. In each case, the improvement in target contrast and/or focus as well as the reduction in azimuth ambiguities is apparent.

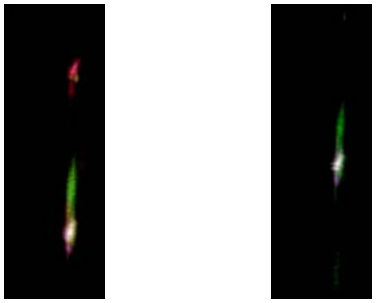

17 Oct. 2005, l22p2 (a342), *E. Cornwallis*

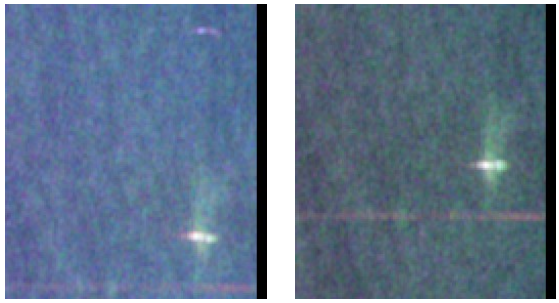

17 Oct. 2005, l22p2 (a342), *Gulf Service*

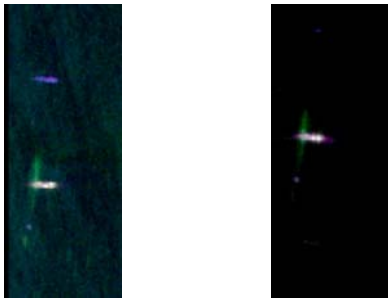

17 Oct. 2005, l22p2 (a342), Target 2

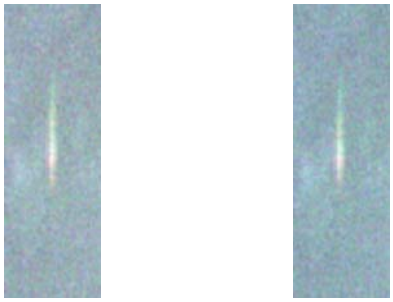

17 Oct. 2005, l22p2 (a342), Target 12

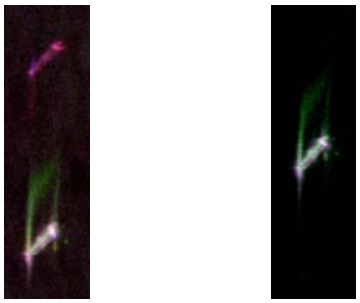

17 Oct. 2005, l26p6 (a345), *Champion*

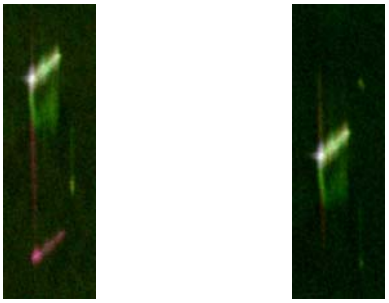

18 Oct. 2005, l31p7 (a354), *Champion*

Figure 17: Representative CHASP processing results (COASP on the left, CHASP on the right).
(Continued on next page.)

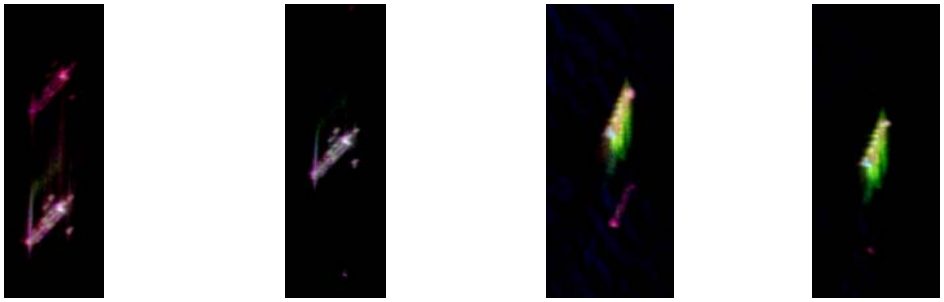

18 Oct. 2005, l31p7 (a354), *Gemini Voyager*

20 Oct. 2005, l41p1 (a358), *Atlantic Concert*

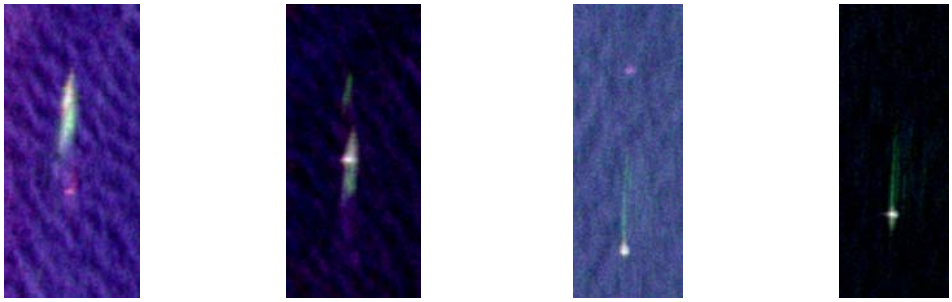

20 Oct. 2005, l41p1 (a358), *Toronto*

20 Oct. 2005, l41p2 (a359), *Dominion Victory*

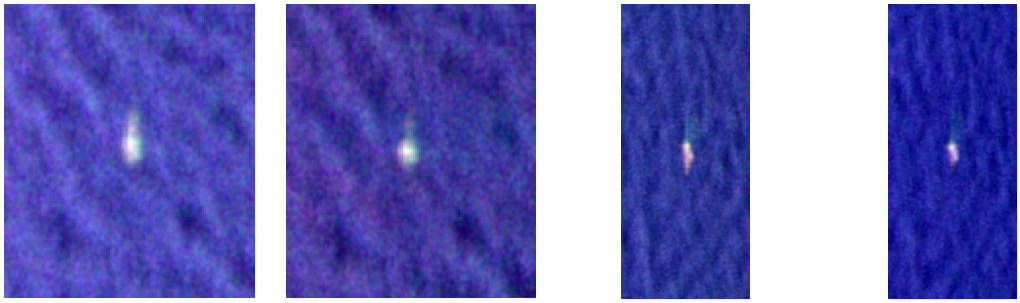

20 Oct. 2005, l41p3 (a360), *Dominion Victory*

20 Oct. 2005, l42p4 (a361), *Dominion Victory*

Figure 17: Concluded.

3.2 Total RCS of Known Vessels

Table 20 through Table 31 present comparisons between the expected and estimated Total RCS values for several of the identified ships. The expected Total RCS is based upon two semi-empirical rule-of-thumb models that have been validated for HH polarization data [20]. The first model is based upon the ship length and the local incidence angle:

$$\sigma_1 = 0.08L^{7/3}(0.78 + 0.11\theta) \tag{8}$$

where σ_1 is the Total RCS in m^2, L is the ship length expressed in meters, and θ is the local incidence angle expressed in degrees. The second model is based solely upon the ship length:

$$\sigma_2 = 1.25L^{1.98} \tag{9}$$

where σ_2 is the Total RCS in m^2. The first model was developed based upon observations of just a few known ships, but compares reasonably well with the second model that was based upon nearly 400 fine mode observations validated with AIS data. In both cases, the Total RCS is assumed to be independent of the ship aspect angle and the ship type. Of course, these are gross simplifications. Nevertheless, these models have proven to provide a helpful point of reference.

In some cases, the Total RCS estimates are biased because a good sample of ocean clutter was not available. As a rule, σ° for the clutter is estimated using the four corners of the image chip around the target. In some cases, however, there were other vessels or land on one side of the target so that the ocean sample could only be taken from two of the corners, which are necessarily at a slightly different incidence angle. Also, ocean clutter is not uniform, which may also cause a biased estimate of the clutter. For larger incidence angles, the estimate of σ° may be biased because system noise was predominant over clutter.

Table 20: Total RCS for 17 Oct. 2005, l22p2 (a342), E. Cornwallis.

	Ground Truth	CHASP	Comments
Identity	*E. Cornwallis*	l22p2	
L [m]	83		
Elevation [deg]		60.17	
Incidence [deg]		60.28	
RCS [dB-m^2]	42, 39		σ_1, σ_2
		39	HH
		29	HV
		28	VH
		35	VV
σ° [dB]			
		-34.5	HH
		-39.9	HV
		-41.2	VH
		-28.8	VV

Table 21: Total RCS for17 Oct. 2005, l22p2 (a342), Toronto.

	Ground Truth	CHASP	Comments
Identity	*Toronto*	l22p2	
L [m]	134		
Elevation [deg]		60.96	
Incidence [deg]		61.04	
RCS [dB-m^2]	47, 43		σ_1, σ_2
		42	HH
		29	HV
		28	VH
		38	VV
σ° [dB]			
		-32.5	HH
		-38.0	HV
		-39.2	VH
		-28.4	VV

Table 22: Total RCS for 17 Oct. 2005, l22p2 (a342), Gulf Service.

	Ground Truth	CHASP	Comments
Identity	*Gulf Service*	l22p2	
L [m]	42		
Elevation [deg]		43.55	
Incidence [deg]		43.61	
RCS [dB-m^2]	34, 33		σ_1, σ_2
		32	HH
		23	HV
		22	VH
		33	VV
σ° [dB]			
		-21.6	HH
		-32.6	HV
		-33.4	VH
		-19.1	VV

Table 23: Total RCS for 17 Oct. 2005, l24p4 (a343), E. Cornwallis.

	Ground Truth	CHASP	Comments
Identity	*E. Cornwallis*	l22p3	
L [m]	83		
Elevation [deg]		41.82	
Incidence [deg]		41.87	
RCS [dB-m^2]	41, 39		σ_1, σ_2
		33	HH
		30	HV
		29	VH
		25	VV
σ° [dB]			
		-15.2	HH
		-30.3	HV
		-31.0	VH
		-13.9	VV

Table 24: Total RCS for 20 Oct. 2005, l41p1 (a358), Atlantic Concert.

	Ground Truth	CHASP	Comments
Identity	*Atlantic Concert*	L41p1	
L [m]	292		
Elevation [deg]		41.52	
Incidence [deg]		41.57	
RCS [dB-m^2]	54, 50		σ_1, σ_2
		54	HH
		46	HV
		45	VH
		54	VV
$\sigma°$ [dB]			
		-12.5	HH
		-27.7	HV
		-28.4	VH
		-11.0	VV

Table 25: Total RCS for 20 Oct. 2005, l41p1 (a358), Dominion Victory.

	Ground Truth	CHASP	Comments
Identity	*Dominion Victory*	l41p1	
L [m]	25		
Elevation [deg]		66.63	
Incidence [deg]		66.77	
RCS [dB-m^2]	31, 29		σ_1, σ_2
		35	HH
		25	HV
		25	VV
		32	VH
$\sigma°$ [dB]			
		-21.2	HH
		-26.2	HV
		-27.7	VH
		-16.9	VV

Table 26: Total RCS for 20 Oct. 2005, l41p2 (a359), Dominion Victory.

	Ground Truth	CHASP	Comments
Identity	*Dominion Victory*	l41p2	
L [m]	25		
Elevation [deg]		59.33	
Incidence [deg]		59.43	
RCS [dB-m^2]	30, 29		σ_1, σ_2
		27	HH
		17	HV
		16	VH
		23	VV
$\sigma°$ [dB]			
		-31.2	HH
		-39.0	HV
		-40.1	VH
		-25.4	VV

Table 27: Total RCS for 20 Oct. 2005, l41p3 (a360), Dominion Victory.

	Ground Truth	CHASP	Comments
Identity	*Dominion Victory*	l41p3	
L [m]	25		
Elevation [deg]		42.66	
Incidence [deg]		42.72	
RCS [dB-m^2]	29, 29		σ_1, σ_2
		37	HH
		21	HV
		20	VH
		35	VV
$\sigma°$ [dB]			
		-19.1	HH
		-33.4	HV
		-34.0	VH
		-16.8	VV

Table 28: Total RCS for 20 Oct. 2005, l42p4 (a361), Dominion Victory.

	Ground Truth	CHASP	Comments
Identity	*Dominion Victory*	l42p4	
L [m]	25		
Elevation [deg]		47.37	
Incidence [deg]		47.44	
RCS [dB-m^2]	29, 29		σ_1, σ_2
		34	HH
		20	HV
		19	VH
		31	VV
$\sigma°$ [dB]			
		-21.2	HH
		-33.5	HV
		-34.1	VH
		-17.6	VV

Table 29: Total RCS for 17 Oct. 2005, l26p6 (a345), Champion.

	Ground Truth	CHASP	Comments
Identity	*Champion*	l26p26	
L [m]	238		
Elevation [deg]		65.57	
Incidence [deg]		65.71	
RCS [dB-m^2]	54, 48		σ_1, σ_2
		48	HH
		35	HV
		35	VH
		45	VV
$\sigma°$ [dB]			
		-28.3	HH
		-32.8	HV
		-34.1	VH
		-22.8	VV

Table 30: Total RCS for 18 Oct. 2005, l31p7 (a354), Champion.

	Ground Truth	CHASP	Comments
Identity	*Champion*	l31p7	
L [m]	238		
Elevation [deg]		68.98	
Incidence [deg]		69.12	
RCS [dB-m^2]	54, 48		σ_1, σ_2
		50	HH
		34	HV
		33	VH
		48	VV
σ° [dB]			
		-32.0	HH
		-32.7	HV
		-36.5	VH
		-22.1	VV

Table 31: Total RCS for 18 Oct. 2005, l31p7 (a354), Gemini Voyager.

	Ground Truth	CHASP	Comments
Identity	*Gemini Voyager*	l31p7	
L [m]	333		
Elevation [deg]		59.37	
Incidence [deg]		59.46	
RCS [dB-m^2]	57, 51		σ_1, σ_2
		55	HH
		48	HV
		48	VH
		56	VV
σ° [dB]			
		-25.2	HH
		-36.3	HV
		-36.3	VH
		-22.7	VV

The estimated Total RCS measurement results are summarized in Figure 18. We see that for the 41° to 67° incidence angle range considered, there is reasonable agreement (to within no worse than 8 dB) between the estimated HH polarization Total RCS values and the model values, as represented by σ_1 (i.e., equation (8)). Furthermore, the estimated VV and HH polarization Total RCS values are well-correlated. Generally, the VV values are a few dB smaller than the HH values. The estimated HV and VH Total RCS values are also well-correlated and fall roughly 10 dB below the estimated HH polarization Total RCS values.

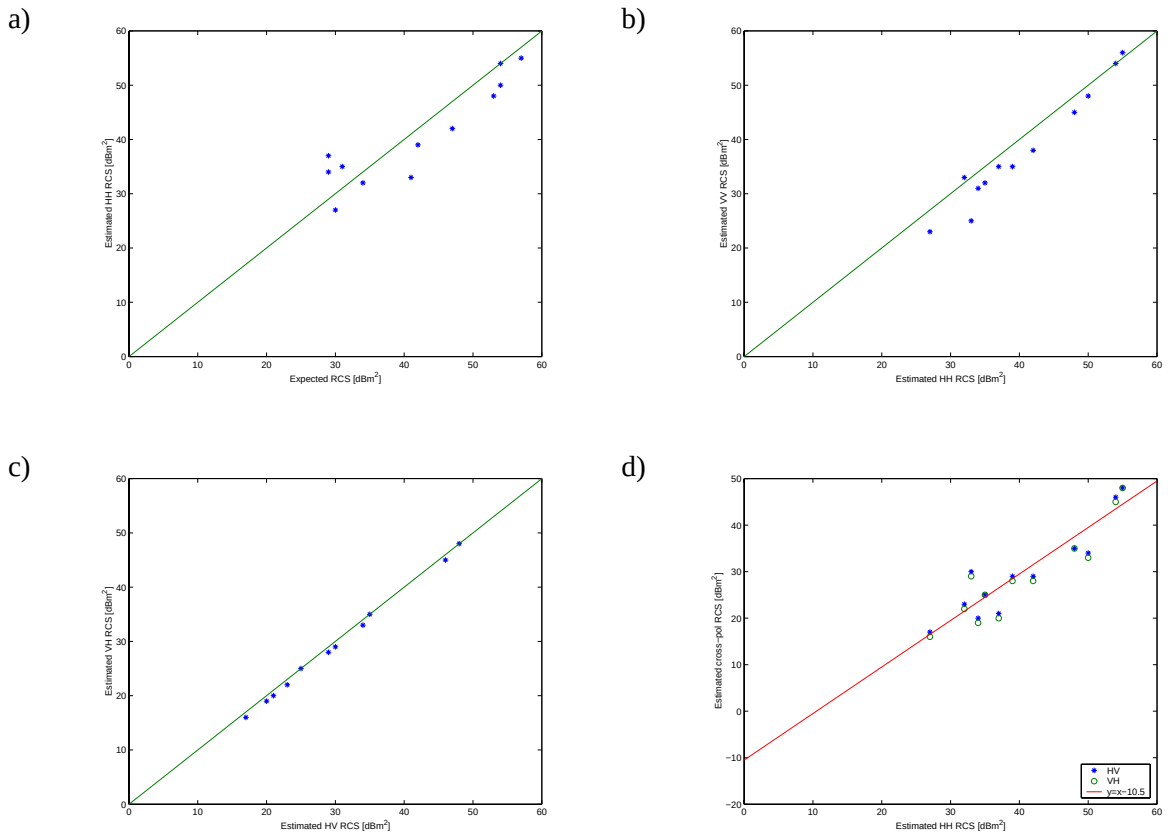

Figure 18: Total RCS scatter plots: a) Estimated HH vs. model; b) Estimated VV vs. estimated HH; c) Estimated VH vs. Estimated HV; d) Estimated cross-polarization vs. Estimated HH. The green-line represents unity slope, the red line is a linear regression fit.

3.3 ROCs for *Dominion Victory*

The detection performance for *Dominion Victory* (25 m) based upon COASP image products is shown in Figure 19, which clearly shows the advantage (i.e., decreased probability of missed detection, decreased probability of false alarm) of a quad polarimetric system, which uses the available amplitude and phase information (triangles). The dual co-polarization system with phase (circles) provides better detection performance than a single channel HH polarization system (asterisks). In principle, a dual polarization system should provide wider swath coverage than a quad polarimetric system. This performance improvement as polarimetric channels are added has been demonstrated previously (see [12] and Annex F).

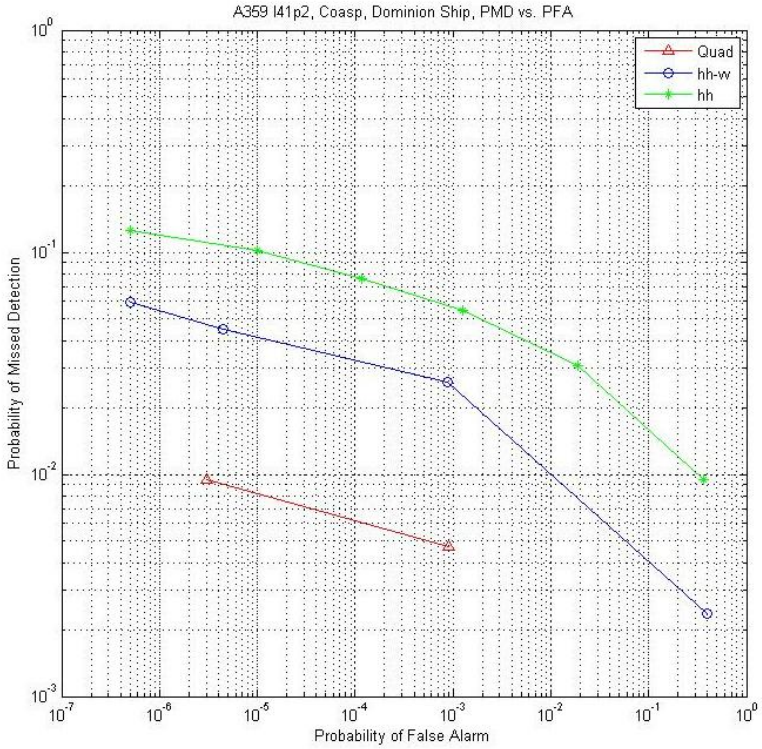

Figure 19: Detection performance for 20 Oct. 2005, l41p2 (a359), Dominion Victory.

By arbitrarily selecting a probability of false alarm of $P_{FA} = 10^{-5}$, the relative improvement in ship detectability may be quantified by comparing the probability of missed detection P_{MD} across the cases considered. In one case (l41p1), *Dominion Victory* could not be detected for $P_{FA} = 10^{-5}$, regardless of the polarimetric modes considered. In this case, the ship was very badly smeared in azimuth. Therefore, the ship image was reprocessed using CHASP to improve the image focus. The ROC was then derived based upon the CHASP image of the ship and the COASP image of the background clutter. In general, we could adequately identify the ship pixels in the COASP image and use the COASP image of both the ship and the background clutter to derive the ROC.

In another case (l41p3), *Dominion Victory* could not be detected for the single channel system for $P_{FA} = 10^{-5}$.

The relative improvement in the detection performance of all 20 Oct. 2005 cases is summarized in Table 32 by taking the ratio of the observed P_{MD} to that of polarimetry P^{Q}_{MD} From the MARSIE data, for the polarimetric imaging of *Dominion Victory*, we observed that from a six-fold to an eleven-fold decrease in the probability of missed detection was achieved by moving from a single polarization to a polarimetric radar system, all else held equal.

Table 32: Values of P_{MD} for $P_{FA} = 10^{-5}$ for Dominion Victory *on 20 Oct. 2005.*

			***Dominion Victory* (25 m)**	
line/pass	**Incidence**		**P_{MD}**	**P_{MD}/P^{Q}_{MD}**
l41p1 (a358) 20 Oct. 2005	66.7°	Quad P_{MD}	0.012	1.00
		HH-VV P_{MD}	0.028	2.33
		HH P_{MD}	0.083	6.92
l41p2 (a359) 20 Oct. 2005	49.4°	Quad P_{MD}	0.008	1.00
		HH-VV P_{MD}	0.040	5.00
		HH P_{MD}	0.090	11.25
l41p3 (a360) 20 Oct. 2005	42.9°	Quad P_{MD}	0.060	1.00
		HH-VV P_{MD}	0.200	3.30
		HH P_{MD}		
l42p4 (a361) 20 Oct. 2005	47.5°	Quad P_{MD}	0.040	1.00
		HH-VV P_{MD}	0.080	2.00
		HH P_{MD}	0.500	6.25

3.4 Polarimetric Decomposition

A total of 10 ships from a selected area of an image acquired on 17 Oct. 2005, l22p2 were detected as shown in the RGB image in Figure 20. The RGB SAR image consists of information from four channels; the magnitude of the HH channel is displayed in Red, the magnitude of VV in Blue, and the magnitude of HV+VH in Green. However, only 3 of these ships have been considered at this time: *Gulf Service* (42 m), *E. Cornwallis* (83 m), and *Toronto* (135 m). Examples of the initial decomposition results are presented in this section. All results considered are presented in Annex D.

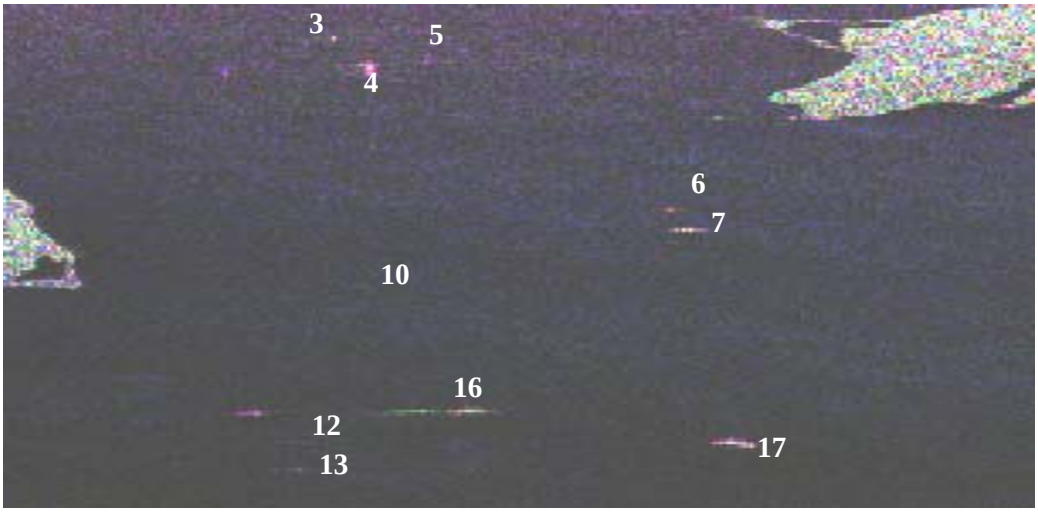

Figure 20: Detected ships in Chedabucto Bay, 17 Oct. 2005, l22p2 (a342).

A RGB image of the *Dominion Victory* from the image of l42p2 is shown in Figure 21a. The ship was moving towards the sensor with a speed of 18 knots during the image acquisition. The incidence angle is approximately 67° and the aspect angle is 171° defined with respect to the antenna bore sight direction, i.e., the ship was imaged towards its bow. The imaging geometry is illustrated in Figure 21b.

a)

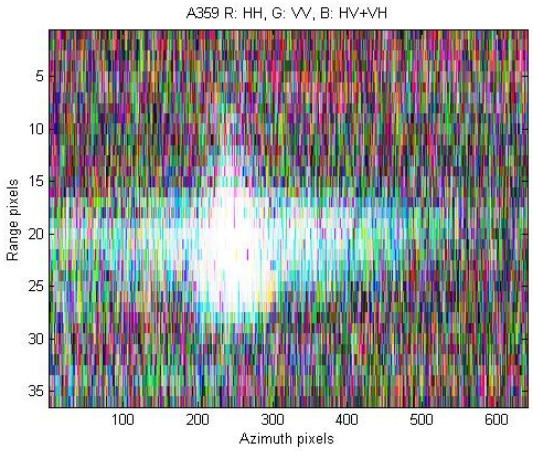

b)

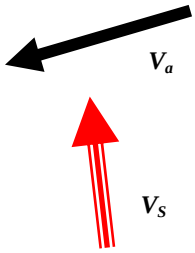

Figure 21: a) Polarimetric image of Dominion Victory, *20 Oct. 2005, l41p2 (a342); b) Image geometry (V_a is the aircraft velocity, V_s is the ship velocity).*

For the Pauli and Cameron decomposition methods, a threshold for each ship was selected based on the ocean $\sigma°$ to reduce the clutter in the decomposition results; the thresholds are listed in Table 33.

Table 33: Decomposition analysis thresholds.

17 Oct. 2005				
Line/Pass	Ship ID, Name	Reference Channel	Ocean $\sigma°$ [dB]	Threshold [dB]
l22p2 (a342)	3, *Gulf Service*	HH	N/A	−15
	16, *E. Cornwallis*	HH	−34.51	−25
	17, *Toronto*	HH	−32.48	−25
20 Oct. 2005				
Line/Pass	Ship Name	Reference Channel	Ocean σ^0 [dB]	Threshold [dB]
l41p1 (a358)	*Dominion Victory*	HH	−21.19	−15
l41p2 (a359)	*Dominion Victory*	HH	−31.19	−25
l41p3 (a360)	*Dominion Victory*	HH	−19.14	−12
l42p4 (a361)	*Dominion Victory*	HH	−21.22	−14

3.4.1 Pauli

The Pauli decomposition result is shown in Figure 22, where each pixel is assigned to one of three classes, depending on which of the components is the largest in amplitude. For class 1, (S_{HH} + S_{VV}) is the largest, for class 2, (S_{HH} − S_{VV}) is the largest, and for class 3, (S_{HV} + S_{VH}) is the largest. Class 1 represents odd bounce (blue), Class 2 represents even bounce (red), and the class 3 represents volume scattering (green). As might be expected, the ship image includes double bounce scattering. Volume scattering also appears in the ship image in some cases. This may be due to multiple bounces from the ship structure or may be caused by uncompensated ship motion during image acquisition and processing.

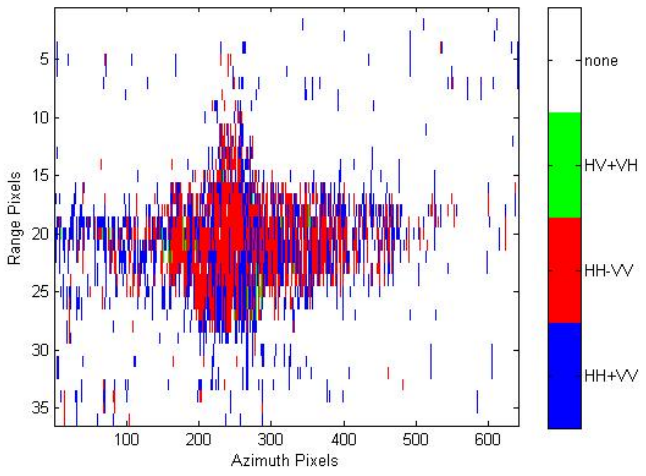

Figure 22: Pauli decomposition image of Dominion Victory, *20 Oct. 2005, l41p2 (a359).*

3.4.2 Cameron

The Cameron decomposition result is shown in Figure 23a. The ship image has been decomposed into six elemental scatterers. In this image, the most dominant component is the quarter wave device, followed by diplane, narrow diplane and cylinder. The distribution of each component is shown in the histogram (Figure 23b).

a) b)

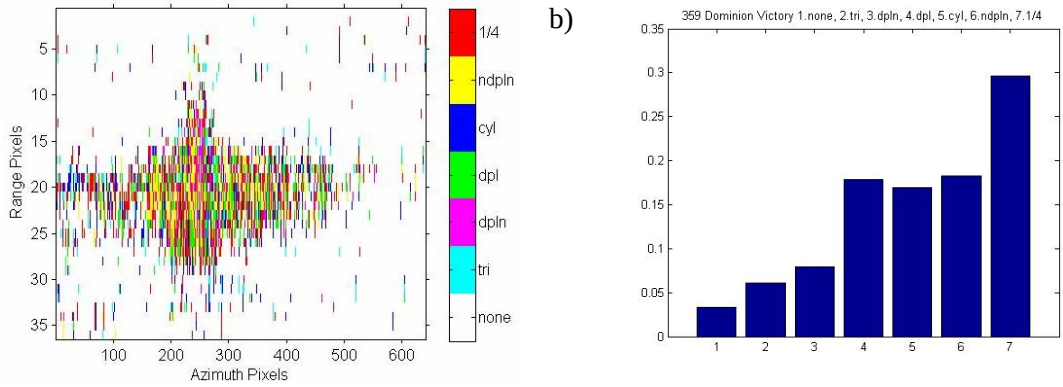

Figure 23: a) Cameron decomposition image of Dominion Victory, *20 Oct. 2005, l41p2 (a359); b) Histogram.*

For the cases studied, the quarter wave device is generally the most dominant component. The fractions of narrow diplane, dipole and cylinder are also high. The fractions of each elemental scatterer from the Cameron decomposition are summarized in Table 34. This distribution of scatterers and their spatial context is potentially useful for ship classification.

Table 34: Summary of elemental scatterer distributions for Cameron decomposition.

17 Oct. 2005, l22p2 (a342)						
Ship ID, Name	trihedral	diplane	dipole	cylinder	narrow diplane	¼-wave
3, *Gulf Service*	0.2168	0.0547	0.1210	0.2263	0.1193	0.2620
16, *E. Cornwallis*	0.0536	0.0514	0.2630	0.2083	0.1517	0.2720
17, *Toronto*	0.1026	0.0357	0.2254	0.2935	0.1243	0.2185
Dominion Victory, 20 Oct. 2005						
	trihedral	diplane	dipole	cylinder	narrow diplane	¼-wave
l41p1 (a358)	0.0943	0.0448	0.2052	0.2206	0.1265	0.3086
l41p2 (a359)	0.0631	0.0819	0.1842	0.1752	0.1887	0.3068
l41p3 (a360)	0.2036	0.0349	0.1771	0.2778	0.0912	0.2153
l42p4 (a361)	0.1488	0.1167	0.1354	0.1388	0.2302	0.2302

3.4.3 SSCM

The SSCM results are presented in terms of the Poincaré sphere angles, longitude 2ψ and latitude 2χ, in Figure 24. The results show that the ship is decomposed into six elemental scatterers, as for the Cameron method.

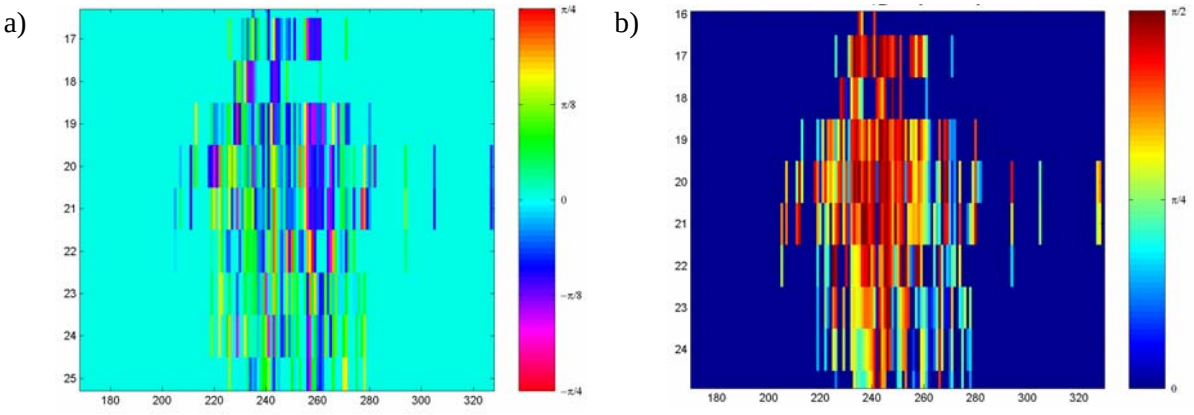

Figure 24: SSCM images Dominion Victory, *20 Oct. 2005, l41p2 (a359): a) Latitude coordinate; b) Longitude coordinate.*

A representative SSCM result presented in terms of six types of symmetric scatterers is shown in Figure 25 and the results for the cases considered are presented in Table 35. We see that the fractions of quarter-wave device, diplane, and dipole are generally high, although there are variations between ships. Furthermore, the distribution of elemental scatterers is different from that of the Cameron decomposition, which was summarized in Table 34. This distribution of scatterers and their spatial context, or even the relative difference in the distribution of scatterers among various decomposition methods such as Cameron and SSCM, is potentially useful information for ship classification. Further study is necessary to explore this issue in more detail.

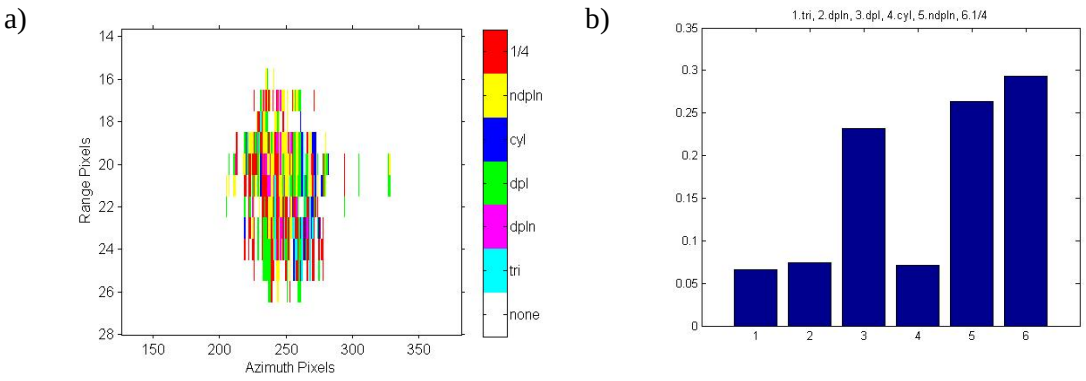

Figure 25: a) SSCM decomposition image of Dominion Victory, *20 Oct. 2005, l41p2 (a359); b) Histogram.*

Table 35: Summary of elemental scatterer distributions for SSCM decomposition.

17 Oct. 2005, l22p2 (a342)						
Ship ID, Name	trihedral	diplane	dipole	cylinder	narrow diplane	¼-wave
3, *Gulf Service*	0.0290	0.0362	0.2971	0.1449	0.2464	0.2464
16, *E. Cornwallis*	0.0952	0.0165	0.2900	0.2332	0.0957	0.2696
17, *Toronto*	0.1148	0.0147	0.2258	0.2735	0.1024	0.2688
Dominion Victory, 20 Oct. 2005						
	trihedral	diplane	dipole	cylinder	narrow diplane	¼-wave
l41p1 (a358)	0.0627	0	0.4649	0.2435	0.0812	0.1476
l41p2 (a359)	0.0665	0.0739	0.2315	0.0714	0.2635	0.2931
l41p3 (a360)	0	0	0.1429	0	0.7143	0.1429
l42p4 (a361)	0	0.0851	0.2340	0	0.6809	0

3.4.4 *H*/α

The *H*/α analysis results are shown in Figure 26, which was obtained by averaging over a 5 by 13 pixel (range by azimuth) kernel. The ocean mostly appears in zones 5 through 9, i.e., medium to low entropy (low entropy dominant), while ship mostly appears in zones 4, 5, and 7, i.e., high to medium entropy (high entropy dominant). Based upon the centre-of-mass of the respective signatures, the ship can be clearly distinguished from ocean. However, for the cases studied, it is apparent that there is often some overlap between the ship and ocean signatures.

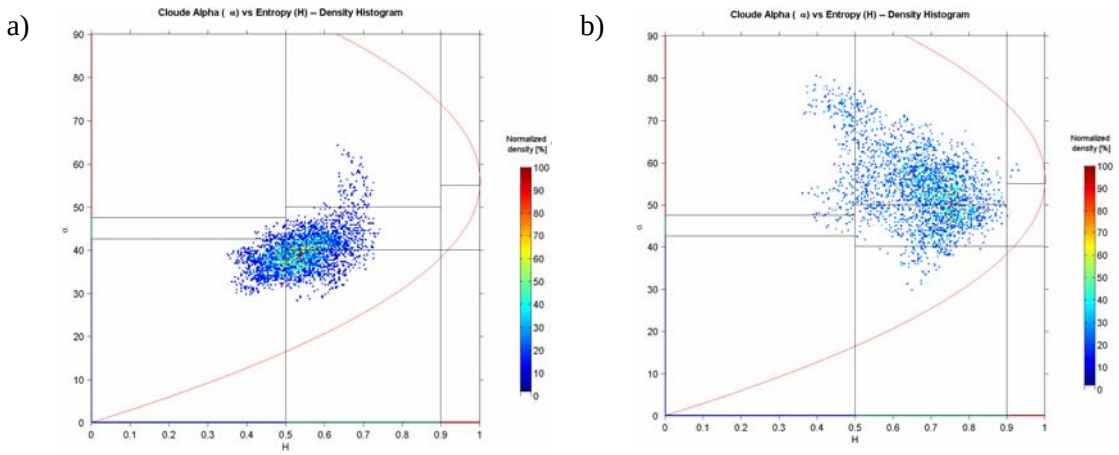

Figure 26: H/α analysis results for Dominion Victory, *20 Oct. 2005, l41p2 (a359): a) Ocean; b) Ship.*

4. Conclusions

The MARSIE trial has provided a vast and valuable data set that has and will be beneficial to the study of polarimetric signatures of ships. Moreover, DRDC Ottawa's ability to collect, process, and analyze the data is significantly better than has been the case for previous ship detection trials. Critical to the improvement in the lab's analysis performance has been the availability of the CHASP processor, which has proven to be a vital tool for the processing and analysis of moving ship targets from the EC CV-580 SAR.

There was an attempt to introduce an automated end-to-end processing chain to carry out the analysis and signature compilation of known ships. Unfortunately, time pressures in the reporting cycle prevented us from seeing this objective through to fruition. However, some elements of an automated chain were used, including target detection, clustering, and land masking through ADSS. A broader ADSS-based analysis chain continues to be a development goal of DRDC Ottawa, and will help to automate any subsequent MARSIE data analysis.

It was found that CHASP processing always improved the ship focus. This improvement is relevant to the PE SOR, which calls for the implementation of tools that enhance the recognition of target characteristics. In addition to focus improvement, CHASP was also able to reliably recover ship velocity information. However, in some cases CHASP was not be able to do this, most likely due to vessel non-linear motion (e.g., circular) imparted on the vessel by the underlying wave field. This could be a significant problem for smaller vessels in higher sea states; further analysis of the effects of non-linear motion is required.

The analysis suggests that CHASP-processed images of ships are a good proxy for RADARSAT-2 images of ships since RADARSAT-2 images will be less susceptible to defocus and the creation of azimuth ambiguities due to target motion.

No systematic attempt has been made so far to completely simulate RADARSAT-2 products from CHASP products, although simulation software is available for this process. The available simulation software amounts to degrading the spatial resolution and increasing the noise floor. Therefore, the polarimetric analysis results that are reported here are probably better than can be expected for RADARSAT-2's polarimetric modes.

The CHASP products include estimates of the Total RCS for each ship considered for each possible linear polarization state. The estimated values for the different polarizations were within the 41° to 67° incidence angle range, and are summarized as follows:

- Estimated HH polarization values were within 8 dB of a rule-of-thumb semi-empirical model for ship Total RCS;
- In general, the estimated HH and VV Total RCS values were within 4 dB of each other with VV values being slightly smaller than the HH values; and
- The estimated HV and VH Total RCS values were well-correlated and were about 10 dB smaller than the HH channel Total RCS values.

As the MARSIE analysis continues, more results of this nature will be collated so that the expected ship detection performance at cross polarization can be better quantified. This could be important for predicting and improving the utility of future SAR missions such as the proposed RADARSAT Constellation mission.

A total of 7 polarimetric images of ships from the MARSIE data set have been studied to date. It is clear that polarimetric SAR can be used for improving ship detection and to provide the surveillance operator with some additional classification information. For example, polarimetric SAR provides both phase and amplitude information, which can reduce the false alarm rate and permit the detection of smaller ships than is possible with single- or dual-channel SAR systems. Based upon the analysis of polarimetric imagery of *Dominion Victory*, more than a 10-fold reduction in the probability of missed detection was observed by introducing polarimetric channels, as compared to a single channel with the same probability of false alarm and all else held equal. Even larger improvements have been noted in other data sets. The increased detection capability offered by polarimetric and dual co-polarization supports PE requirements according to the PE SOR.

The results thus far demonstrate that polarimetric SAR provides information that goes beyond point target detection. For example, polarimetric data could improve the way in which candidate ship targets are recognized or classified in terms of:

- The size and shape of the vessel;
- The presence of any prominent structures that are "visible" in the image of the vessel (e.g., higher RCS structures, flight decks, king posts, etc.);
- The direction and speed of the vessel;
- The proximity to other vessels operating in a similar manner (especially for the case of smaller vessels); and
- The overall vessel structure from the nature and distribution of constituent elemental scatterers.

Four polarimetric target decomposition methods were applied to the MARSIE data in order to characterize the targets of interest in terms of their elemental scatterers. These methods included Pauli, Cameron, SSCM, and H/α. Each method provided different information about the target. It was apparent that the Cameron and SSCM methods offered the most potential for target classification since decomposition to a variety of scatterer types was possible, along with the spatial context of the various scatterers. The Pauli method, although very simple, could be used to efficiently distinguish the target of interest (predominantly double bounce scattering) from the surrounding ocean (predominantly single bounce scattering). The H/α method appeared to be less useful for ship classification since there was often overlap between the ocean and ship in some analysis zones. However, this method has recently been further developed [15] and these extensions should be investigated. For the same ship, the decomposition results do vary from case to case, no doubt depending on the geometry and ship velocity.

4.1 Recommendations

Based upon these results, aside from compiling the polarimetric signatures of other known vessels in the MARSIE data set, the following polarimetric issues are relevant to the Polar Epsilon SOR and CONOPS and are recommended for further study:

- The effects of acquisition geometry, target motion, environmental conditions, etc. on the observed polarimetric signature;
- The relationship between the elemental scatterer distributions between the Cameron and SSCM polarimetric decomposition methods;
- The relationship between target features and the elemental scatterers derived from the Cameron and the SSCM polarimetric decomposition methods;
- The feasibility of applying polarimetric decomposition methods to automatic target recognition (ATR) by using scattering elements or estimated scatterer orientation angles as target features in target classification software such as the ATR Workbench [7] or eCognition [1]; and
- The simulation of RADARSAT-2 polarimetry signatures from CHASP products.

Polar Epsilon should consider using the MARSIE trial dataset to further enhance their operational system's target detection and classification performance and to reduce false alarm rates. There is strong evidence that a significant improvement could be realized as compared to lower resolution, single polarization acquisition modes.

Given the rather narrow swath of the RADARSAT-2 polarimetric modes, it is recommended that Polar Epsilon use polarimetry for surveillance of spatially constrained maritime areas of interest including:

- Choke points (such as most of the North West Passage);
- Straits, channels, and confined waterways;
- Specific fishery zones;
- Port surveillance; and
- Arctic Archipelago surveillance.

References

[1] Anon.; Statement of Operational Requirement, 00000625, Polar Epsilon (Joint Space-Based Wide Area Surveillance and Support); Project Sponsor: Deputy Chief of the Defence Staff, 13 Oct. 2004.

[2] Benz, U., and E. Pottier; Object Based Analysis of Polarimetric SAR data in Alpha-Entropy-Anisotropic Decomposition by using Fuzzy Classification by eCognition; Proc. 2001 International Geoscience and Remote Sensing Symposium (IGARSS2001), 9-13 July 2001, Sydney, Australia, Vol. 3, pp 1427-1429.

[3] Cameron, W.L., N.N. Youssef, and L.K. Leung; Simulated Polarimetric Signatures of Primitive Geometrical Shapes; *IEEE Transactions on Geoscience and Remote Sensing*, Vol. 34, No. 3, pp 793-803, 1996.

[4] Cloude, S.R., and E. Pottier; A Review of Target Decomposition Theorems in Radar Polarimetry; *IEEE Transactions on Geoscience and Remote Sensing*, Vol. 34, No. 2, pp 498-518, 1996.

[5] Cloude, S.R., and E. Pottier; An Entropy Based Classification Scheme for Land Applications of Polarimetric SAR. *IEEE Transactions on Geoscience and Remote Sensing*, Vol. 35, No. 1, pp 68-78, 1997.

[6] Dias, J.M.B., and P.A.C. Marques; Multiple moving target detection and trajectory estimation using a single SAR sensor; *IEEE Transactions on Aerospace and Electronic Systems*, Vol. 39, No. 2, pp 604-624, 2003.

[7] English, R.A., S.J. Rawlinson, and N.M. Sandirasegaram; ATR Workbench for Automating Image Analysis; Algorithms for Synthetic Aperture Radar Imagery X, Proceedings of SPIE Vol. 5095, pp 349-357, 2003.

[8] English, R.A., C. Liu, D. Schlingmeier, and P.W. Vachon; CoCoNaut Polarimetric SAR Signature Trial; DRDC Ottawa TM, in preparation, April 2006.

[9] Kirscht, M.; Detection and Imaging of Arbitrary Moving Targets with Single-channel SAR; *IEE Proceedings on Radar, Sonar, and Navigation*, Vol. 150, No. 1, pp 7-11, 2003.

[10] Liu, C., L. Gallop and D. Schlingmeier; Quest-2003 Polarimetric Signature Trial; DRDC Ottawa TM 2004-207.

[11] Liu, C., N. Sandirasegaram, R.A. English and D. Schlingmeier; MarCoPola Polarimetric SAR Trial: Signatures of Multiple Vessels with Aligned Operating Conditions; DRDC Ottawa TM 2005-134.

[12] Liu, C., P.W. Vachon, and G.W. Geling; Improved ship detection using polarimetric SAR data; *Canadian Journal of Remote Sensing*, Vol. 31, No. 1, pp 122-131, 2005.

[13] Liu, C., and A. Meek; Likelihood Ratio Test Polarimetric SAR Ship Detection Application; DRDC Ottawa TM 2005-243.

[14] Livingstone, C.E., A.L. Gray, R.K. Hawkins, P.W. Vachon, T.I. Lukowski, and M. Lalonde; The CCRS airborne SAR systems: Radar for remote sensing research; *Canadian Journal of Remote Sensing*, Vol. 21, No. 4, 1995, pp 468-491.

[15] Pottier, E.; Polarimetry: From Basics to Applications, IGARSS 2003, Toulouse, France, 21-25 July 2003.

[16] Redding, N.J., D.I. Kettler, G. Blucher, and P.G. Perry; The Analysts' Detection Support System for Deploying a Network of Target Detection and Recognition Algorithms in SAR Exploitation; *Proceedings of the International Radar Conference*, Adelaide, 3-5 September 2003, pp. 448-453.

[17] Soumekh, M.; Reconnaissance with Ultra Wideband UHF Synthetic Aperture Radar; *IEEE Signal Processing magazine*, pp. 21-40, 1995.

[18] Touzi, R., and F. Charbonneau; Characterization of Target Symmetric Scattering Using Polarimetric SARs; *IEEE Transactions on Geoscience and Remote Sensing*, Vol. 40, No. 11, pp 2507-2516, 2002.

[19] Touzi, R., F. Charbonneau, R.K. Hawkins, and P.W. Vachon; Ship detection and characterization using polarimetric SAR; *Canadian Journal of Remote Sensing*, Vol. 30, No. 3, pp 552-559, 2004.

[20] Vachon, P.W., J.W.M. Campbell, C. Bjerkelund, F. W. Dobson, and M.T. Rey; Ship detection by the RADARSAT SAR: Validation of detection model predictions; *Canadian Journal of Remote Sensing*, Vol. 23, No. 1, 1997, pp 48-59.

[21] Vachon, P.W., and M.V. Dragošević; COASP and CHASP Processors for Strip-map and Moving Target Processing of EC EV-580 Synthetic Aperture Radar Data: Algorithms and Software Description; DRDC Ottawa TM 2006-066, May 2006, 128 pages.

[22] Vachon, P.W., R.A. English, and J. Wolfe; Validation of RADARSAT-1 Vessel Signatures with AISLive Data; in press, *Canadian Journal of Remote Sensing*, 2006.

[23] Yeremy, M., J.W.M. Campbell, K. Mattar, and T. Potter; Ocean Surveillance with Polarimetric SAR; *Canadian Journal of Remote Sensing*, Vol. 27, No. 4, 2001, pp 328-343.

Annex A EC CV-580 SAR Flight Activity Summary[4]

A.1 Trial Objectives

Using the Environment Canada (EC) CV-580 Polarimetric synthetic aperture radar (SAR):

- To acquire Polarimetric SAR data of Maritime Sensor Integration Experiment (MARSIE) Trial[5] events as a RADARSAT-2 polarimetric mode proxy sensor;
- To acquire Polarimetric SAR data for analysis of signatures of known vessels (i.e. both the vessel and its motion are known), especially for smaller boats;
- To acquire Polarimetric SAR data to contribute to the ongoing assessment by DRDC Ottawa and Polar Epsilon of the RADARSAT-2 Polarimetric modes for vessel detection and classification.

A.2 Trial Plan

To achieve these objectives, the intention was to carry out five flights of the EC CV-580 Polarimetric SAR during the MARSIE Trial. The flight program was to be comprised of over flights of two Rendezvous events (Rendezvous' 2 and 3, scheduled for 14 and 21 Oct. near N45.5 W51.0), two transfer events (Transfers 2 and 3, scheduled for 17 and 24 Oct. near Janvrin Point), and 1 RCMP training event (scheduled for 18 Oct. near Janvrin Point). In each case we expected to obtain imagery of the participating fishing trawler played by *Dominion Victory*, outfitted with a ship motion sensing package, three small boats near the Janvrin Point location, each outfitted with GPS receivers, other participating vessels including HMCS *Toronto* and the *Strait Signet*, and other larger vessels of opportunity, as identified in AIS data. All events would be imaged at a nominal incidence angle of 50°, including a SAR Calibration Site that would be established at Charlottetown.

A.3 Actual Trial Events

Aircraft and radar readiness delayed our deployment to YYG (Charlottetown) until 16 Oct. Furthermore, the time of the planned Rendezvous events were moved ahead by about one day (to 13 and 20 Oct.) due to revisions to the ACL sailing schedule. And furthermore, foul weather and Fishing Trawler (i.e., *Dominion Victory*) readiness conspired to cause Rendezvous 2 to be completely missed (i.e., the event never happened as planned). Instead, we decided to combine imaging of the second transfer event with several passes over *Dominion Victory* on 17 Oct. as she

[4] Report prepared by P.W. Vachon and circulated informally on 27 October 2005.

[5] The MARSIE Trial consisted of a Maritime Incursion Scenario (MIS) that was played out 3 times with 1 week intervals off the East Coast of Canada in October 2005. In each MIS, a Freighter carried a Contraband Package from Europe to Canada, which it threw overboard at the Rendezvous Point (nominally N45.5° W51°) on the Grand Banks. A Fishing Trawler recovered the Contraband Package and transported it to Chedabucto Bay, where the Contraband Package could be transferred from the Fishing Trawler to shore near Janvrin Point by various smaller boats. Key imaging opportunities included the 3 Rendezvous events and the 3 Transfer events.

was en route back to the Rendezvous Point. However, *Dominion Victory*'s departure was delayed until 18 Oct., so this plan was commuted to 18 Oct. and combined with imaging of the RCMP Training exercises. Unfortunately, the Medium Power Amplifier (MPA) failed during Flight 2, forcing use of the Low Power Amplifier (LPA) for the balance of the trial. The MPA provides roughly 10 times the transmitted power of the LPA, so this failure increases the noise floor of the acquired radar imagery by about 10 dB. Rendezvous 3 occurred more-or-less as projected except that *Dominion Victory* proceeded to St. John's rather than back to Chedabucto Bay following retrieval of the Contraband Package due to a poor weather forecast. Transfer 3 occurred more or less as projected with *Dominion Victory* and *Strait Signet* participating in Chedabucto Bay. The actual flights and key MARSIE Trial events imaged are summarized in Table 36.

Table 36: Summary of EC CV-580 Flights for MARSIE.

Flight	Date Oct. 2005	$T_{takeoff}$ [UTC]	$T_{landing}$ [UTC]	Elapsed [hours]	AIS	Comments
	16	17:22	20:51	3.5	Yes	Transit from YOW to YYG; Calibration Site at YYG; troubleshooting of RTP2 Azimuth Correlator problems (no opportunity to test MPA).
1	17	12:07	16:17	4.2	Yes	Transfer 2/RCMP Training; airborne photography support; Calibration Site at YYG; test of MPA.
2	18	11:59	17:16	5.3	Yes	Transfer 2/RCMP Training; airborne photography support; *Dominion Victory*; Calibration Site at YYG.
	20	12:26	13:53	1.5	Yes	Transit from YYG to YYT to refuel.
3	20	17:00	22:37	5.6	Yes	Rendezvous 3 (*Dominion Victory*, *Atlantic Concert*), N46:52 W51:31, 17:30 UTC; Calibration Site at YYG.
4	24	22:23	02:06	3.7	Yes	Transfer 3; Calibration Site at YYG; landing on 25 Oct.
	25	16:43	19:27	2.8	Yes	Transit from YYG to YOW; Calibration Site at Connaught Range.
Total				26.6		

Notes for Table 36:

- Automatic Identification System (AIS) Data recording onboard the EC CV-580 is summarized below.
- YOW is Ottawa airport; YYG is Charlottetown airport; YYT is St. John's airport.
- Participating Vessels are summarized below.
- Transfer and RCMP Training events occurred near the trial site at Janvrin Point (N45.53° W61.20°), which is located on Janvrin Island in Chedabucto Bay (most activities took place in or near Macdonald's Cove, the body of water between Janvrin Point and Thomas Head, centred roughly on N45.54° W 61.19°; all flight lines were centred on this point and were designed with a nominal incidence angle of 50°).
- Airborne Photography support is summarized below.

A.4 MARSIE Trial Player Vessels

The following vessels had scripted roles in the MARSIE Trial. Certain of them were outfitted with special equipment for the Trial, as noted.

- HMCS *Toronto*

- Halifax-Class Multi-Role Patrol Frigate
- Length: 134 m
- Equipment: AIS Receiver
- http://www.navy.forces.gc.ca/toronto/home/index_e.asp

- CCGS *E. Cornwallis*
  - Light Icebreaker – Major Navaids Tender
  - Length: 83 m
  - Equipment: AIS Transponder
  - http://www.ccg-gcc.gc.ca/fleet-flotte/vessels-navires/ships_e.asp?refNum=C-2
- *Dominion Victory*
  - Multi-Purpose Diving Support Vessel
  - Operator: Dominion Diving Ltd.
  - Length: 25 m
  - Equipment: ship motion sensor (SMS) system and AIS-in-a-Box from DRDC Atlantic
  - MARSIE Trial role: Fishing Trawler
  - http://www.dominiondiving.com/index.html
  - http://forms.cta-otc.gc.ca/CVIS/Ship_e.cfm?ShipID=320748
- *Strait Signet*
  - Offshore Support/Research Vessel
  - Operator: Superport Marine Services Ltd.
  - Length: 32 m
  - MARSIE Trial role: backup Fishing Trawler for Chedabucto Bay activities
  - http://www.superport.ns.ca/signetlyt.pdf
  - http://forms.cta-otc.gc.ca/CVIS/Ship_e.cfm?ShipID=328504
- *Atlantic Concert*
  - Container Vessel
  - Operator: Atlantic Container Line (ACL)
  - Length: 292 m
  - Equipment: AIS transponder
  - MARSIE Trial Role: the third ACL freighter participating in the MARSIE Trial, she dropped the Contraband Package for Rendezvous 3 while en route from Liverpool to Halifax
  - http://www.aclcargo.com/vesselSpecs.php

- Transfer Event boats
  - Equipment: GPS receivers from DRDC Atlantic
  - MARSIE Trial role: transfer of Contraband Package from Fishing Trawler to shore
    - *Cajun Spirit*; 11 m sailboat
    - *J. Franklin Wright*; 13 m fishing boat
    - RHIB
    - Several zodiacs

A.5 SAR Calibration Site

DRDC Ottawa (D. Schlingmeier, L. Gallop, and either D. Lamothe or G. Duff) established an EC CV-580 SAR Calibration Site in an open field near the Charlottetown airport passenger terminal. A reference survey monument near Souris (about 100 km away) was used as the absolute position reference. The Calibration Site consisted of two DRE-series trihedral corner reflectors (TCRs) mounted on tripods, two active radar calibrators (ARCs) (borrowed from CCRS) and an Ashtech GPS receiver. The four calibration devices were setup along a 150 m long line centred at N46.28 W 63.14 (east of Brackley Road, south of Sherwood Road at an elevation of 54.6 m above mean sea level), oriented at 91° T, with calibration devices (ordered west to east) TCR1 (DREP), ARC1 (1-2756), TCR2 (DREV), and ARC2 (1-2542). The calibration devices were oriented parallel to the line, looking north, with an incidence angle of 50°. The Calibration Site was imaged twice as the last activity of each flight (once left looking on a heading of 271° T and once right looking on a heading of 91° T). The site was not secure; the TCRs were left deployed, but the ARCS and GPS receiver were re-deployed prior to each flight. The GPS receiver was operating in time for each EC CV-580 take-off. The Calibration Site activities were very successful; both ARCs were observed each time that the site was imaged.

A.6 SAR Data QC

During the transit from YOW to YYG, several data takes, including two passes over the Calibration Site at YYG, were acquired. This permitted troubleshooting and correction of a problem with the Azimuth Correlator in RTP2, but did not allow time to test the MPA, which was eventually tested at the end of Flight 1. Following the transit to YYG and the first three MARSIE Trial flights, the raw SAR signal data tapes were sent by courier to R. Hawkins (CCRS) for QC testing. In each case, the QC results for the raw SAR signal data were reported as good.

A.7 AIS Data Reception on the EC CV-580

One of DRDC Ottawa's AI3000 AIS Receiver was installed on the EC CV-580 for the duration of the MARSIE Trial. During each flight, serial AIS data from the AI3000 AIS Receiver were recorded on a notebook computer running Windows XP using the ShipPlotter version 8.3 software; software configuration and operating procedures were provided by D. Brookes (DRDC Ottawa). Separate log files are available for each flight date. Table 37 indicates the ships that were seen in the AIS data within the areas of interest; each ship was verified through the ISR

(Internet Ships Registry) database (i.e., Lloyd's Registry) when possible. Although the exact useful range of the AIS equipment on the EC CV-580 has not been quantified, it can be stated that it was possible to receive AIS data from ships that were 100's of kilometres away.

Table 37: Summary of AIS data received on the EC CV-580 for MARSIE Trial areas of interest.

Ship	IMO	Length [m]	Type	Comments
17 Oct 2005; Chedabucto Bay				
Gulf Service	7902051	42	Tug	Not found in ISR database.
Champion	9252979	238	Crude Oil Tanker	
Eastern Power	8819225	225	Bulk Cargo Carrier	
18 Oct. 2005; Chedabucto Bay				
Gemini Voyager	9174218	333	Crude Oil Tanker	
Ambassador	8016653	222	Bulk Cargo Carrier	
Eastern Power	8819225	225	Bulk Cargo Carrier	
Champion	9252979	238	Crude Oil Tanker	
20 Oct. 2005; Grand Banks				
Atlantic Concert	8214164	292	Container/Ro-Ro Cargo Ship	
24 Oct 2005; Chedabucto Bay				
Seapromise	9247479	183	Chemical/Products Tanker	
Eagle Boston	9111620	253	Crude Oil Tanker	
Atlantic Fir	9324916	31	Tug	
Chepstow	9142966	100	LPG Tanker	
Atlantic Beech	6912427	33	Tug	Not found in ISR database.

Notes for Table 37:

- Call sign and MMSI are also available for unique vessel identification.
- Length overall is noted.

A.8 Airborne Photography

Airborne Photography was carried out for Flights 1 and 2 by J. Lang (DRDC Ottawa) from a Cessna aircraft that operated in the Janvrin Point area. The flights coincided with the duration of the EC CV-580 flights. The objective was, for validation purposes, to photograph any targets that might be imaged by the airborne SAR within the trial area. These flights including sample photographs are summarized in a separate report[6].

[6] See Annex B.

A.9 Commercial Satellite Imagery

RADARSAT-1 and Envisat ASAR imagery were also acquired during the MARSIE Trial. The EC CV-580 flights were timed with MARSIE Trial events (e.g., Rendezvous or Transfer) rather than satellite pass times. The acquired CSI are summarized in a separate report[7].

A.10 Baseline EC CV-580 SAR Configuration and Operation

- C-band Polarimetry
- MPA, if available
- SAW^{-1}: Out
- Mode: Nadir
- Motion Compensation: Off
- Range Gate Delay Update: Off
- Sensitivity Time Control: Test
- Depression Angle: 35°
- Gains (coarse and fine): dependent on amplifier available and surface wind speed (i.e. backscatter)
- Real-Time Processing: Dual-Near (HH on RTP1, VV on RTP2, checking both periodically)
- MAID and HSR recording monitored periodically throughout each flight
- Routine check of RTP2 output and presence of signal in all channels
- Noise recording following each pass: 30 seconds of noise; plus 30 seconds with maximum fine gains; plus 30 seconds from the built-in test equipment (i.e., BITE noise source)

A.11 Flight 1

The plan was to acquire 6 passes over Janvrin Point, imaging the transfer/training events 6 times (with 6 different aspect angles), followed by two passes over the calibration site at YYG. The CV-580 was assigned a nominal operation time of 9:30 to 11:00 (local time, 12:30 to 14:00 UTC) over Janvrin Point, coincident with an airborne photography flight. The airspace restriction was actually for the airborne photography flight, to prevent conflict with a UAV that was scheduled for launch at 11:00 (it turned out that the launch never happened and the photography activities continued until 11:30). HMCS *Toronto*, CCGS *E. Cornwallis*, *Dominion Victory*, *Strait Signet*, and the 3 small transfer boats were all expected to be operating in the Janvrin Point area at the time of the flight. The first line was flown with SAW^{-1} In to permit inspection of the imagery. All subsequent lines were flown with SAW^{-1} Out to reduce the dynamic range of the raw SAR data to allow recording of signal data from the larger vessels in the area with less danger of signal data saturation. Two lines were lost due to a MAID failure; it was judged that the lines could not

[7] Contact P.W. Vachon for more information.

be re-flown at that time due to fuel and alternate airport uncertainties. One calibration line was lost due to a MAID failure, but it was repeated. The MPA was successfully tested following a swap over from LPA (requiring about 20 minutes) during the third Calibration line at the end of the flight.

Table 38: Summary of Flight 1, 17 Oct. 2005.

l	p	Hdg [deg T]	Look	SAW^{-1}	T_{on} [UTC]	T_{off} [UTC]	Comments
21	1	180	Left	In	12:45:04	12:51:47	LPA; Janvrin Point, MAID failure, but line completed; data probably not usable.
22	**2**	45	Left	Out	13:05:48	13:12:43	LPA; Janvrin Point.
23	**3**	270	Left	Out	13:26:20	13:31:21	LPA; Janvrin Point.
24	**4**	90	Right	Out	13:43:42	13:48:21	LPA; Janvrin Point.
25	5	225	Right	Out			LPA; MAID failure, line aborted.
26	**6**	0	Right	Out	14:24:37	14:29:36	LPA; Janvrin Point, planned line was shifted 1 nm west.
27	**7**	271	Left	Out	14:48:49	14:54:21	LPA; calibration.
28	8	91	Right	Out			LPA; MAID failure, line aborted.
28	**9**	91	Right	Out	15:26:37	15:30:39	LPA; calibration, repeat of l28p8.
27	10	271	Left	In	15:56:00	16:01:25	MPA test; calibration.

Notes for Table 38 through Table 41:

- Processing priority for trial data are indicated by bold Line (l) and Pass (p) numbers.
- The aircraft heading (Hdg) is a nominal value.
- SAW^{-1} In indicates that hardware range compression using a surface acoustic wave (SAW) device was enabled; SAW^{-1} Out indicates that range compression will be done post flight in software. SAW^{-1} Out reduces the dynamic range of the raw data, thus reducing the risk of raw data saturation, but at the expense of a reduced ability to carry out real-time QC of radar operation (i.e., the RTP imagery are defocused).
- T_{on} is the "on" time for the helical scan recorder (HSR) for signal data recording.
- T_{off} is the transmitter "off" time; transmitter off is normally followed by noise recording for radar calibration purposes.

A.12 Flight 2

The plan was to acquire 6 passes over Janvrin Point, imaging the transfer/training events 6 times (with 6 different aspect angles), followed by 3 passes over *Dominion Victory* as she was in transit to the Rendezvous Point to search for the Contraband Package that was dropped a few days earlier for Rendezvous 2, followed by two passes over the calibration site at YYG. Again, the CV-580 was assigned a nominal operation time of 9:30 to 11:00 (local time, 12:30 to 14:00 UTC), coincident with an airborne photography flight. The airspace restriction was actually for the airborne photography flight, to prevent conflict with a UAV that was scheduled for launch at 11:00. HMCS *Toronto*, CCGS *E. Cornwallis*, *Dominion Victory*, *Strait Signet*, and the 3 small transfer boats were all expected to be operating in the Janvrin Point area during this flight. The 6 passes over Janvrin Point were very successful and the radar appeared to work well. The CV-580 was forced to change flight levels several times during the early passes due to aircraft icing problems. *Dominion Victory* might be visible in several of the Janvrin Point passes, especially the east-west oriented lines. Unfortunately, several problems arose with the *Dominion Victory* passes towards the end of the flight. Real time planning for the moving target acquisitions proved

to be difficult. Furthermore, a flight management system problem arose after Pass 8 and persisted for nearly an hour, resulting in a gap of nearly one hour in imaging activities. Once these issues were resolved, the flight program continued, but the MPA promptly failed. Considering the time needed to change over to LPA (roughly 20 minutes), we were forced to return to YYG to complete the calibration lines with the LPA. All lines were flown with SAW^{-1} Out. *Dominion Victory* may have been imaged 3 or more times during this flight.

Table 39: Summary of Flight 2, 18 Oct. 2005.

l	p	Hdg [deg T]	Look	T_{on} [UTC]	T_{off} [UTC]	Notes
31	**2**	180	Left	12:39:47	12:45:59	MPA; Janvrin Point; planned line was shifted 1 nm west.
32	**3**	45	Left	13:00:47	13:07:38	MPA; Janvrin Point.
33	**4**	270	Left	13:20:08	13:26:10	MPA; Janvrin Point; *Dominion Victory* near beginning of line?
33	**5**	90	Right	13:43:08	13:49:09	MPA; Janvrin Point; line extended east, *Dominion Victory* near end of line?
32	**6**	225	Right	14:00:28	14:08:00	MPA; Janvrin Point;
31	**7**	0	Right	14:18:06	14:23:40	MPA; Janvrin Point; planned line was shifted 1 nm west.
34	**8**	135	Left	14:46:29	14:52:00	MPA; line planned for *Dominion Victory* at 45° aspect.
35	9	270	Right			MPA failure; line aborted, return to YYG.
37	**10**	271	Left	16:34:47	16:41:31	LPA; calibration.
37	**11**	91	Right	16:52:17	16:57:40	LPA; calibration.

A.13 Flight 3

Due to the northward change in the Rendezvous Point location to N46:52 W51:31, the plan became to move the EC CV-580 to St. John's the morning of 20 Oct., to re-fuel there, then to over fly the Rendezvous event with 5 passes starting at 17:30 UTC, the revised time of Rendezvous 2, followed by transit back to Charlottetown with two passes over the calibration site at YYG.. The over flight of the Rendezvous was meant to be composed of one pass over *Atlantic Concert* (parallel to her track), followed by four passes over *Dominion Victory* (in transit to Chedabucto Bay following the Contraband Package recovery, i.e., moving target with aspect angles of 180°, 45°, 90°, and 0°). Two lines were added to this program to allow time for recovery of the Contraband Package and to make up for at least two lines over *Dominion Victory* that were lost during Flight 2. As of the departure from YYG, we were aware that the *Dominion Victory* and HMCS *Toronto* were both in the vicinity of the revised Rendezvous Point. We were also expecting MPA (i.e., Aurora) and PAL participation near the Rendezvous location. Of course, it took *Dominion Victory* rather longer than anticipated to recover the Contraband Package. Furthermore, we learned that *Dominion Victory* would go to St. John's following pickup of the Contraband Package since there was a gale warning for her routing back to Chedabucto Bay; we were given a new heading of 331° T for their routing back to St. John's. Therefore, to allow time for the Contraband Package recovery and in order to get additional images of the *Dominion Victory*, several lines were dynamically planned and added to the program. Due to strong headwinds and turbulence at altitude, the Calibration Site was imaged at a lower altitude than during other flights. All data were acquired with LPA and SAW^{-1} Out on this flight.

Table 40: Summary of Flight 3, 20 Oct. 2005.

l	p	Hdg [deg T]	Look	T_{on} [UTC]	T_{off} [UTC]	Notes
41	**1**	75	Right	17:29:37	17:33:26	Over Rendezvous Point at 17:30; Vessels noted in radar data; delayed response to BITE On command.
41	**2**	255	Left	17:50:10	17:55:44	Vessels noted in radar data.
41	**3**	75	Right	18:09:55	18:14:17	Vessels noted in radar data.
42	**4**	286	Left	18:28:22	18:33:30	Vessel noted in radar data.
42	**5**	106	Right	18:43:??	18:48:47	*Dominion Victory* visual with a reported heading of 260° T.
44	**6**	350	Left	19:10:40	19:14:33	*Dominion Victory* recovering buoy, may not have been imaged.
45	**7**	286	Left	19:39:23	19:44:33	Attempted 45° aspect; *Dominion Victory* visual; reported new track of 316° T rather than 331° T as expected.
37	**8**	271	Left	21:54:05	21:57:38	Calibration; 16,000', line re-planned.
37	**9**	91	Right	22:11:18	22:14:17	Calibration; 16,000', line re-planned.

A.14 Flight 4

The plan was to acquire 6 passes over Janvrin Point (with 6 different aspect angles), followed by two passes over the calibration site at YYG. The CV-580 was assigned a nominal operation time of 18:00 to 19:30 (local time, 21:00 to 23:30 UTC) corresponding to night time activities. Line 1 was re-planned in comparison to that of Flights 1 and 2 so that it looked towards the west rather than the east. *Dominion Victory*, *Strait Signet*, and the 3 small transfer boats were expected to be operating in the Janvrin Point area. Departure was delayed by 1.5 hours due to a problem with the ADC board in RTP2 (eventually solved by a swap of the ADC boards between RTPs). Janvrin Operations (R. Schwartz) advised that operations could continue until midnight (local), if necessary, but with zero contingency for deferring the activities until the next day. The mission was flown at 19,000' rather than the planned 22,000' due to moderate to severe turbulence at higher altitudes, except for the Calibration Site lines which were flown at 17,000' for the same reason. There was a delayed response to the BITE On command for all lines. All data were acquired with LPA and SAW^{-1} In on this flight. The latter was chosen since we were expecting to image smaller boats only and this choice would permit real-time verification that boats were present and visible in the real-time data.

Table 41: Summary of Flight 4, 24/25 Oct. 2005.

l	p	Hdg [deg T]	Look	T_{on} [UTC]	T_{off} [UTC]	Notes
1	1	180	Right	22:52:57	22:57:29	Janvrin Point; 6 boats reported in MacDonald's Cove, 2 visible in real-time data; range/azimuth blocks of focus/defocus (cf. 24 Sept. 2004 CoCoNaut data acquired off Tofino); data probably not usable.
2	2	45	Left	23:10:14	23:14:52	Janvrin Point; at least 2 boats visible in real-time data; Motion Compensation fault causes lose of BITE noise; range/azimuth blocks of focus/defocus persists; data probably not usable; ERU reset.
3	**3**	270	Left	23:26:10	23:32:48	Janvrin Point; at least 4 boats visible in real-time data; focus problem resolved.

3	**4**	90	Right	23:44:00	23:49:23	Janvrin Point; at least 4 boats visible in real-time data; BITE noise lost.
2	**5**	225	Right	00:00:32	00:05:03	Janvrin Point; boats visible.
1	**6**	0	Left	00:16:25	00:20:29	Janvrin Point; boats visible.
2	7	225	Right	00:31:56	00:37:04	Janvrin Point; make up for loss of l2p2 (repeat of l2p5); range/azimuth blocks of focus/defocus returns; line aborted; ERU reset.
1	**8**	0	Left	00:47:57	00:51:15	Janvrin Point; make up for loss of l1p1 (repeat of l1p6); boats visible.
4	**9**	271	Left	01:25:12	01:30:15	Calibration; line moved 1.0 nm south relative to plan; ARC "blooming" on Cross Polarization Channel.
4	**10**	91	Right	01:43:23	01:47:30	Calibration; line moved 1.0 nm south relative to plan; ARC "blooming" on Cross Polarization Channel.

A.15 Summary

The EC CV-580 SAR program for the MARSIE Trial faced many logistic, aircraft, and radar problems. Nevertheless, the program appears to have returned 23 successful radar passes (4 on 17 Oct., 7 on 18 Oct., 7 on 20 Oct. and 5 on 24 Oct.) that include known vessels and specific MARSIE Trial events. Also, 11 passes over the Calibration Site at YYG were acquired; Calibration Site operations were flawless.

A.16 EC CV-580 SAR Data Analysis Plans

- The SAR signal data (all MARSIE Trial passes and Calibration Site passes) will be stripped from HSR to Exabyte tape by MDA Geospatial Services (formerly RSI).
- All passes will be processed to image form and calibrated using COASP and associated calibration routines; polarimetric vessel detection software will be used to locate vessels of interest; Polarimetric SAR images of key MARSIE Trial events will be prepared for distribution.
- Position and motion records for key participating vessels will be obtained and correlated temporally and spatially with the EC CV-580 SAR coverage and detected vessels.
- Vessels of interest will be extracted and re-focussed with CHASP; SAR-derived motion parameters will be compared to available vessel motion data.
- Standard polarimetric signatures will be compiled for each known and refocused vessel; results will be interpreted in the RADARSAT-2 polarimetry context.

A.17 Acknowledgements

The successful EC CV-580 SAR program described in this report was made possible by the expertise and dedication of many individuals. In particular, B. Healey and W. Chevrier (pilots); R. Whetter and D. Percy (SAR operators); M. Kalus (aircraft engineer); J. Zandbergen (mission planner); R. Hawkins of CCRS (EC CV-580 SAR consultant); Radar Systems Section engineers and technicians; D. Schlingmeier, L. Gallop, D. Lamothe, and G. Duff (Calibration Site

operations and trial logistics); G. Geling and A. Cond (MARSIE Trial coordination and Trial Operations); and the entire MARSIE Trial team.

A.18 Lessons Learned

- Onboard AIS data were very helpful for tracking trial activities and observing what was happening during the trial. For dynamic flight line planning, it would have been very beneficial to have been receiving real-time AIS data from HMCS *Toronto*, *Dominion Victory*, *Strait Signet*, and even the smaller transfer event boats. The AIS recording software can accommodate GPS input, which would be helpful since the AIS platform location is changing.
- The EC CV-580 mission planning software (SARNAV, developed at CCRS ca. 1990) is antiquated and cumbersome for real-time flight line planning, especially when dealing with moving targets; this resulted in several lost lines and considerable lost time in flight. If DRDC Ottawa is going to continue to use this facility, then flight planning operations must be improved.
- A local Ottawa mission should be considered prior to the primary mission to exercise the Calibration Site and radar equipment. Perhaps this should be planned routinely as a direct trial expense? This would force aircraft and radar readiness in advance of departure for actual trial activities and would reduce risk during the actual trial activities. The testing should involve data QC and processing of raw SAR signal data to image form.
- MAID (housekeeping data) recording failed several times, resulting in several lost flight lines. We are certainly looking forward to the new disk-based data recording system for the EC CV-580 SAR that is being developed by DRDC Ottawa. Unfortunately the new recording system was not ready for this trial, but should be commissioned during the fall of 2005. Availability of this system will permit routine operation with SAW^{-1} In (improving data QC) and opens up the possibility of polarimetric data processing during a trial on a Linux-based PC. Furthermore, this will obviate the need for deploying a data stripper to the field or returning raw SAR signal data tapes to Ottawa for tape verification.
- The BITE On command circuitry failed to respond at the end of certain flight lines on 20 and 24 Oct. until a gentle vibration was manually applied by hand to the ERU control board. This board was replaced prior to MARSIE by the X-Band equivalent following modifications by RS; this new board responded in the same way as the original C-Band board. This suggests that this problem, which has persisted for a long time, originates in the back plane of the ERU card cage.
- During the flight of 24/25 Oct., the real time imagery showed range/azimuth blocks with a focus/defocus pattern that was cured for the subsequent pass by resetting the ERU. The data were acquired with SAW^{-1} In, permitting real-time data QC. This pattern appears to be the same as was observed on 24 Sept. 2004 (CoCoNaut) when the data were acquired with SAW^{-1} Out; real-time data QC was not possible in that case. We need to watch for this effect in the SAW^{-1} Out data that were acquired during MARSIE. The observed pattern could be evidence of oscillator drift, for example. It is recommended that the ERU be reset prior to each pass.

- The detailed scripting that was carried out in advance of the trial was not closely followed as only the basic trial activities were conserved. Actual events were invariably negotiated on a day-to-day and case-by-case basis via telephone. The Communications Plan, which was circulated with the Trial Plan as Annex G, was the most important document during the Trial.
- To reduce the cost of conducting trials, DRDC Ottawa should look into the concept of deploying a minimal (i.e., "lean-and-mean") Calibration Site, which might be composed of one TCR, one ARC, and one GPS receiver, perhaps with just one or two attendants, and just a single pass over the Calibration Site. Also, DRDC Ottawa needs to study alternate sources or approaches to acquiring reference GPS data. Calibration Site logistics were greatly simplified by using a consistent Look direction and a single incidence angle.
- Radar and data QC support provided by R. Hawkins (CCRS) was invaluable during the preparation and execution phases of this trial.

Annex B Summary of Photo Survey Flights for MARSIE[8]

B.1 Introduction

As part of the MARSIE Trial, Photo Survey Flights were carried out from a Cessna 172 aircraft operated by Eastern Air Services Inc. out of Trenton, Nova Scotia. Flight operation were carried out in the Janvrin Point area at the same time as EC CV-580 SAR flights that occurred on 17 and 18 Oct. 2005, as summarized in Table 42. The objective of the Photo Survey Flights was, for validation purposes, to photograph any targets that might be imaged by the airborne SAR within the trial area.

Table 42: Summary of coincident Photo Survey and EC CV-580 flights during MARSIE.

Date Oct. 2005	Photo Survey Start [UTC]	Photo Survey Stop [UTC]	EC CV-580 Start [UTC]	EC CV-580 Stop [UTC]
17	12:59	14:21	13:05	14:29
18	12:41	13:59	12:40	14:23

Notes for Table 42:

- Photo Survey Start and Stop times correspond to the times of the first and last photographs taken in the Janvrin Point area, respectively.
- EC CV-580 Start and Stop times correspond to the start time of the first successful SAR pass over Janvrin Point and the end time of the last successful SAR pass over the Janvrin Point area, respectively.

On both days it was overcast and rather dark for photography. It was necessary to use a high ISO setting on the camera in order to shoot at a high enough shutter speed to minimize camera vibrations. The resulting images are slightly grainy, but show good detail of the targets. Sample photographs follow below[9].

B.2 17 Oct. 2005

Photographs are available of:

- 18 vessels (MARSIE players and targets of opportunity) and 2 buoys;
- Janvrin Point site, including test vehicles, parked cars, Coyotes, UAV launch site, and hyperspectral targets (fabric squares on the ground).

In all, 548 photographs were taken during the first flight. Each photograph has GPS data (time and location) embedded in the file except for 34 images taken from 13:44 to 13:56 UTC for which the GPS failed due to a defective battery. Also, attitude heading reference system (AHRS) data are available for photos taken from 12:59 to 13:36 UTC. At the latter time, the battery for laptop that was recording the AHRS data failed.

[8] Report prepared by J. Lang and P.W. Vachon and circulated informally on 2 November 2005.
[9] All photographs in this Annex were taken by J. Lang.

B.3 18 Oct. 2005

Photographs are available of:

- 17 different vessels (MARSIE players and targets of opportunity); and
- Overviews of Chedabucto Bay and the Janvrin Point site.

In all, 618 photographs were taken during the second flight. During this flight, the GPS and AHRS both worked well.

Figure 27: Photograph of Janvrin Point (foreground, left) with CCGS E. Cornwallis *in the distance.*

Figure 28: Photograph of CCGS E. Cornwallis *and some player vessels.*

Figure 29: Photograph of Dominion Victory.

Figure 30: Photograph of HMCS Toronto *and a player vessel.*

*Figure 31: Photograph of commercial shipping in Chedabucto Bay (*Eastern Power*).*

*Figure 32: Photograph of commercial shipping in Chedabucto Bay (*Gemini Voyager*).*

*Figure 33: Photograph of commercial shipping in Chedabucto Bay (*Champion*).*

Figure 34: Photograph of a RHIB.

Figure 35: Photograph of Strait Signet *and a Zodiac.*

Figure 36: Photograph of J. Franklin Wright.

Annex C EC CV-580 Data Processing Report[10]

C.1 Purpose

This report summarizes the available EC CV-580 SAR data that were acquired during the MARSIE Trial. All of the EC CV-580 SAR data have been processed using the Configurable Airborne SAR Processor (COASP); we can now take stock of exactly what data we have available and the way ahead to meaningfully complete the data analysis.

C.2 Data Summary

Table 43 summarizes the data transcription[11], COASP processing, and calibration outcomes for the MARSIE data. Most of the data were transcribed by MDA Geospatial Services under contract (a few cases were transcribed by CCRS). The processing and calibration were carried out at DRDC Ottawa. Section C.3 contains a summary of the processing steps taken.

Table 43: Summary of EC CV-580 SAR Processing for MARSIE (continued on next page).

Date	l/p	Ref	Cal	Inc	SAW	Amp	Lk	COASP	Cal Used	Comments
16 Oct. 2005	p11p3	a341	Y	50.6	IN	LPA	R	Y		transcribed by CCRS
17 Oct. 2005	l22p2	a342			OUT	LPA	L	Y	346	1/19
17 Oct. 2005	l23p3	a343			OUT	LPA	L	Y	346	2/19
17 Oct. 2005	l24p4	a344			OUT	LPA	R	Y	346	3/19
17 Oct. 2005	l26p6	a345			OUT	LPA	R	Y	346	4/19
17 Oct. 2005	l27p7	a346	Y	50.4	OUT	LPA	L	Y		
17 Oct. 2005	l28p9	a347	Y	50.7	OUT	LPA	R	Y		
17 Oct. 2005	l27p10	a348	Y	51.8	IN	MPA	L	Y		bad PRF/V after line 79,250, cal site OK
18 Oct. 2005	l31p2	a349			OUT	MPA	L	Y	hybrid	5/19, RAW data drop-outs, low priority
18 Oct. 2005	l32p3	a350			OUT	MPA	L	Y	hybrid	6/19, RAW data drop-outs, low priority
18 Oct. 2005	l33p4	a351			OUT	MPA	L	Y	hybrid	7/19, RAW data drop-outs, low priority
18 Oct. 2005	l33p5	a352			OUT	MPA	R	Y	hybrid	8/19, RAW data drop-outs, low priority
18 Oct. 2005	l32p6	a353			OUT	MPA	R			high BER, could not be transcribed
18 Oct. 2005	l31p7	a354			OUT	MPA	R	Y	hybrid	9/19
18 Oct. 2005	l34p8	a355			OUT	MPA	L	Y		focus/defocus problem, not usable
18 Oct. 2005	l37p10	a356	Y	51.0	OUT	LPA	L	Y		
18 Oct. 2005	l37p11	a357	Y	51.5	OUT	LPA	R	Y		

[10] Derived and updated from a report prepared by P.W. Vachon and T. Potter that was circulated informally on 26 January 2006.

[11] Transcription refers to the transfer (i.e., reading, re-formatting, and writing) of the RAW signal data from helical scan tape as recorded on the aircraft to machine-readable Exabyte tape.

Table 43: Concluded.

Date	l/p	Ref	Cal	Inc	SAW	Amp	Lk	COASP	Cal Used	Comments
20 Oct. 2005	l41p1	a358			OUT	LPA	R	Y	366	10/19
20 Oct. 2005	l41p2	a359			OUT	LPA	L	Y	366	11/19
20 Oct. 2005	l41p3	a360			OUT	LPA	R	Y	366	12/19
20 Oct. 2005	l42p4	a361			OUT	LPA	L	Y	366	13/19
20 Oct. 2005	l42p5	a362			OUT	LPA	R	Y	366	in 5 parts due to high BER, no ships
20 Oct. 2005	l44p6	a363			OUT	LPA	L	Y	366	14/19
20 Oct. 2005	l45p7	a364			OUT	LPA	L	Y	366	15/19
20 Oct. 2005	l37p8	a365	Y	50.9	OUT	LPA	L	Y		transcribed by CCRS, bad Cal parameters
20 Oct. 2005	l37p9	a366	Y	52.0	OUT	LPA	R	Y		transcribed by CCRS
24 Oct. 2005	l3p3	a367			IN	LPA	L	Y	341	16/19
24 Oct. 2005	l3p4	a368			IN	LPA	R	Y	341	17/19
24 Oct. 2005	l2p5	a369			IN	LPA	R			bad MAID file, can't be processed
24 Oct. 2005	l1p6	a370			IN	LPA	L	Y	341	18/19
24 Oct. 2005	l1p8	a371			IN	LPA	L	Y	341	19/19
24 Oct. 2005	l4p9	a372	Y	51.1	IN	LPA	L	Y		ARCs unstable (blooming), not usable
24 Oct. 2005	l4p10	a373	Y	50.8	IN	LPA	R	Y		ARCs unstable (blooming), not usable

Notes for Table 43:

- l/p = Line and Pass number
- Ref = internal reference number for each data set
- Cal = indication as to whether or not it was a calibration line (Y for yes)
- Inc = incidence angle at the calibration site
- SAW = use of the SAW^{-1} range compression device (IN if so, OUT if not)
- Amp = amplifier used, either the low power amplifier (LPA) or the medium power amplifier (MPA)
- Lk = look direction (R for right, L for left)
- COASP = indication if data have been processed with this processor (Y for yes)
- Cal Used = data used for calibration processing (the case of hybrid is described below)

Several passes were lost during the data transcription process due to a too high bit-error rate (BER). Also, several processing problems were encountered due to bad MAID data. In future, these types of problems will be eliminated once the new data recording system is completed.

Two calibration passes were lost due to ARC instabilities, which lead to “blooming” of their signatures in the SAR image. The instability is thought to arise from local atmospheric conditions (temperature and moisture). The gain will be adjusted downward if this problem is noted in future.

One pass was lost due to a checkerboard focus/defocus pattern that has been seen several times previously. This problem is now known to be associated with the exciter receiver unit (ERU). Future acquisitions will involve an ERU re-set prior to each pass.

Several problems were encountered with the calibration data, which require a match between use of the SAW^{-1} device and the amplifier used. The biggest problem was caused by failure of the

MPA during the 18 Oct. flight. The "hybrid" calibration approach referred to in Table 1 used mean phase corrections from the LPA SAW-OUT calibration cases acquired and calibration constant adjustments from LPA SAW-OUT cases acquired using historical LPA versus MPA calibration data.

In total, 19 project lines were successfully returned (acquired, processed with COASP, and calibrated), as enumerated in the comments column of Table 1. The survey image from each successful case is shown below.

C.3 Processing Procedures

To process EC CV-580 data to a calibrated polarimetric SAR image, the following input data sets are required:

- Primary base station GPS data;
- Secondary base station GPS data;
- Aircraft GPS data;
- Aircraft MAID data (i.e. aircraft housekeeping from INS and other sources); and
- Raw SAR signal data (transcribed from HSR to Exabyte tape).

The GRAFNAV software is used to process the GPS data. The primary GPS base station position is determined by referencing it to a known survey monument. From this, a GPS solution for the position of the secondary base station is determined. The aircraft GPS data is then differentially corrected using concurrent data from the 2 GPS base stations to produce the reference aircraft track for motion compensation.

The corrected GPS, MAID, and SAR signal data are then transferred to a workstation. The signal data is contained in 4 separate files, one for each polarization channel (i.e. VV, VH, HV, and HH). At the end of each flight line, three types of noise are usually recorded: transmitter off, BITE noise source on, and BITE noise source on with maximum gain. The noise is used in the radiometric calibration procedure. 4096 samples of noise are used and must be self consistent; a statistical quality control (QC) program is run to allow the user to identify good noise samples. The noise samples are processed separately and their power determined. The noise is usually also examined visually for errors.

Next, the program InQC is run for aircraft motion compensation. InQC processes MAID, GPS and ancillary signal data. Several plots and a log file are generated for QC checks. InQC produces the PRF file, which contains the necessary motion compensation parameters and is one of the required inputs for the COASP processing program.

COASP itself consists of a number of separate processes that carry out pixel alignment, data transposition, motion compensation, antenna pattern correction, application of K' (radiometric calibration), phase angle corrections, and several other operations. Range compression is carried out if the SAW^{-1} range compression device was not used during data acquisition.

If the data are from a calibration line, then only the portion of the image that is over the calibration site is processed with COASP. The pixel coordinates of the calibration devices are determined and the TARGANAL program is run to measure and analyze the responses of ARC and corner reflector calibration devices. These results are in turn used by another program called GENCAL that estimates K' and phase angle corrections. The image is then re-processed with COASP to apply the calibration parameters; the response of the calibrators is measured again and several QC procedures are carried out.

The elapsed time required for COASP to process an entire image is a function of the hardware and the number of users. Three to four hours is typical for a full scene on the present SGI hardware at DRDC Ottawa (known locally as Pigpen). Of course, data download, processor setup, and data archive operations are also time consuming for the operator.

After initial COASP processing, the program CHASP can be used to carry out a detailed analysis of individual targets. Doppler centroid and Doppler rate, interpreted as target motion, can be estimated and corrected.

After processing, a Matlab™ program is used to create a colour composite RGB survey image that is re-sampled to approximately the correct geometric perspective.

C.4 Survey Images

Following are survey images from the nineteen COASP-processed EC CV-580 SAR MARSIE data sets. In each case the available channels have been combined as Red=|VV|, Blue=|HH|, and Green=|HV|+|VH|. Various histogram stretches have been applied; depending on the image dynamic range, the results are not always attractive. The images are presented in a slant-range format with azimuth time increasing from right-to-left and slant range, covering 16.3 km, increasing from top-to-bottom. Janvrin Point (the focal point of the MARSIE activities in Chedabucto Bay) has been labelled with a green arrow when it is present in the image. All of the available data acquired from each pass is shown in each case.

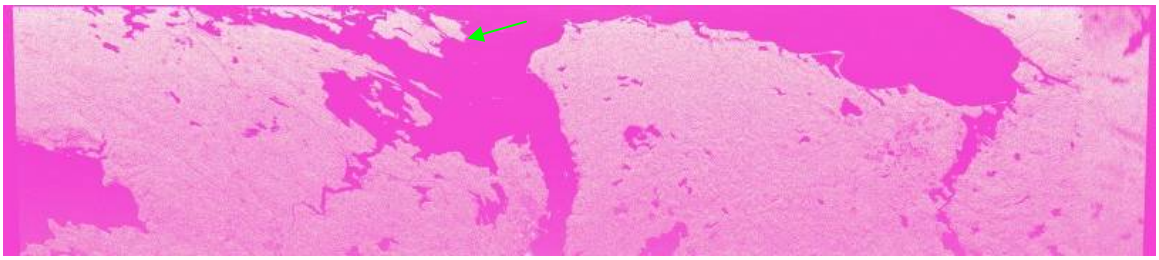

Figure 37: Survey Image from 17 Oct. 2005, l22p2 (a342).

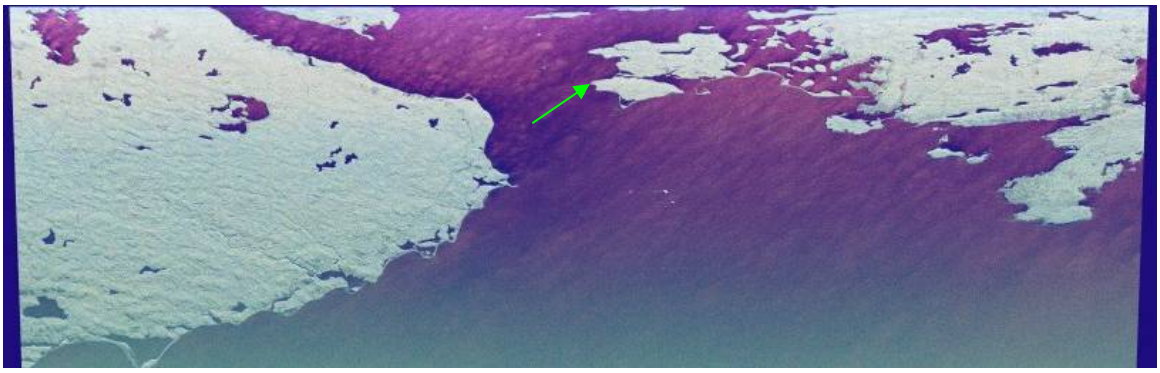

Figure 38: Survey Image from 17 Oct. 2005, l23p3 (a343).

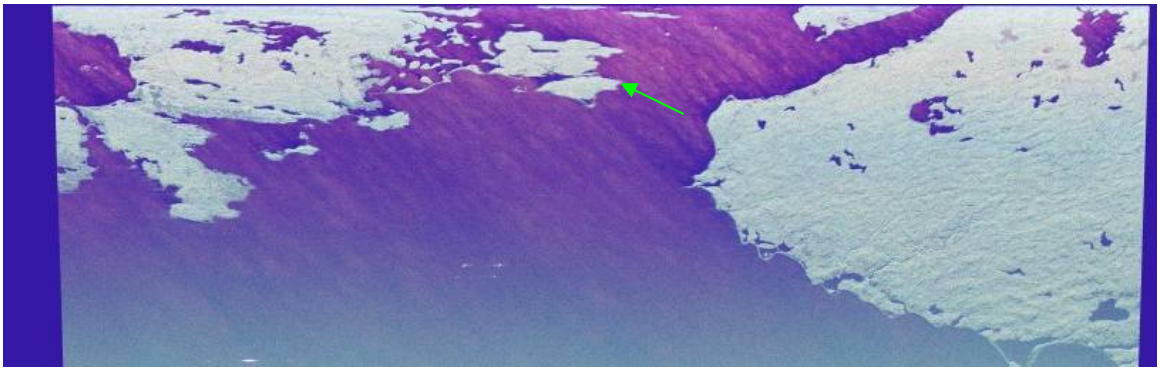

Figure 39: Survey Image from 17 Oct. 2005, l24p4 (a344).

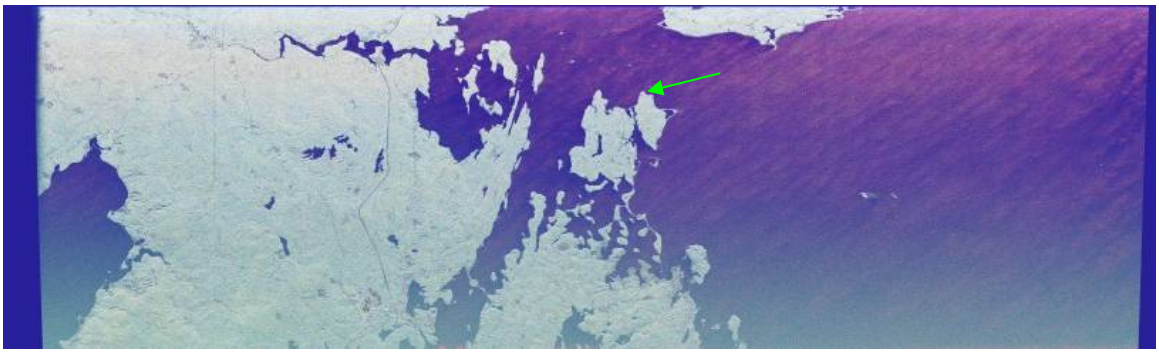

Figure 40: Survey Image from 17 Oct. 2005, l26p6 (a345).

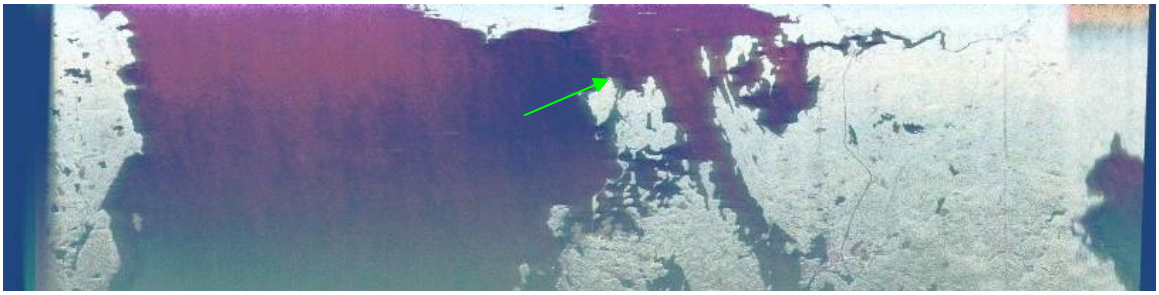

Figure 41: Survey Image from 18 Oct. 2005, l31p2 (a349).

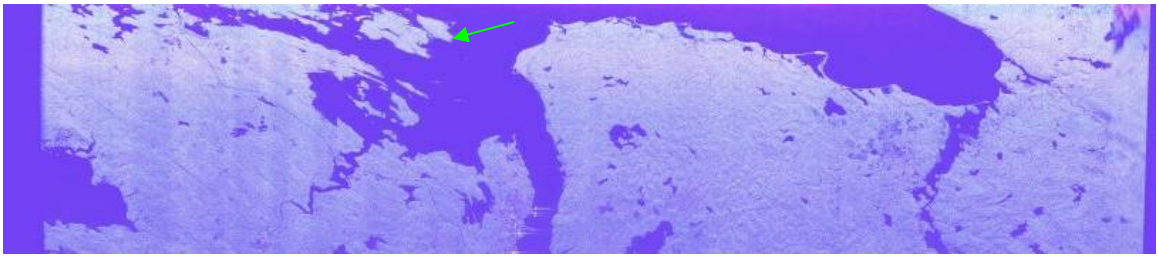

Figure 42: Survey Image from 18 Oct. 2005, l32p3 (a350).

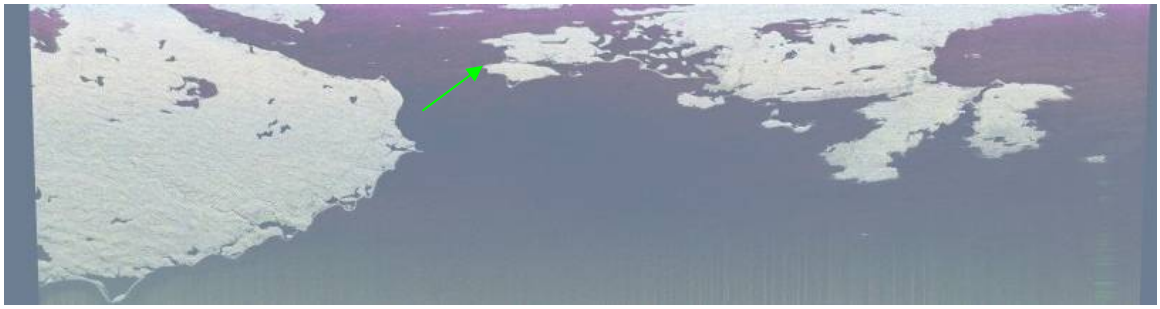

Figure 43: Survey Image from 18 Oct. 2005, l33p4 (a351).

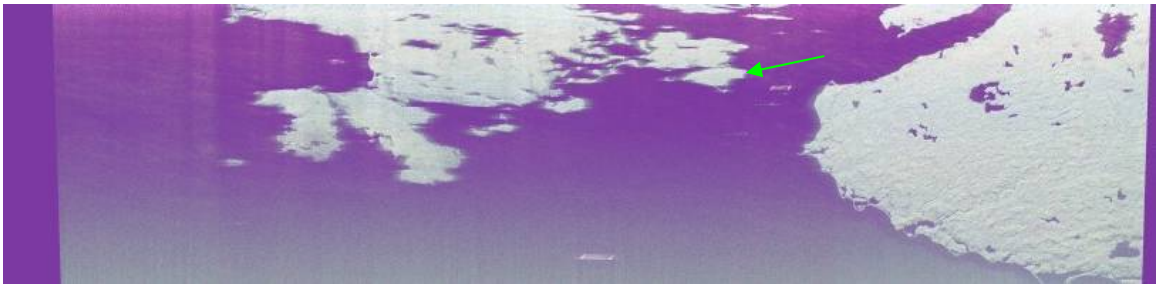

Figure 44: Survey Image from 18 Oct. 2005, l33p5 (a352).

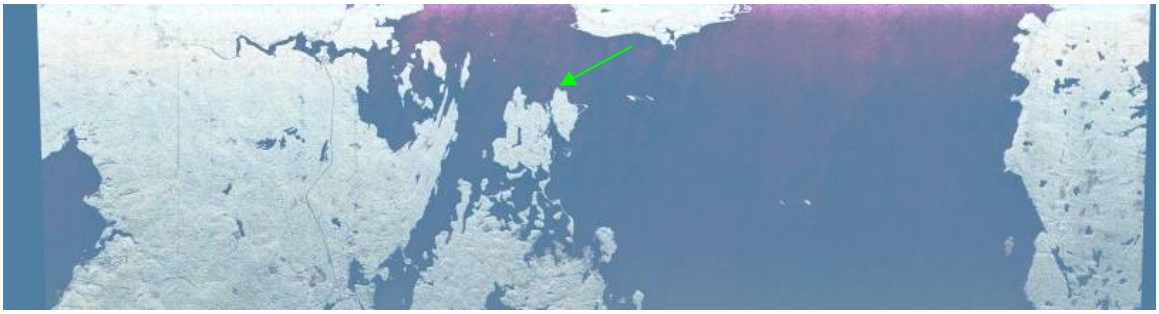

Figure 45: Survey Image from 18 Oct. 2005, l31p7 (a354).

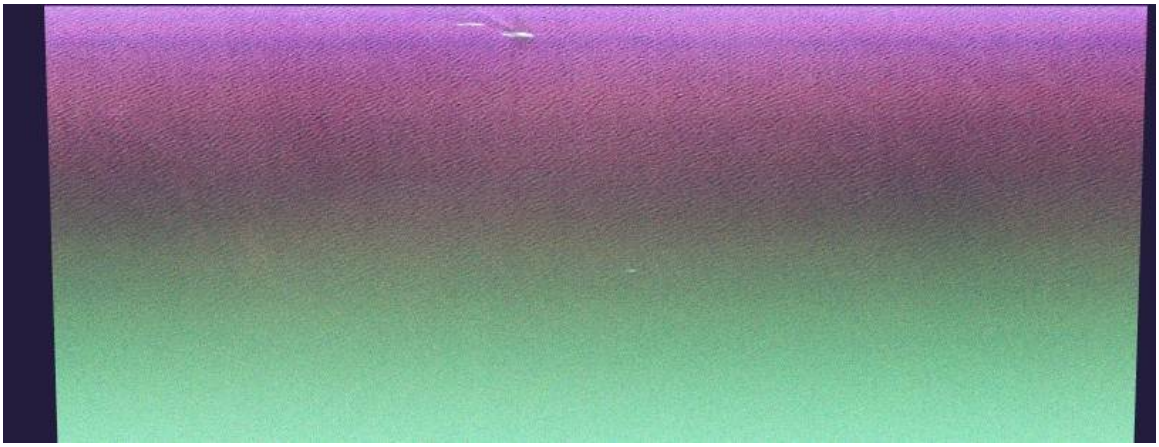

Figure 46: Survey Image from 20 Oct. 2005, l41p1 (a358).

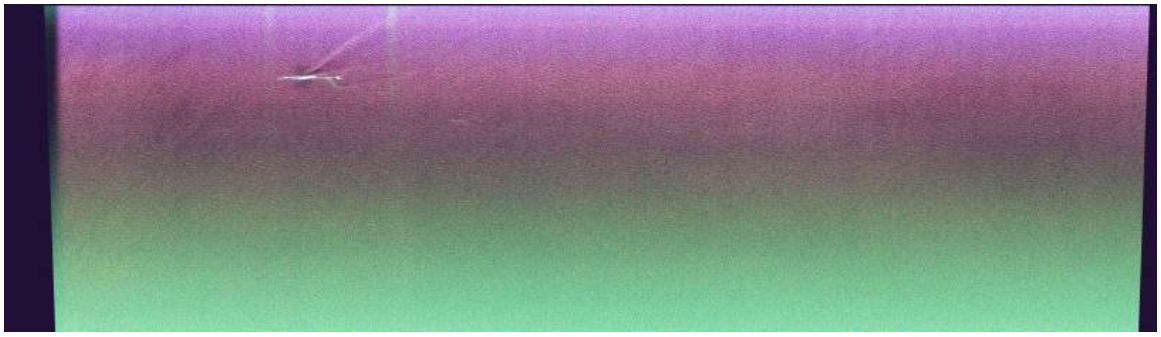

Figure 47: Survey Image from 20 Oct. 2005, l41p2 (a359).

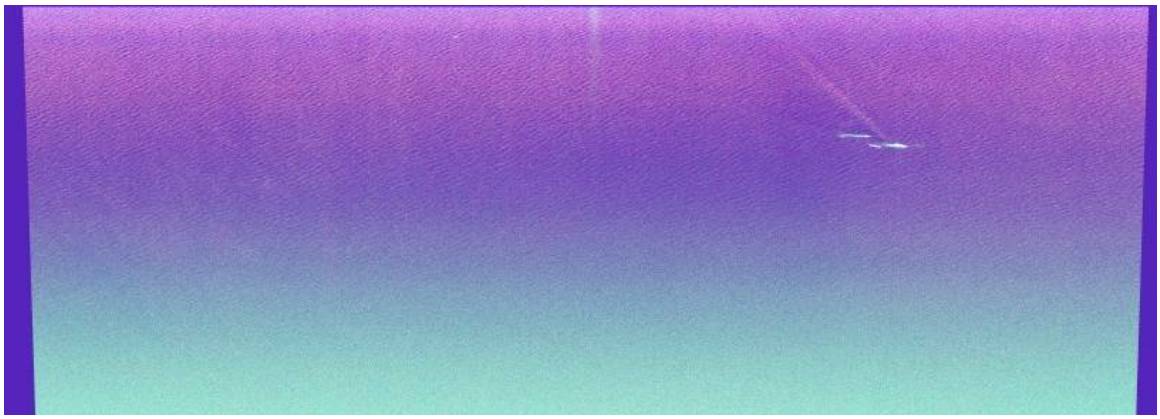

Figure 48: Survey Image from 20 Oct. 2005, l41p3 (a360).

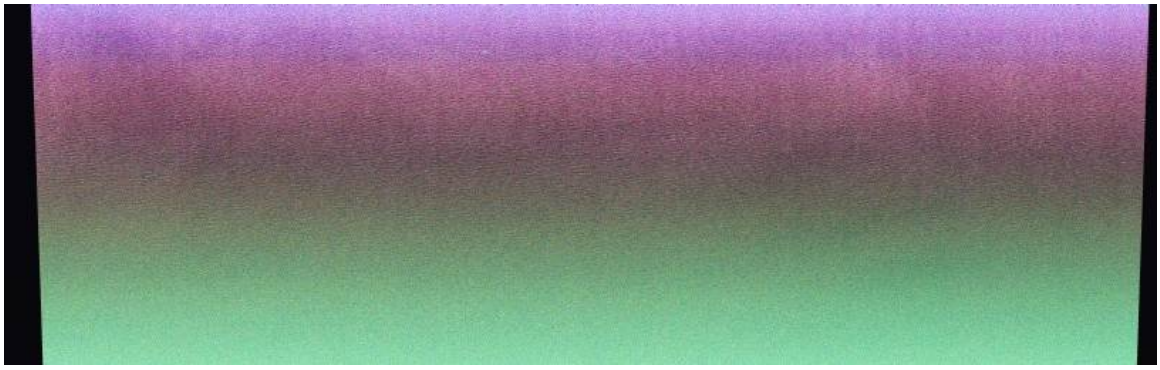

Figure 49: Survey Image from 20 Oct. 2005, l42p4 (a361).

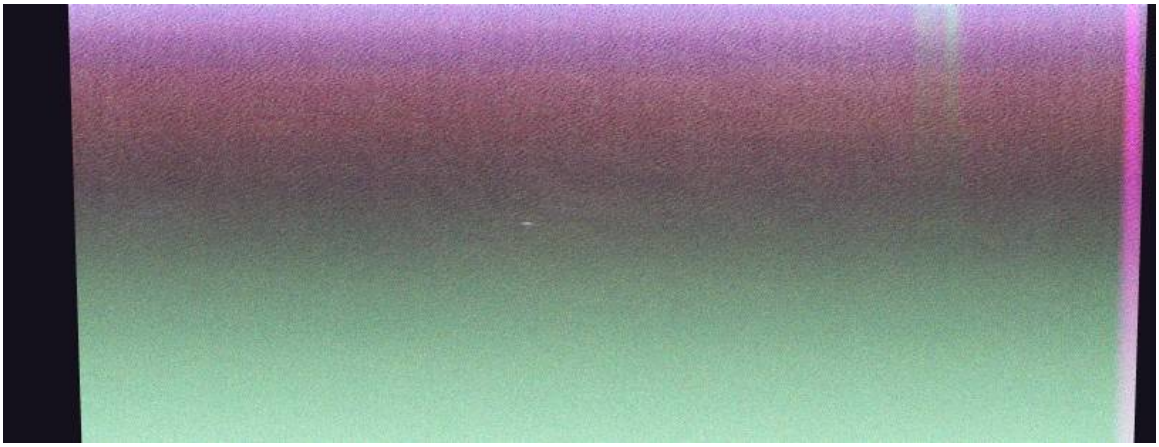

Figure 50: Survey Image from 20 Oct. 2005, l42p6 (a363).

Figure 51: Survey Image from 20 Oct. 2005, l45p7 (a364).

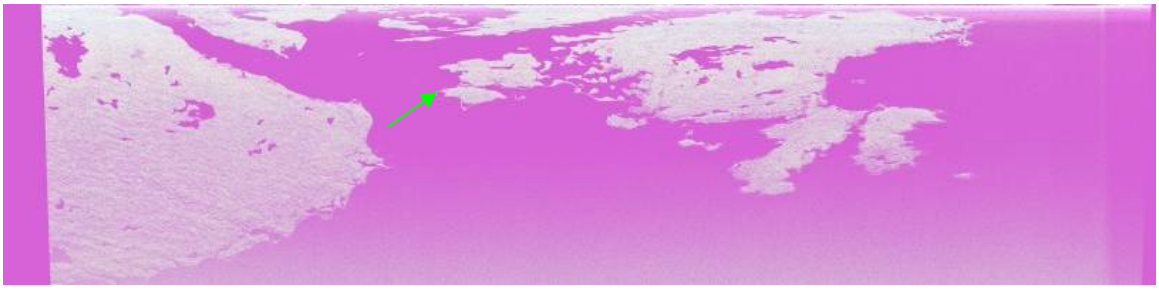

Figure 52: Survey Image from 24 Oct. 2005, l3p3 (a367).

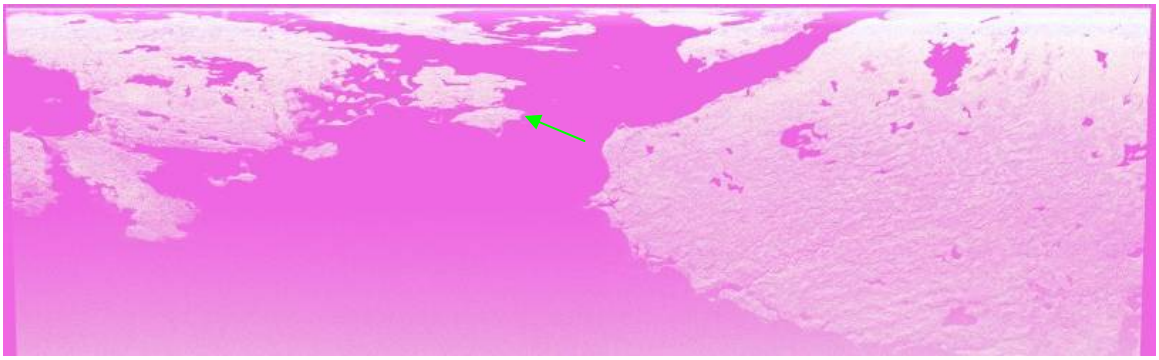

Figure 53: Survey Image from 24 Oct. 2005, l3p4 (a368).

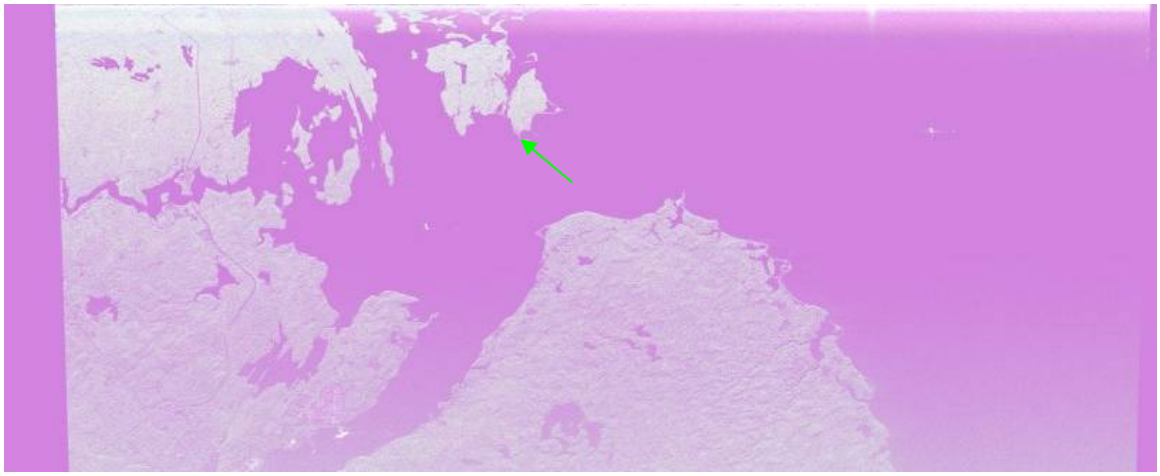

Figure 54: Survey Image from 24 Oct. 2005, l1p6 (a370).

Figure 55: Survey Image from 24 Oct. 2005, l1p8 (a371).

C.5 Next Steps

- Polarimetric vessel detection software will be used to locate vessels of interest.
- Position and motion records for key participating vessels will be correlated temporally and spatially with the EC CV-580 SAR coverage and detected vessels.
- Vessels of interest will be extracted and re-focussed with CHASP; SAR-derived motion parameters will be compared to available vessel motion data; the RCS for small known targets will be measured and tabulated.
- Standard polarimetric signatures will be compiled for each known and refocused vessel; results will be interpreted in the RADARSAT-2 polarimetry context.

Annex D Polarimetric Analysis Results

Initial polarimetric analysis results from MARSIE are catalogued in this Annex. The data considered were acquired on 17 Oct. and 20 Oct. 2005. The image acquisition geometry is illustrated in Figure 56. The *Dominion Victory* (25 m) results appear in Figure 57 (l41p1), Figure 58 (l41p3), and Figure 59 (l42p4); the *Gulf Service* (42 m) results appear in Figure 60, the *E. Cornwallis* (83 m) results in Figure 61, and the *Toronto* (135 m) results in Figure 62.

a)

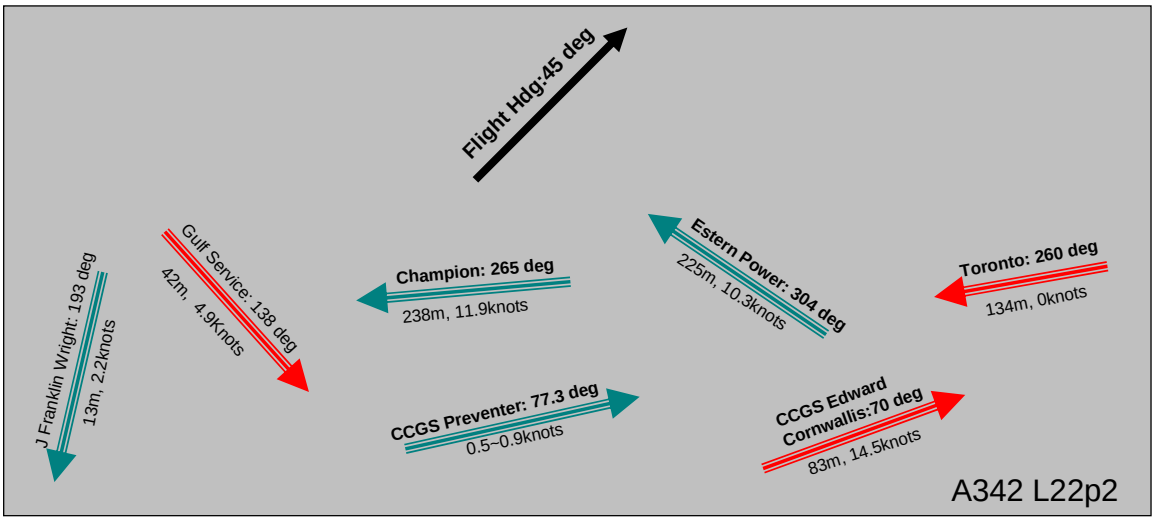

b) Marsie trial on Oct. 20, 2005

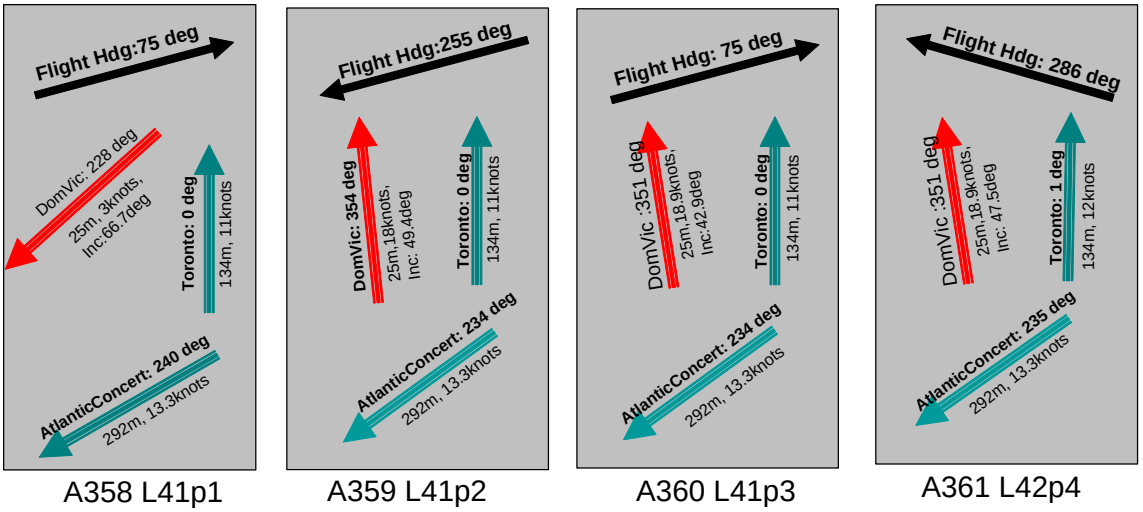

Notes:

Flight Headings: obtained from “MARSIE Trial:EC cv580 SAR Flight Activity Summary”, Paris W. Vachon, Oct. 27, 05

Ship Courses: obtained from Nathan’s ground truth info

Figure 56: Acquisition geometry: a) 17 Oct. 2005, l22p2; b) 20 Oct. 2005.

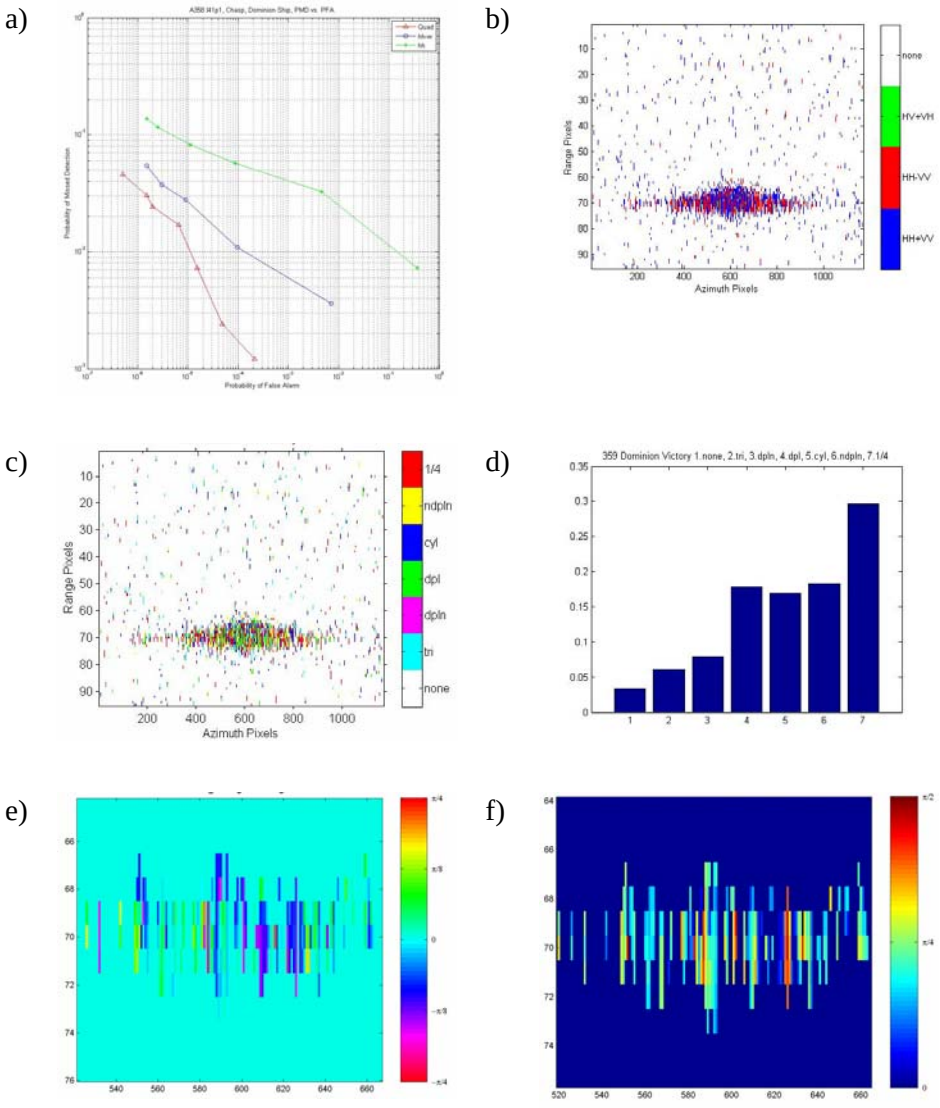

Figure 57: Dominion Victory, *20 Oct. 2005, l41p1 (a358): a) Detection performance; b) Pauli decomposition image; c) Cameron decomposition image; d) Cameron histogram; e) SSCM latitude; f) SSCM longitude; g) SSCM decomposition image; h) SSCM histogram; i) H/α analysis for ocean; j) H/α analysis for ship. (Continued on next page.)*

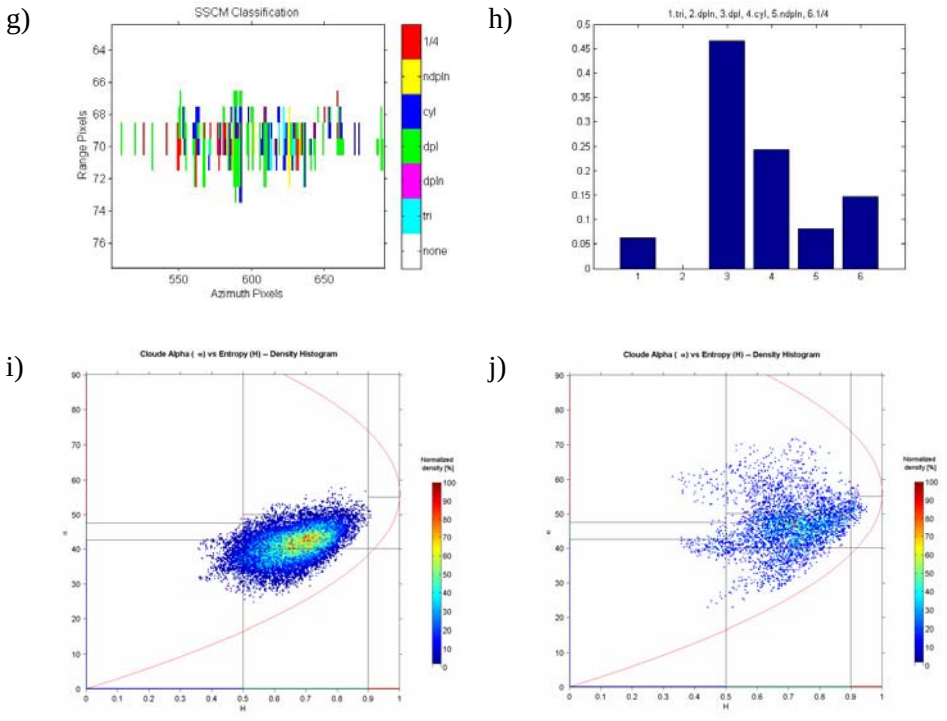

Figure 57: Concluded.

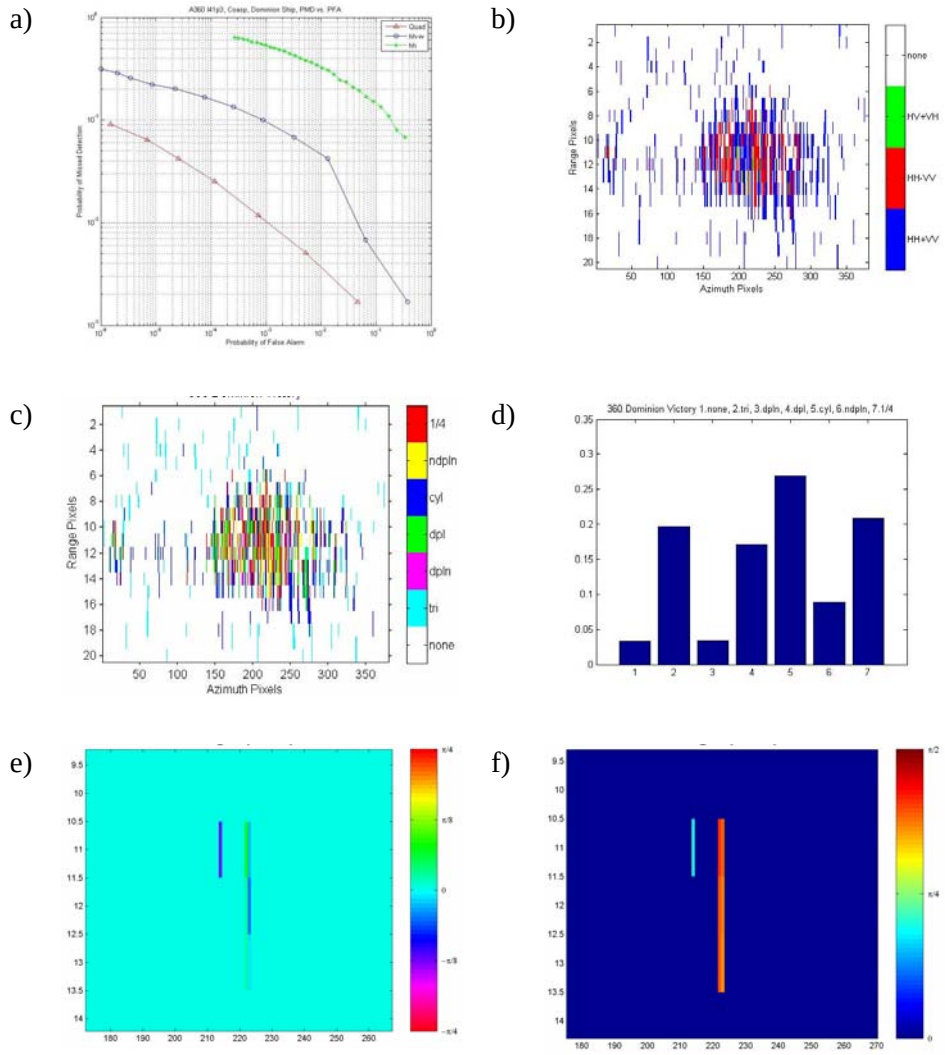

Figure 58: Dominion Victory, *20 Oct. 2005, l41p3 (a360): a) Detection performance; b) Pauli decomposition image; c) Cameron decomposition image; d) Cameron histogram; e) SSCM latitude; f) SSCM longitude; g) SSCM decomposition image; h) SSCM histogram; i) H/α analysis for ocean; j) H/α analysis for ship. (Continued on next page.)*

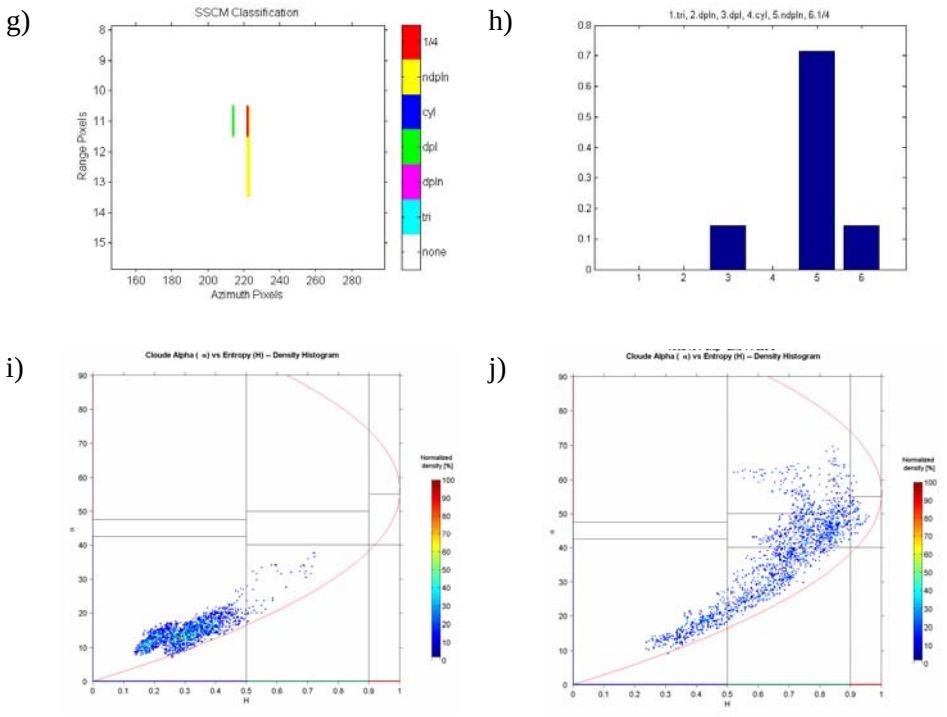

Figure 58: Concluded.

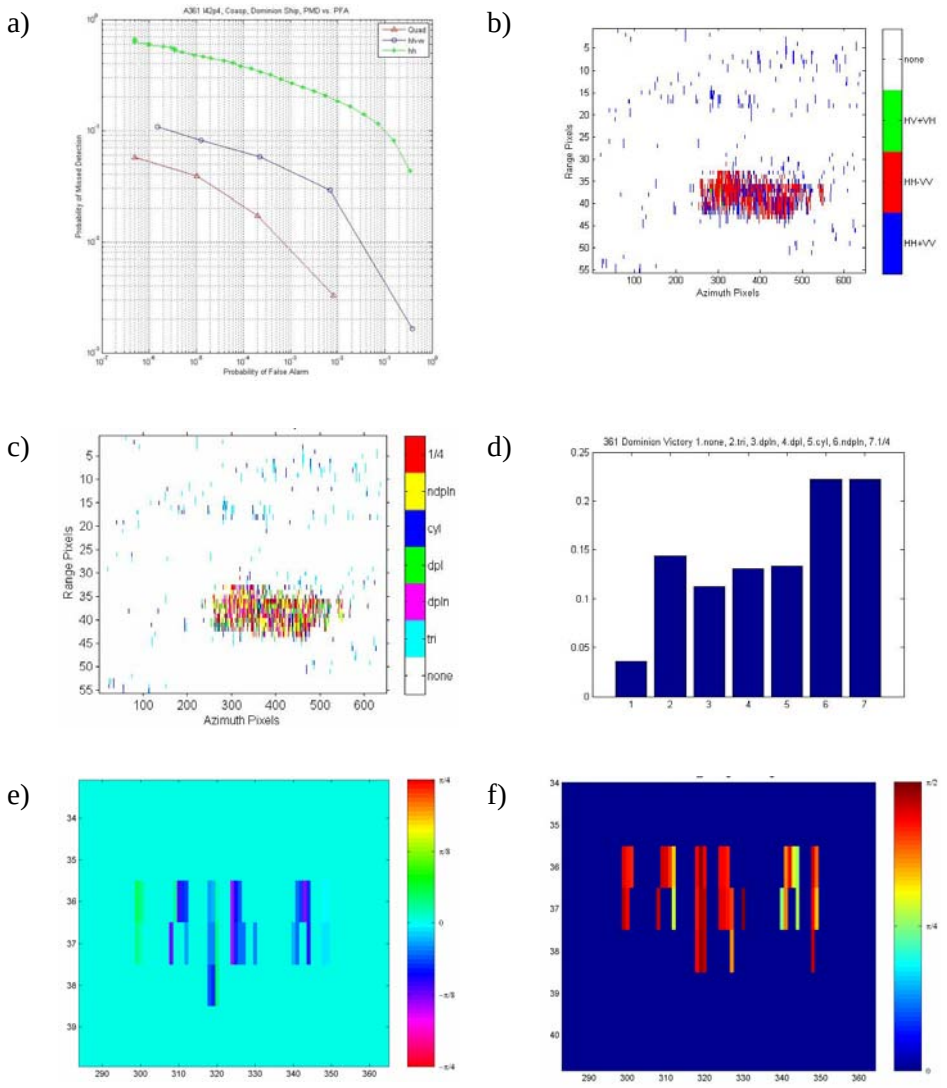

Figure 59: Dominion Victory, *20 Oct. 2005, l42p4 (a361): a) Detection performance; b) Pauli decomposition image; c) Cameron decomposition image; d) Cameron histogram; e) SSCM latitude; f) SSCM longitude; g) SSCM decomposition image; h) SSCM histogram; i) H/α analysis for ocean; j) H/α analysis for ship. (Continued on next page.)*

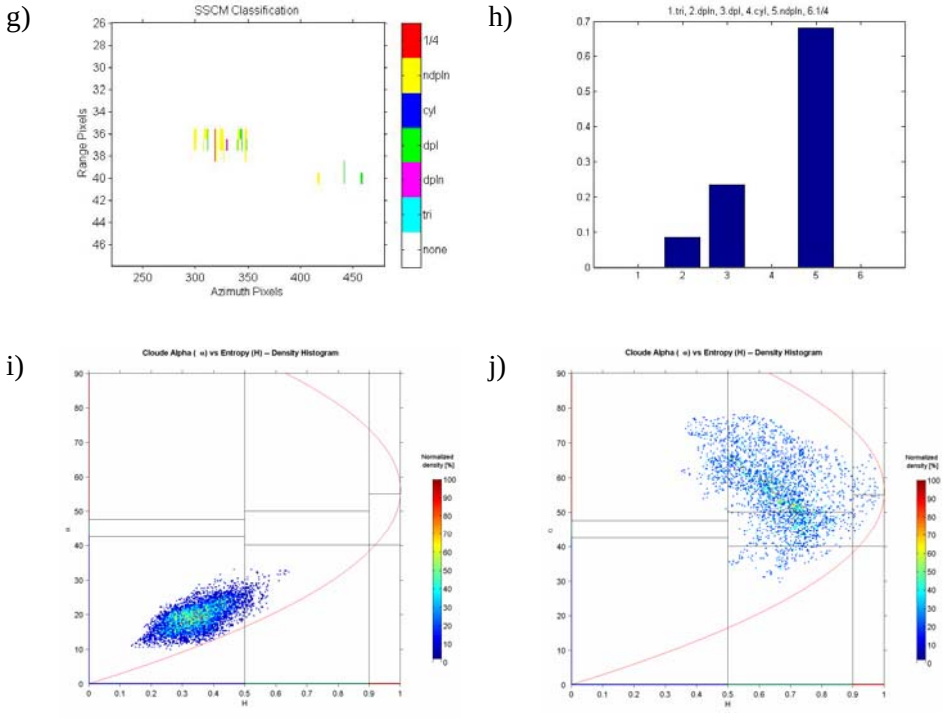

Figure 59: Concluded.

a) N/A

b)

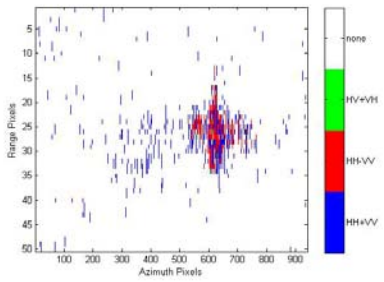

c)

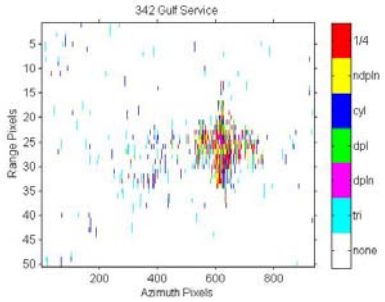

d)

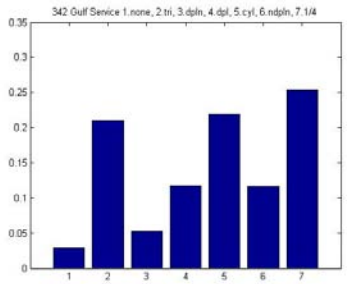

e)

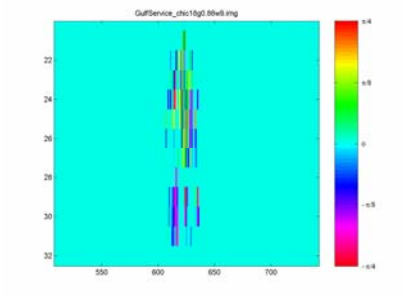

f)

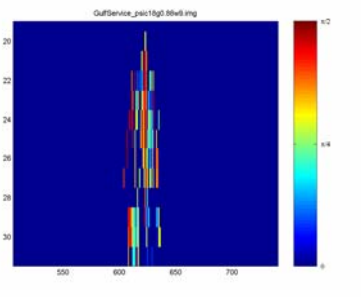

Figure 60: Gulf Service, *17 Oct. 2005, l22p2 (a342): a) Detection performance; b) Pauli decomposition image; c) Cameron decomposition image; d) Cameron histogram; e) SSCM latitude; f) SSCM longitude; g) SSCM decomposition image; h) SSCM histogram; i) H/α analysis for ocean; j) H/α analysis for ship.* *(Continued on next page.)*

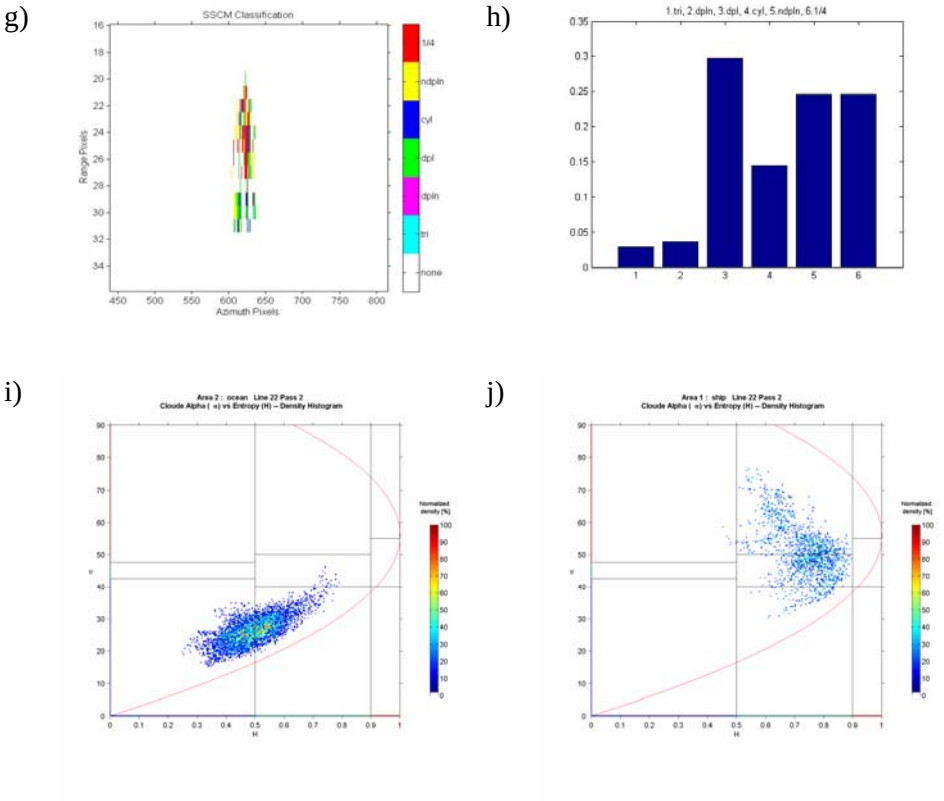

Figure 60: Concluded.

a) N/A

b)

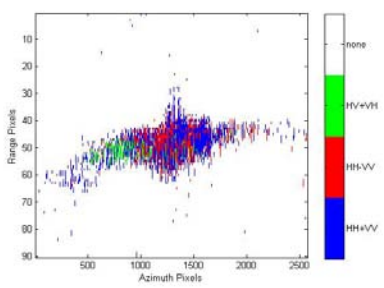

c)

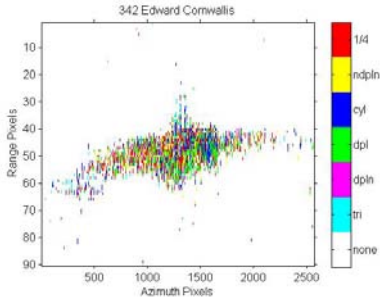

d)

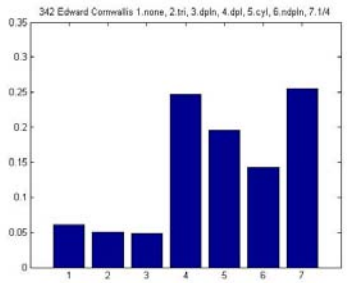

e)

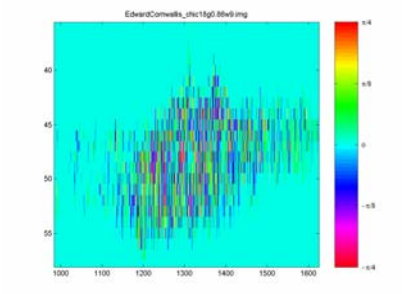

f)

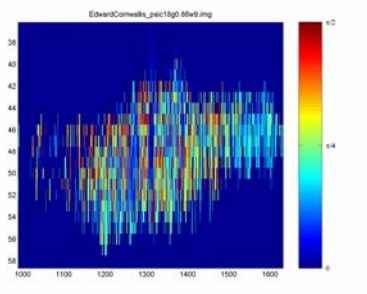

Figure 61: E. Cornwallis, *17 Oct. 2005, l22p2 (a342): a) Detection performance; b) Pauli decomposition image; c) Cameron decomposition image; d) Cameron histogram; e) SSCM latitude; f) SSCM longitude; g) SSCM decomposition image; h) SSCM histogram; i) H/α analysis for ocean; j) H/α analysis for ship.* *(Continued on next page.)*

g)

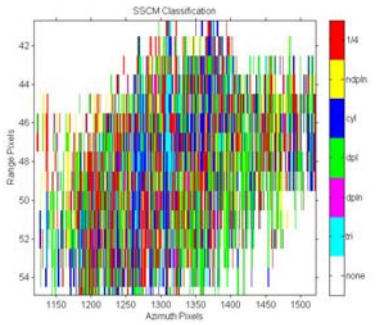

h)

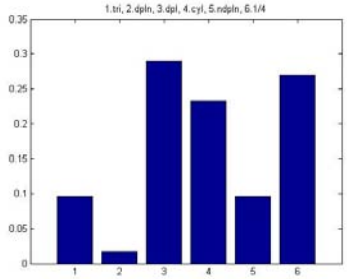

i)

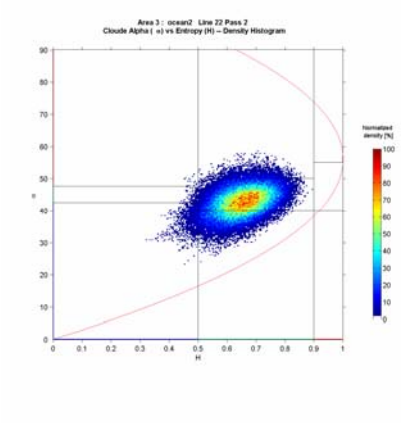

j)

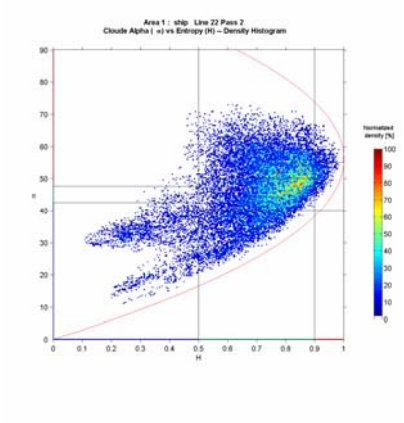

Figure 61: Concluded.

a) N/A

b)

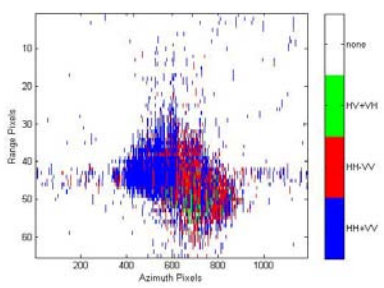

c)

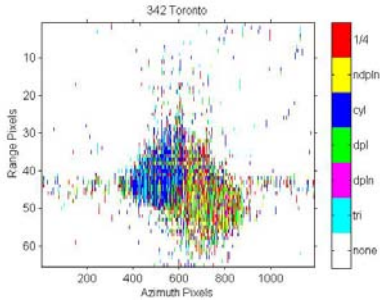

d)

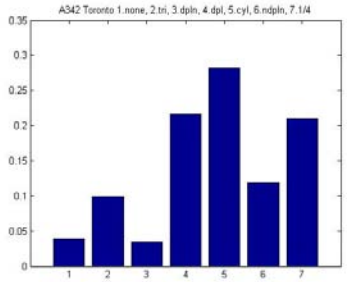

e)

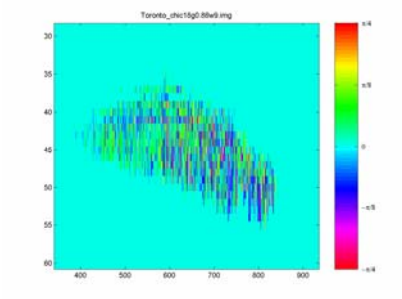

f)

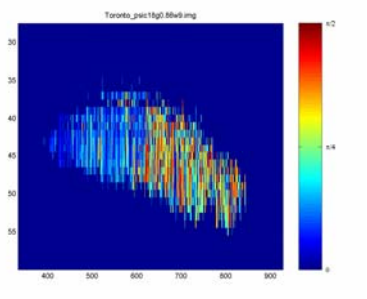

Figure 62: Toronto, *17 Oct. 2005, l22p2 (a342): a) Detection performance; b) Pauli decomposition image; c) Cameron decomposition image; d) Cameron histogram; e) SSCM latitude; f) SSCM longitude; g) SSCM decomposition image; h) SSCM histogram; i) H/α analysis for ocean; j) H/α analysis for ship.* *(Continued on next page.)*

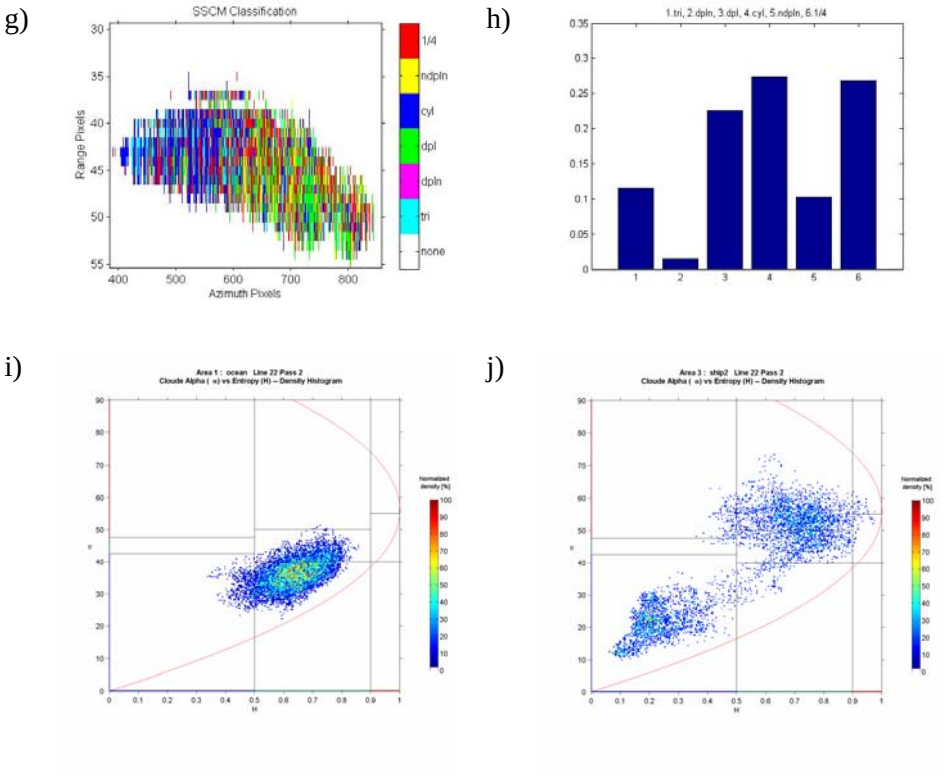

Figure 62: Concluded.

Annex E CHASP Processing of RADARSAT-1 Data

E.1 Introduction

This Annex discusses the applicability of the chip-based adaptive SAR processor (CHASP) to RADARSAT-1 data processing. Test results using RADARSAT-1 Fine mode data are presented. There is strong evidence that some, if not all, of CHASP's adaptive algorithms are relevant to RADARSAT processing, and that CHASP's core functionality can provide useful target motion information. However, the overall procedure, currently implemented as two interactive wrapper programs (referred to as "wrap" and "view123"), is likely to differ for the processing of RADARSAT-1 data as compared to EC CV-580 SAR data.

E.2 Comparison of the EC CV-580 SAR and RADARSAT-1

As described in [21], CHASP has been developed primarily to auto-focus moving ship data acquired by the EC CV-580 SAR. However, CHASP also has the potential to process ship imagery from other SAR data sources as long as the data are suitably pre-processed. Specifically, the data must be range compressed prior to processing with CHASP. Appropriate gain and radiometric corrections should also be applied to ensure radiometrically calibrated (at least relatively calibrated) input to CHASP. New CHASP modifications are being implemented so that azimuth-compressed single-look complex (SLC) data can be accepted for further processing. However, SLC data should be pre-processed in a customized way, leaving as broad an azimuth bandwidth available as possible with no azimuth spectral shaping. Under such conditions, SLC data can still be used for fine Doppler centroid (DC) tuning, frequency tracking, and for inter-look and multi-look operations.

When CHASP methods are applied to RADARSAT-1 data, their performance may differ from the EC CV-580 SAR case. Significant system differences between the two SARs imply differences in sensitivity of the various CHASP algorithms.

Typical properties of the EC CV-580 SAR data include:

- The pulse repetition frequency (PRF) is constantly adjusted along track to maintain PRF/V (i.e., the along-track sample spacing) as nearly constant;
- The effective radar speed is equal to the ground speed and is independent of range;
- There is a relatively wide beam width in azimuth, implying aspect angle diversity during formation of the synthetic aperture (i.e., the ship signature is acquired over different aspect angles);
- The real-time antenna steering approximately compensates for aircraft attitude variations to ensure that the DC is close to zero for stationary targets;
- The interval of DC/PRF offsets induced by ship motion is relatively large and could cause a PRF ambiguity for the ship;

- Based upon our experience, the best way to estimate the DC/PRF offset of a ship is to minimize ghosts (i.e., azimuth ambiguities) in the image;
- The interval of relative velocity offsets induced by ship motion is relatively large and could cause azimuth smearing;
- The nominal azimuth resolution is high and the azimuth sample spacing is relatively small, so inter-look cross-correlation can be performed without a need for over sampling;
- The slant range sample spacing is constant, but the slant range resolution depends on the SAW status (i.e., compression in real time via a surface acoustic wave device, leading to increased dynamic range and possible signal data saturation; or compression in software, leading to a lower range resolution but a reduction in the possibility of signal data saturation);
- The synthetic aperture is long, corresponding to thousands of coherently processed pulses;
- Non-uniform target motion (sway, heave or surge) is evident in many cases due to the long aperture and high sensitivity, thus hampering ship velocity estimation; and
- Typically, a ship covers many image pixels.

Typical properties of RADARSAT-1 data, in comparison to EC CV-580 SAR data, include:

- The Doppler bandwidth is larger and the PRF is higher;
- The effective radar speed is different from the ground speed and from the orbital speed, and is much higher and slightly range dependent so that PRF/V varies slightly with slant range;
- The azimuth beam width is very small such that the aspect angle is almost constant and, consequently, there are fewer power fluctuations during formation of the synthetic aperture;
- The DC/PRF for clutter can be very large and include large ambiguity numbers for most cases of interest, such that the DC/PRF must be estimated for the background clutter;
- The interval of DC/PRF offsets induced by ship motion are relatively narrow such that they do not cause much defocusing;
- It is harder to estimate the line of sight (LOS) component of the ship velocity from the Doppler shifts of a ship since both clutter and target DC offsets must be estimated with high accuracy;
- The interval of relative PRF/V offsets induced by ship motion is practically negligible such that they only contribute in a minor way to azimuth smearing. As such, map-drift or frequency tracking are much less sensitive to the along-track component of the ship velocity, which makes velocity estimation more difficult;
- The azimuth resolution and sample spacing are much larger such than the inter-look cross-correlation peaks, which are always on a sub-pixel level, so that over sampling is required;
- The slant range resolution and sample spacing depend on the beam mode and the slant range sample size is larger such that target motion induced range migration is less pronounced;

- The synthetic aperture is shorter, corresponding to several hundreds of coherently processed pulses;
- Non-uniform target motion does not play a major role since the target exposure time is too short and the algorithm sensitivity is too low;
- A relatively small number of pixels belong to the ship.

The main quantitative differences between the EC CV-580 SAR and RADARSAT-1 are listed in Table 44. These differences in basic SAR properties translate into much lower sensitivity of the CHASP algorithms to ship motion for RADARSAT-1 as compared to the EC CV-580 SAR. Unlike the EC CV-580 SAR case, with CHASP processing of RADARSAT-1 data there is less opportunity for focus improvement by means of DC and DR adjustment.

Table 44: Comparison of SAR system parameters.

	EC CV-580 SAR	RADARSAT-1
PRF	≈ 300 Hz	≈ 1300 Hz
Effective platform speed	≈ 140 m/s	≈ 7000 m/s
Azimuth beam width	3.03°	≈ 0.3°
Dwell time	∈(3, 5) s	≈ 0.5 s
Coherently processes pulses	∈(1000, 2000)	≈ 600
Azimuth sample spacing	≈ 0.4 m	≈ 5 m
Slant range sample spacing	4 m	∈{5.14, 8.117, 11.6} m
Typical clutter DC/PRF	≈ 0	∈(−7, 7)
Motion-induced DC/PRF offset	∈(−1, 1)	∈(−0.2, 0.2)
Motion-induced $\Delta V / V$	∈(−0.1, 0.1)	≈ 0

E.3 Estimation of LOS Speed

The ships that are analyzed and presented in this Annex were taken from a RADARSAT-1/AISLive Fine mode data set that was acquired in early 2005 [22]; their location, size, and velocity is known from the associate automatic identification system (AIS) data. CHASP processing in this case is concerned with estimating basic ship parameters and comparing them to the available ground truth. Besides the LOS velocity component, estimation of length and orientation is important, because these can provide an estimate of the relative heading (i.e., with respect to RADARSAT-1 ground track).

Two data sets were analyzed in detail. The first data set was an F1 mode image, acquired along orbit 48,187 on 27 Jan. 2005 in the Dover Strait area. This case is a descending pass with a positive DC, which does not vary significantly across the swath. The elevation angles were between 33.3° and 35.3°. The second data set was an F5 mode image, acquired along orbit 48,280 on 2 Feb. 2005, also in the Dover Strait area. This case is an ascending pass with a negative DC. The elevation angles were between 39.7° and 41.1°.

The data were first range compressed using the commercially available EV-APP SAR processor[12]. All analyzed ships are clearly visible in the range compressed data. Their lengths ranged from 28 m to 289 m.

Image chips of interest were defined based upon the available AISLive data. Processing parameters for the chips of interest (i.e., DC/PRF and PRF/V) were extracted using EV-APP, but they were verified/corrected using CHASP algorithms from DC estimation for the clutter. Any error in the clutter DC estimates would affect the velocity estimate of each ship.

The processing parameters for the considered ships are shown in Table 45 and Table 46 for the 27 Jan. and 2 Feb. cases, respectively. The ship parameters derived from the AISLive data and verified in the internet ships register (ISR) database are shown in Table 47 and Table 48 for the 27 Jan. and 2 Feb. cases, respectively.

The azimuth displacement in these tables and the corresponding DC offsets were calculated using the LOS component of the ship velocity, based upon the AISLive information. The CHASP-derived local DC estimates for the ocean clutter may differ slightly from those provided by EV-APP. However, it may be better to rely only upon the CHASP estimates of the required processing parameters. A background clutter DC/PRF uncertainty of 0.03 was found when comparing estimates from EV-APP with those from CHASP. This difference amounts to a LOS speed uncertainty of more than 1 m/s.

Table 45: Processing parameters for the 27 Jan. 2005 ships.

Ship	DC/PRF	PRF/V [m^{-1}]
1	5.0909000	181940
2	5.001350	0.181907
3	5.060000	0.181930
4	5.022777	0.181915
5	5.018300	0.181913
6	5.116700	0.181954
7	5.212800	0.181994
8	5.216600	0.181995
9	5.045570	0.181925
10	5.241560	0.182006
11	5.219400	0.181996
12	5.039110	0.181922
13	5.092170	0.181944
14	5.216700	0.181996
15	5.090700	0.181943
16	5.012510	0.181911
17	5.058000	0.181930
18	5.000500	0.181906
19	5.129600	0.181959
20	5.053000	0.181928

[12] A Microsoft Canada (formerly Vexcel Canada) product.

Table 46: Processing parameters for the 2 Feb. 2005 ships

Ship	DC/PRF	PRF/V [m^{-1}]
1	5.562200	0.184563
2	5.551983	0.184532
3	5.561286	0.184560
4	5.544297	0.184511
5	5.563453	0.184567
6	5.531869	0.184480
7	5.537169	0.184493
8	5.565725	0.184574
9	5.539227	0.184498

Table 47: Ship parameters derived from AISLive data for 27 Jan. 2005.

Ship	Length [m]	Rel. Head. [°]	LOS Speed [m/s]	Az. Disp. [m]	DC/PRF Offset
1	180	15	6.41	-854	-0.17
2	225	117	-1.705	225	0.047
3	89	307	2.37	-314.5	-0.065
4	95	86	0.21	28	-0.005
5	264	119	-2.80	288.7	0.077
6	86	310	3.11	-419	-0.0856
7	64	314	2.54	-343	-0.07
8	171	311	3.45	-466	-0.095
9	111	123	-2.00	277	0.055
10	89	310	3.765	-415	-0.1035
11	94	311	2.65	-354	-0.073
12	92	90	-0.01	2.00	0.000
13	88	311	2.78	-371	-0.0765
14	100	317	3.675	-496	-0.101
15	289	314	3.825	-504	-0.105
16	275	298	3.41	-508	-0.0935
17	155	96	-0.36	48.3	0.01
18	121	125	-2.67	273	0.073
19	248	308	3.38	-452	-0.093
20	88	98	-0.46	60	-0.013

Table 48: Ship parameters derived from AISLive data for 2 Feb. 2005.

Ship	Length [m]	Rel. Head. [°]	LOS Speed [m/s]	Az. Disp. [m]	DC/PRF Offset
1	185	214.5	-3.28	-489	0.089192
2	82	58.5	2.06	306	-0.056142
3	135	304	4.00	596	-0.108770
4	99	213	-3.44	-507	-0.093542
5	28	118.5	-3.64	-544	0.098981
6	144	37.5	4.31	632	-0.117173
7	90	34	3.66	538	-0.099525
8	83	358	4.37	653	-0.118831
9	213	68	2.64	388	-0.071788

CHASP was used to process all of the noted ships in chips of 200 samples in slant range and 2048 samples in azimuth. Ideally, there should be just one ship in each processed chip. Due to the high ship density, in some cases there were several ships in a single chip. In these cases, the ships were selected via a configuration file and were processed one at a time using a procedure that has not yet been automated.

CHASP estimates of the azimuth position of the ship response before focusing as well as the azimuth position of the focused ship response are both used for frequency tracking. The difference between the two positions can be used for ship velocity estimation. When the "ZD_frame" option is turned off, the difference between these two positions is only due to the uncompensated DC, which includes the background estimation error and the DC offset due to ship motion. Assuming that the background (i.e., reference) DC is known (i.e., has been well estimated by the SAR processor), then the displacement is directly proportional to the LOS component of the ship's velocity. The results of this estimation are presented in Figure 63. Generally, there is good agreement between the computed and the available AISLive validation data values.

It is apparent that a LOS velocity estimate and a heading estimate, as derived from the estimated ship signature orientation for example, would suffice to estimate the s hip velocity in a number of favourable cases.

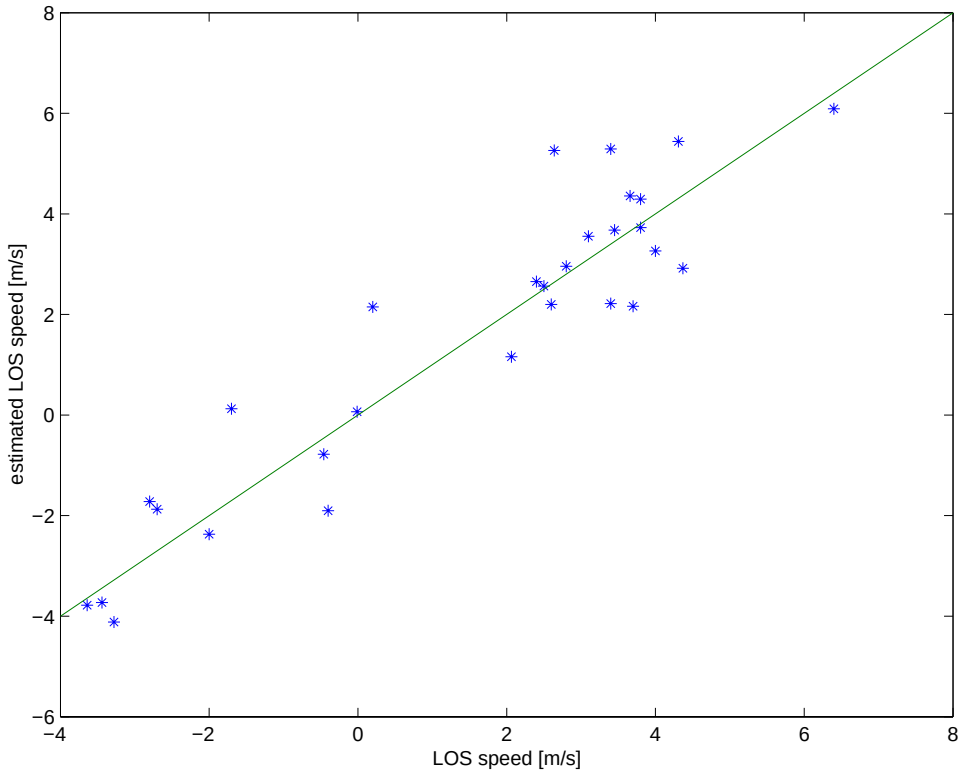

Figure 63: Scatter plot of ship speed estimated from azimuth displacement and ship speed from AISLive data. The green line represents unity slope.

E.4 Estimation of Along-Track Speed

The along-track speed is very difficult to estimate directly due to low sensitivity and complex ship structure. Here we consider just one example. Tracking results for Ship 8 from 27 Jan. 2005 data set data set as taken directly from CHASP header file (mid-aperture speed, mean speed, standard deviation, all normalized by the SAR effective speed) are:

- vel_a_cenT: −0.0010688324
- vel_a_meanT: −0.0009741914
- vel_a_stdT: 0.0001274157

According to the AISLive data (from the available LOS component, incidence angle and heading), the along track speed is 6.1 m/s. Relative to the sensor effective speed of 7063.28155185 m/s, this would cause a relative velocity offset of just 0.00086, which is somewhat lower than the mean velocity estimate found in the header.

It must be noted that the effective antenna speed for this beam varies from 7066.96990548 m/s at near range to 7062.16221909 m/s at far range. There are SAR algorithms that consider this speed

to be constant and independent of range. Clearly, the accuracy of the ship's speed estimate depends on the accuracy of the reference speed (i.e., the effective satellite speed). In terms of PRF/V, the nominal value is 0.181995 and the adjusted value would be 0.1821526 (both in units of 1/m). In terms of DR, the nominal value is −1753.3, and the adjusted value would be −1750 (both in units of Hz/s).

The result of the multi-look procedure for Ship 8 is −0.000977 for the relative speed adjustment (corresponding to a misregistration of $1/8^{th}$ of an azimuth pixel). This result is in good agreement with the tracking result and with expectation based on the AISLive data, for the relative speed offset.

The tracking procedure and the correlation procedure did not work for any of the cases considered.

E.5 Issues to Consider

- CHASP algorithms use as a reference the background DC/PRF and PRF/V, and high accuracy is needed in their estimation. If these values are derived from a commercial SAR processor, then their accuracy will be unknown. In this case they may have to be estimated or refined; if they are not refined, then the auto-focusing parameters of a ship cannot be used to derive the ship velocity.
- In principle, it is possible to estimate the velocity of a ship based on its azimuth displacement and bearing, and the background DC. The most favourable relative heading is 0° (i.e., heading perpendicular to the ground track) and the least favourable is 90° (i.e., heading parallel to the ground track).
- Velocity estimation based on DR adjustment is not straightforward. Non-uniform motion along the LOS may influence the estimate of the along-track speed (both for the tracking method and for the look correlation method). This is supported both analytically and by simulations, but we have not found clear evidence of such nonlinearities as exists for the EC CV-580 SAR.
- Ship size estimation cannot be improved significantly by refocusing based on adaptive estimation of Doppler parameters (DC/PRF and PRF/V). In particular, the stretching of the azimuth length of a ship cannot be explained solely by its along-track motion, which is on the order of a pixel or less. Pitching of the ship could be responsible via introduction of different azimuth displacement for different parts of the ship. The complex structure of the ship could also contribute to this effect via interference (as observed in slow time). This is supported both analytically and by simulations.

Annex F Quantification of the Benefit of Polarimetry for Ship Detection[13]

Over the years, DRDC Ottawa has been involved in the acquisition of a number of airborne polarimetric SAR data sets of known vessels under known environmental conditions. Specific trials of interest include CRUSADE 2000 [23], Quest-2003 [10], and MarCoPola 2004 [11]. While our ability to acquire, process, and analyze data from the EC CV-580 SAR has recently improved, these historical data sets have provided the opportunity to evaluate the benefits of polarimetric SAR for vessel detection [12]. One approach applied statistical decision theory to the polarimetric scattering matrix. Gaussian statistics were assumed in order to determine a decision variable. The detection performance was quantified by estimating receiver operating characteristics (ROCs), which show the probability of missed detection (PMD) as a function of the probability of false alarm (PFA). These curves illustrate the trade-off between PFA and PMD: a lower PFA is accompanied by a higher PMD.

This methodology has been applied to SAR images of known ships from the noted trials to calculate the performance of a number of different SAR systems, including single channel, dual channel, and quad polarimetric. Amplitude-only and amplitude plus phase were also considered. In this Annex, we present a synthesis of the results for three detection systems: polarimetric, dual co-polarization with phase, and HH polarization. We reduced the calculated ROCs to a single number whenever possible[14] by choosing a fixed value for the PFA[15] of $(10)^{-5}$, and by comparing the PMD for each of the radar cases mentioned to that of polarimetric detection, resulting in an estimate of the relative increase in PMD for the radar choices considered. These results appear in Table 49 through Table 52 for the available data sets. Other PFAs could be chosen for this analysis. However, the relative performance of PMD is expected to be similar to those presented here. Similarly, PMD could have been held constant, rather than PFA, to provide a similar inter-comparison.

From the Tables, we note the following:

- Aside from the CRUSADE data, all cases tabulated are for relatively calm conditions;
- For a PFA of $(10)^{-5}$, and normalizing the PMD to that of polarimetry, we found an increase of PMD for dual-co polarization with phase, and a larger increase of PMD for HH polarization, thus providing a quantification of the benefit of polarimetry for vessel detection;
- The benefits of polarimetry for ship detection appear to be larger for smaller vessels; and

[13] Derived and updated from a report prepared by P.W. Vachon and C. Liu that was circulated informally on 10 March 2006.

[14] Not all cases of PMD and PFA can be calculated, depending upon the number of samples actually available for statistical analysis.

[15] This choice permits some detection performance intercomparison via the relative PMD. The ROCs show the relative performance more broadly as a function of PFA. The representative trend in PMD for this specific PFA appears to apply to other PFA choices.

- Dual co-polarization with phase could be an interesting option for RADARSAT-2, especially if it can be provided with a larger swath width than will be available for polarimetric modes[16].

Table 49: Values of P_{MD} for $P_{FA} = 10^{-5}$ derived from the CRUSADE Trial data acquired in March 2000 off St. John's. Wind and wave observations are available as noted.

						***A.S. Pierce* (35 m)**		***Arctic Pride* (18.3 m)**		***Quebec* (135 m)**	
Line/Pass	**Wind Speed [m/s]**	**Wave Height [m]**	**Incidence**			**P_{MD}**	**P_{MD}/P^{Q}_{MD}**	**P_{MD}**	**P_{MD}/P^{Q}_{MD}**	**P_{MD}**	**P_{MD}/P^{Q}_{MD}**
l2p2 (a147) 22 Mar. 2000	12.9		*A.S. Pierce*: 34.7°	Quad	P_{MD}	1.20E-01	1.00				
				HH-VV	P_{MD}	5.60E-01	4.67				
				HH	P_{MD}						
l12p12 (a149) 22 Mar. 2000	12.9		*A.S. Pierce*: 33.7°	Quad	P_{MD}						
				HH-VV	P_{MD}						
				HH	P_{MD}						
l7p7 (a192) 24 Mar. 2000	7.7		*A.S. Pierce*: 46.0°	Quad	P_{MD}						
				HH-VV	P_{MD}	1.30E-02					
				HH	P_{MD}	1.20E-01					
l10p10 (a195) 24 Mar. 2000	7.7		*A.S. Pierce*: 55.9°	Quad	P_{MD}	2.30E-02	1.00				
				HH-VV	P_{MD}	7.00E-02	3.04				
				HH	P_{MD}	1.50E-01	6.52				
l3p1 (a199) 28 Mar. 2000	6.7	1	*Arctic Pride*: 53.1°	Quad	P_{MD}	1.00E-01	1.00	6.00E-03	1.00	1.00E-01	1.00
			A.S. Pierce: 29.4°	HH-VV	P_{MD}	2.70E-01	2.70	7.00E-02	11.67	2.30E-01	2.30
			Quebec: 37.4°	HH	P_{MD}			3.00E-01	50.00		
l10p10 (a200) 28 Mar. 2000	6.7	1	*Arctic Pride*: 33.3°	Quad	P_{MD}	8.00E-03	1.00	8.00E-02	1.00	9.00E-02	1.00
			A.S. Pierce: 35.4°	HH-VV	P_{MD}	2.30E-01	28.75	2.80E-01	3.50		
			Quebec: 38.0°	HH	P_{MD}	4.40E-01	55.00	4.00E-01	5.00		
l9p11 (a201) 28 Mar. 2000	6.7	1	*Arctic Pride*: 27.5°	Quad	P_{MD}	2.00E-01	1.00	1.00E-01	1.00		
			A.S. Pierce: 25.7°	HH-VV	P_{MD}			5.40E-01	5.40		
			Quebec: 28.7°	HH	P_{MD}						
l5p7 (a155) 30 Mar. 2000	7.7	3 to 4	*Arctic Pride*: 50.9°	Quad	P_{MD}			8.00E-04	1.00		
				HH-VV	P_{MD}			1.00E-02	12.50		
				HH	P_{MD}			8.00E-02	100.00		

[16] This might be feasible relative to already-defined polarimetry modes since the image quality requirements on the cross-polarization channels could be relaxed.

Table 50: Values of P_{MD} for $P_{FA} = 10^{-5}$ derived from the Quest-2003 Trial data acquired in Oct. 2003 off Halifax. Wind and wave observations are available as noted.

					Quest (76 m)	
Line/Pass	**Wind Speed [m/s]**	**Wave Height [m]**	**Incidence**		**P_{MD}**	**P_{MD}/P^{Q}_{MD}**
l1p2 (a278) 6 Oct. 2003	3.3	2	52.28°	Quad P_{MD}		
				HH-VV P_{MD}		
				HH P_{MD}		
l2p3 (a279) 6 Oct. 2003	3.3	2	48.03°	Quad P_{MD}	1.00E-01	1.00
				HH-VV P_{MD}		
				HH P_{MD}	2.10E-01	2.10
l3p4 (a280) 6 Oct. 2003	3.3	2	68.54°	Quad P_{MD}		
				HH-VV P_{MD}		
				HH P_{MD}		
l5p6 (a282) 6 Oct. 2003	1.6	1.9	57.3°	Quad P_{MD}	8.10E-03	1.00
				HH-VV P_{MD}	1.80E-02	2.22
				HH P_{MD}	6.00E-02	7.41
l6p7 (a283) 6 Oct. 2003	1.6	1.9	42.38°	Quad P_{MD}		
				HH-VV P_{MD}		
				HH P_{MD}	2.10E-02	
l1p1 (a288) 7 Oct. 2003	6	1.6	41.52°	Quad P_{MD}	1.50E-02	1.00
				HH-VV P_{MD}	8.00E-02	5.33
				HH P_{MD}	4.10E-01	27.33
l2p2 (a289) 7 Oct. 2003	6.8	1.6	40.42°	Quad P_{MD}	6.00E-02	1.00
				HH-VV P_{MD}	6.00E-01	10.00
				HH P_{MD}		
l3p3 (a290) 7 Oct. 2003	7.5	1.6	35.63°	Quad P_{MD}	5.80E-02	1.00
				HH-VV P_{MD}	4.20E-01	7.24
				HH P_{MD}		
l4p4 (a291) 7 Oct. 2003	7.5	1.6	27.23°	Quad P_{MD}	1.10E-01	
				HH-VV P_{MD}		
				HH P_{MD}		
l6p6 (a293) 7 Oct. 2003	7.6	1.6	45.43°	Quad P_{MD}		
				HH-VV P_{MD}	1.70E-02	
				HH P_{MD}	1.20E-01	

Table 51: Values of P_{MD} for $P_{FA} = 10^{-5}$ derived from the MarCoPola Trial data acquired on 23 March 2004 off Halifax. Wind and wave observations are available as noted.

					Quest (76 m)		*Grenfell* (68.5 m)		*Sambro* (16.3 m)	
Line/Pass	**Wind Speed [m/s]**	**Wave Height [m]**	**Incidence**		**P_{MD}**	**P_{MD}/P^{Q}_{MD}**	**P_{MD}**	**P_{MD}/P^{Q}_{MD}**	**P_{MD}**	**P_{MD}/P^{Q}_{MD}**
l1p3 (a301) 23 Mar. 2004			*Quest*: 45.5°	Quad P_{MD}						
			Grenfell: 41.°	HH-VV P_{MD}			1.20E-01		2.70E-01	
			Sambro: 52.4°	HH P_{MD}	3.10E-01		4.00E-01		5.00E-01	
l2p4 (a302) 23 Mar. 2004			*Quest*: 43.9°	Quad P_{MD}						
			Grenfell: 39.6°	HH-VV P_{MD}	3.00E-01		4.00E-01		3.00E-01	
			Sambro: 51.5°	HH P_{MD}	5.00E-01		6.00E-01		6.00E-01	
l3p5 (a303) 23 Mar. 2004			*Quest*: 36.2°	Quad P_{MD}	2.50E-01	1.00	1.10E-01	1.00		
			Grenfell: 44.1°	HH-VV P_{MD}	7.00E-01	2.80	3.80E-01	3.45		
			Sambro: 27.1°	HH P_{MD}			6.00E-01	5.45		
l4p6 (a304) 23 Mar. 2004			*Quest*: 46.5°	Quad P_{MD}					2.30E-02	1.00
		0.3	*Grenfell*: 37.8°	HH-VV P_{MD}	4.10E-01		7.00E-01		3.10E-01	13.48
			Sambro: 51.1°	HH P_{MD}	6.40E-01		8.00E-01		6.00E-01	26.09
l5p7 (a305) 23 Mar. 2004			*Quest*: 34.6°	Quad P_{MD}	5.30E-01					
		0.2	*Grenfell*: 45.7°	HH-VV P_{MD}			5.40E-01			
			Sambro: 31.9°	HH P_{MD}			8.00E-01			
l6p8 (a306) 23 Mar. 2004			*Quest*: 44.7°	Quad P_{MD}						
		0.2	*Grenfell*: 42.2°	HH-VV P_{MD}	3.70E-02				4.50E-02	
			Sambro: 56.8°	HH P_{MD}	3.00E-01		2.10E-01		1.20E-01	
l7p9 (a307) 23 Mar. 2004			*Quest*: 38.6°	Quad P_{MD}	1.60E-01	1.00			3.80E-02	1.00
		0.2	*Grenfell*: 43.6°	HH-VV P_{MD}	5.30E-01	3.31			1.70E-01	4.47
			Sambro: 51.7°	HH P_{MD}	8.00E-01	5.00	6.20E-01		5.00E-01	13.16
l8p10 (a308) 23 Mar. 2004			*Quest*: 47.7°	Quad P_{MD}					1.00E-01	1.00
		0.3	*Grenfell*: 38.4°	HH-VV P_{MD}			2.40E-01		7.00E-01	7.00
			Sambro: 36.1°	HH P_{MD}	3.00E-01		6.00E-01			

Table 52: Values of P_{MD} for $P_{FA} = 10^{-5}$ derived from the MarCoPola Trial data acquired on 24 March 2004 off Halifax. Wind and wave observations are available as noted.

						***Divecom III* (13.3 m)**		***Grenfell* (68.5 m)**		***Sambro* (16.3 m)**	
Line/Pass	**Wind Speed [m/s]**	**Wave Height [m]**	**Incidence**			**P_{MD}**	**P_{MD}/P^{Q}_{MD}**	**P_{MD}**	**P_{MD}/P^{Q}_{MD}**	**P_{MD}**	**P_{MD}/P^{Q}_{MD}**
l1p1 (a309) 24 Mar. 2004			*Divecom III*: 36.1°	Quad	P_{MD}	6.50E-01				3.00E-01	1.00
			Grenfell: 44.9°	HH-VV	P_{MD}					6.60E-01	2.20
			Sambro: 35.1°	HH	P_{MD}						
l2p2 (a310) 24 Mar. 2004			*Divecom III*: 47.2°	Quad	P_{MD}	9.50E-02				1.60E-01	
			Grenfell: 39.9°	HH-VV	P_{MD}			4.40E-01			
			Sambro: 30.9°	HH	P_{MD}			6.50E-01			
l3p3 (a311) 24 Mar. 2004			*Divecom III*: 40°	Quad	P_{MD}			2.80E-01	1.00	2.10E-01	1.00
			Grenfell: 39.3°	HH-VV	P_{MD}			6.10E-01	2.18	5.50E-01	2.62
			Sambro: 47.5°	HH	P_{MD}			8.10E-01	2.89		
l4p4 (a312) 24 Mar. 2004			*Divecom III*: 43.4°	Quad	P_{MD}	3.00E-01		1.40E-01	1.00		
			Grenfell: 36.4°	HH-VV	P_{MD}			8.00E-01	5.71		
			Sambro: 28.8°	HH	P_{MD}			8.40E-01	6.00		
l5p5 (a313) 24 Mar. 2004			*Divecom III*: 29.6°	Quad	P_{MD}			4.30E-01	1.00	5.90E-01	
			Grenfell:38.3°	HH-VV	P_{MD}			8.50E-01	1.98		
			Sambro: 46.8°	HH	P_{MD}						

List of acronyms

ACL	Atlantic Container Lines
ADSS	Analysts' Detection Support System
AHRS	Attitude and Heading Reference System
AIS	Automatic Identification System
ARC	Active Radar Calibrator
ASAR	Advanced SAR instrument on Envisat
ASCII	American Standard Code for Information Interchange
ATA	Adaptive Threshold Algorithm
ATR	Automatic Target Recognition
AVMS	AIS Vessel Management System
BER	Bit Error Rate
BITE	Built-In Test Equipment
CCGS	Canadian Coast Guard Ship
CCRS	Canada Centre for Remote Sensing
CHASP	Chip-based Adaptive SAR Processor
CNR	Clutter-to-Noise Ratio
COASP	Configurable Airborne SAR Processor
COE	Common Operating Environment
CONOPS	Concept of Operations
CRB	Cramer-Rao Lower Bound
CV-580	Consolidated Vultee Convair 580 (aircraft)
DC	Doppler Centroid
DND	Department of National Defence
DR	Doppler Rate
DRDC	Defence R&D Canada
EC	Environment Canada
ERU	Exciter, Receiver Unit
GPS	Global Positioning System
HH	Horizontal transmit, Horizontal receive
HMCS	Her Majesty's Canadian Ship
HV	Horizontal transmit, Vertical receive

JIIFC	Joint Information and Intelligence Fusion Capability
JIOC	Joint Information Operations Centre
L	Left
l#p#	Line number, Pass number
LOS	Line of Sight
LPA	Low Power Amplifier
MARSIE	Maritime Sensor Integration Experiment
MIS	Maritime Incursion Scenario
MPA	Medium Power Amplifier
MSOC	Maritime Security Operations Centre
N	No
OTH	Over The Horizon
PC	Personal Computer
PE	Polar Epsilon
PolSAR	Polarimetric SAR
PFA	Probability of False Alarm
PMD	Probability of Missed Detection
PRF	Pulse Repetition Frequency
QC	Quality Control
R	Right
R&D	Research & Development
RCS	Radar Cross Section
RGB	Red, Green, Blue
RMP	Recognized Maritime Picture
ROC	Receiver Operating Characteristic
ROI	Region of Interest
RTP	Real Time Processor
SAR	Synthetic Aperture Radar
SAW	Surface Acoustic Wave
SCNR	Signal to Clutter and Noise Ratios
SD	Standard Deviation
SLA	Service Level Arrangement
SLC	Single Look Complex
SNR	Signal-to-Noise Ratio

SOR	Statement of Operational Requirements
SSCM	Symmetric Scattering Characterization Method
TCR	Trihedral Corner Reflector
TR	Target Response
TTCP	The Technical Cooperation Program
UAV	Unmanned Aerial Vehicle
UTC	Universal Time Coordinated
VH	Vertical transmit, Horizontal receive
VV	Vertical transmit, Vertical receive
Y	Yes
YOW	Ottawa airport
YYG	Charlottetown airport
YYT	St. John’s airport

This page intentionally left blank.

Distribution list

Document No.: DRDC Ottawa TM 2006-202

LIST PART 1: Internal Distribution by Centre:

4	Library DRDC Ottawa
1	Dragošević, Marina
1	Geling, Gary
1	Kashyap, Nathan
1	Kraft, James
1	Liu, Chen
1	Livingstone, Chuck
1	Meek, Allan
1	Potter, Terry
1	Sabry, Ramin
1	Schlingmeier, David
1	Secker, Jeff
5	Vachon, Paris
1	Wilcox, Caroline
1	Yue, Bing
22	TOTAL LIST PART 1

LIST PART 2: External Distribution by DRDKIM

1	DRDKIM
2	Library and Archives Canada
1	CISTI
1	Butler, Maj Peter, DJCP
1	Howes, LCol Jeff, DPDOIS, Polar Epsilon
1	Quinn, LCdr Robert, DJCP
1	Samoluk, LCdr Andy, DJCP
1	Tunaley, J.K.E., DPDOIS, Polar Epsilon
9	TOTAL LIST PART 2

31 TOTAL COPIES REQUIRED

This page intentionally left blank.

DOCUMENT CONTROL DATA

(Security classification of title, body of abstract and indexing annotation must be entered when the overall document is classified)

1. ORIGINATOR (The name and address of the organization preparing the document. Organizations for whom the document was prepared, e.g. Centre sponsoring a contractor's report, or tasking agency, are entered in section 8.)

Defence R&D Canada - Ottawa
3701 Carling Avenue
Ottawa, Ontario
K1A 0Z4

2. SECURITY CLASSIFICATION (Overall security classification of the document including special warning terms if applicable.)

UNCLASSIFIED

3. TITLE (The complete document title as indicated on the title page. Its classification should be indicated by the appropriate abbreviation (S, C, R or U) in parentheses after the title.)

Processing and Analysis of Polarimetric Ship Signatures from MARSIE: Report on Results for Polar Epsilon

4. AUTHORS (last name, followed by initials – ranks, titles, etc. not to be used)

Vachon, P.W.; Dragošević, M.; Kashyap, N.; Liu, C.; Schlingmeier, D.; Meek, A.; Potter, T.; Yue, B.; Kraft, J.

5. DATE OF PUBLICATION (Month and year of publication of document.)	6a. NO. OF PAGES (Total containing information, including Annexes, Appendices, etc.)	6b. NO. OF REFS (Total cited in document.)
October 2006	140	23

7. DESCRIPTIVE NOTES (The category of the document, e.g. technical report, technical note or memorandum. If appropriate, enter the type of report, e.g. interim, progress, summary, annual or final. Give the inclusive dates when a specific reporting period is covered.)

Technical Memorandum

8. SPONSORING ACTIVITY (The name of the department project office or laboratory sponsoring the research and development – include address.)

Polar Epsilon SLA

9a. PROJECT OR GRANT NO. (If appropriate, the applicable research and development project or grant number under which the document was written. Please specify whether project or grant.)	9b. CONTRACT NO. (If appropriate, the applicable number under which the document was written.)
15ec05-01	

10a. ORIGINATOR'S DOCUMENT NUMBER (The official document number by which the document is identified by the originating activity. This number must be unique to this document.)	10b. OTHER DOCUMENT NO(s). (Any other numbers which may be assigned this document either by the originator or by the sponsor.)
DRDC Ottawa TM 2006-202	

11. DOCUMENT AVAILABILITY (Any limitations on further dissemination of the document, other than those imposed by security classification.)

(X) Unlimited distribution
( ) Defence departments and defence contractors; further distribution only as approved
( ) Defence departments and Canadian defence contractors; further distribution only as approved
( ) Government departments and agencies; further distribution only as approved
( ) Defence departments; further distribution only as approved
( ) Other (please specify):

12. DOCUMENT ANNOUNCEMENT (Any limitation to the bibliographic announcement of this document. This will normally correspond to the Document Availability (11). However, where further distribution (beyond the audience specified in (11) is possible, a wider announcement audience may be selected.))

13. ABSTRACT (A brief and factual summary of the document. It may also appear elsewhere in the body of the document itself. It is highly desirable that the abstract of classified documents be unclassified. Each paragraph of the abstract shall begin with an indication of the security classification of the information in the paragraph (unless the document itself is unclassified) represented as (S), (C), (R), or (U). It is not necessary to include here abstracts in both official languages unless the text is bilingual.)

This report presents the initial analysis of a polarimetric synthetic aperture radar (SAR) data set that was acquired during the Oct. 2005 Maritime Sensor Integration Experiment (MARSIE). MARSIE, as part of a larger TTCP activity, was designed to explore the benefits of sensor fusion to solve the target detection and tracking problem. The MARSIE trial was conducted off the East Coast of Canada and brought many sensors to bear on a set of known ship targets that were engaged in a simulated maritime incursion scenario. The Environment Canada CV-580 polarimetric SAR was used as a proxy sensor for RADARSAT-2 polarimetry. MARSIE polarimetry results include observations of ship target radar cross section for co-polarization and cross-polarization channels, the reduction in the probability of missed detection for polarimetric relative to single channel radar operation, and the potential benefit of polarimetric target decomposition to generate ship target classification features and to segment the ship target of interest from the ocean background. A main recommendation of this report is that polarimetry could improve Polar Epsilon (PE) ship detection performance and enhance the PE concept of operations for the surveillance of spatially constrained maritime operational areas of interest such as choke points.

523H

14. KEYWORDS, DESCRIPTORS or IDENTIFIERS (Technically meaningful terms or short phrases that characterize a document and could be helpful in cataloguing the document. They should be selected so that no security classification is required. Identifiers, such as equipment model designation, trade name, military project code name, geographic location may also be included. If possible keywords should be selected from a published thesaurus, e.g. Thesaurus of Engineering and Scientific Terms (TEST) and that thesaurus identified. If it is not possible to select indexing terms which are Unclassified, the classification of each should be indicated as with the title.)

MARSIE, Polar Epsilon, polarimetric decompostion, polarimetry, SAR, ship detection, ship signatures, synthetic aperture radar

Defence R&D Canada

Canada's leader in Defence
and National Security
Science and Technology

R & D pour la défense Canada

Chef de file au Canada en matière
de science et de technologie pour
la défense et la sécurité nationale

www.drdc-rddc.gc.ca